Hydrogen Production in Supercritical Water

by

Adam Joseph Byrd

A dissertation submitted to the Graduate Faculty of
Auburn University
in partial fulfillment of the
requirements for the Degree of
Doctor of Philosophy
Auburn, Alabama
August 6, 2011

Keywords: Hydrogen Production, Supercritical Water,
Renewable Energy, Hydrothermal Stability

Approved by

Ram B. Gupta, Chair, Professor of Chemical Engineering
Sushil Adhikari, Assistant Professor of Biosystems Engineering
Mario R. Eden, Associate Professor of Chemical Engineering
Yoon Y. Lee, Professor of Chemical Engineering
Christopher B. Roberts, Professor of Chemical Engineering

Abstract

Hydrogen has been considered as an environmentally friendly energy carrier for the future. It is not found freely in nature but must be obtained by processing hydrogen containing compounds. Current industrial-scale hydrogen production relies on the fossil fuel feedstocks. The processing of fossil fuels for hydrogen production may represent a more efficient use, but ultimately still contributes greenhouse gases into the atmosphere. Fossil fuels are not the only possibility for a hydrogen containing feedstock, however. Biomass and biomass-derived materials also can be processed to generate hydrogen. Carbon dioxide generated during hydrogen production from biomass will later be fixed by plants during photosynthesis, thus creating a closed loop with no net increase in CO_2.

The properties of water above its critical point (T: 374°C, P: 221 bar) are markedly different than under ambient conditions, making it interesting both as solvent and reactant. In the supercritical phase the dielectric constant of water is greatly reduced and accordingly it behaves as an organic solvent, easily dissolving many organic species and gases while precipitating polar salts. As a homogenous phase with low viscosity and high diffusivity, transport limitations can be overcome in supercritical water. Physical properties of supercritical water such as density, heat capacity, and ion product can be tuned by small changes in temperature and pressure to enhance reaction rate and reduce volume requirement for reactors. A further benefit conferred by the supercritical water

process is that water is compressed in the liquid state allowing the produced hydrogen to be obtained directly at high pressure without the need for energy intensive compression.

Four biomass-derived compounds have been examined as feedstocks for hydrogen production in supercritical water by catalytic reforming in a continuous flow reactor. The flow-type reactor allowed the attainment of short residence times of seconds unavailable to previous researchers operating batch reactors. First, glucose was used as a model compound for biomass (Chapter 2). The presence of the ruthenium catalyst greatly increased the conversion and hydrogen yield from glucose while significantly reducing char and tar formation. Feed concentrations of up to 5 wt% glucose gave a hydrogen yield near the theoretical maximum at 700°C with a residence time of only two seconds. Ethanol (Chapter 3) was investigated as a feedstock for hydrogen production as it is already produced for use as an automotive fuel additive, however its conversion to hydrogen for use in a fuel cell would greatly increase its efficiency. Full conversion to gaseous products was seen above 700°C with no coke formation being observed below 10 wt% ethanol feed. Varying pressure from 221 to 276 bar had little effect on the gas yields. The third biomass-derived feedstock used was glycerol (Chapter 4), which is obtained as a byproduct from biodiesel manufacturing by transesterification of vegetable oils. Hydrogen yields near the theoretical limit were obtained for dilute solutions with a 1s residence time at 800°C, while hydrogen yields dropped with longer residence times due to methanation. Feed concentrations of up to 40 wt% glycerol were also gasified at 800°C and 1 s residence time with no coke formation and the yield of product gases closely following equilibrium values. Liquefied switchgrass biocrude was evaluated as the fourth feedstock for hydrogen production in Chapter 5. Nickel, cobalt, and ruthenium

catalysts were prepared on titania, zirconia, and magnesium aluminum spinel supports to create a suite of nine catalysts. These were evaluated for hydrogen production by gasification of switchgrass biocrude in supercritical water at 600°C and 250 bar. Magnesium aluminum spinel was seen to be an inappropriate support as reactors quickly plugged. Ni/ZrO_2 gave 0.98 mol H_2/mol C, the highest hydrogen yield of all tested catalysts; however, over time, increase in pressure drop lead to reactor plugging with all zirconia supported catalysts. Titania supported catalysts gave lower conversions, however they did not plug during the course of the study. Charring of all catalysts was seen to occur at the entrance of the reactor as the biocrude was heated. All support materials suffered significant surface area loss due to sintering.

The severity of water's critical point can lead to sintering and phase transformations of catalyst support materials. Cerium-coated γ-alumina (Chapter 6) and binary oxides of aluminum, titanium, and zirconium (Chapter 7) were synthesized as potential catalyst supports and evaluated for their stability in hot compressed water. γ-Al_2O_3 modified with 1-10 wt% Ce was examined, specifically in the temperature range of 500 – 700°C at 246 bar. Transformations of the γ phase were slowed but not prevented. Based on X-ray analysis, the transformation of γ -Al_2O_3 proceeded through the κ phase toward the stable α phase. Reduced cerium species were seen to be oxidized in the supercritical water environment, and low Ce-loading supports maintained the highest BET surface areas. The stabilization was greatest at 700°C, where Ce-modified aluminas retained significantly higher specific surface areas than unmodified alumina. Binary oxides of aluminum, titanium, and zirconium with 1:1 mole ratios of the component metals were synthesized by a coprecipitation method. Their stability in sub- and

supercritical water was evaluated at 25 MPa over a temperature range of 350 – 650 °C for a period of three hours by XRD and BET studies. The compound $ZrTiO_4$ was crystallographically stable at all conditions. It maintained its surface area in subcritical water, although it sintered and lost much of its pore volume in supercritical water. ZrO_2/Al_2O_3 maintained high surface area up to 450°C, but sintered above this temperature as a result of phase transformation of both ZrO_2 and Al_2O_3. The TiO_2/Al_2O_3 mixed oxide, while having the highest initial surface area, sintered extensively following all hydrothermal treatments. Alumina in the TiO_2/Al_2O_3 system hydrolyzed in subcritical water and transformed to corundum in supercritical water, while anatase titania was transformed to rutile only at 650°C.

Acknowledgements

I wish to offer my thanks to my advisor Dr. Ram B. Gupta, whose continued guidance and advice has been inestimable in my dissertation research. He has provided encouragement in the face of difficulty as well as a model of excellence in all endeavors.

I thank the members of my research group both past and present who have helped me along the way. Dr. Ganesh Sanganwar, Dr. Sandeep Kumar, Dr. K.K. Pant, Dr, Melinda Hemingway, Dr. Lingzhao Kong, Hema Ramsurn, Courtney Ober, and Siddharth Gumuluru are all owed many thanks for long and helpful discussions of research topics. I also thank Dr. Sachin Nair for assistance with BET measurements and Dr. Aimee Poda for her help with operation of TGA-MS.

I must also pay homage to the memory of my grandfather Joseph V. Saliga, who provided the inspiration and dedication to do research in the field of hydrogen production.

Finally I wish to acknowledge the financial support of the Department of Energy through the NETL Consortium of Fossil Fuel Science, DOD/TACOM/TARDEC, and the Alabama Centre for Paper and Bioresource Engineering.

Table of Contents

Abstract....ii

Acknowledgements....vi

List of Tables....xii

List of Figures....xiii

1. Introduction....1

1.1 Hydrogen Properties....2

1.2 Supercritical Water Background and Properties....3

1.3 Hydrogen Production from Hydrocarbons....5

1.4 Hydrogen Production from Biomass and Model Compounds....8

1.4.1 Aqueous Phase Reforming....8

1.4.2 Gasification....8

1.4.3 Supercritical Water Gasification....9

1.5 Water Electrolysis....13

1.6 Other Relevant Previous SCW work....13

1.6.1 Supercritical water oxidation (SCWO)....13

1.6.2 Corrosivity in SCW environment....17

1.7 References....20

2. Hydrogen Production from Glucose....27

2.1 Abstract....27

2.2 Introduction....27

2.3 Experimental Section....30

2.3.1 Materials....30

2.3.2 Apparatus....30

2.3.3 Experimental Procedure....32
2.4 Results and Discussion....33
2.4.1 Effect of Ru/Al_2O_3 Catalyst....33
2.4.2 Effect of Residence Time....37
2.4.3 Effect of Temperature....38
2.4.4 Effect of Glucose Concentration....40
2.4.5 Reaction Mechanism....41
2.5 Conclusions....44
2.6 Acknowledgement....45
2.7 References....46
3. Hydrogen Production from Ethanol....49
3.1 Abstract....49
3.2 Introduction....49
3.3 Experimental Section....53
3.4 Results and Discussion....56
3.4.1 Effect of Ru/Al_2O_3 Catalyst....56
3.4.2 Effect of Residence Time....62
3.4.3 Effect of Pressure....65
3.4.4 Effect of Temperature....65
3.4.5 Effect of the Ethanol Concentration....67
3.4.6 Reaction Mechanism and Kinetics....69
3.5 Conclusions....73
3.6 Acknowledgment....74
3.7 References....75
4. Hydrogen Production from Glycerol....78
4.1 Abstract....78
4.2 Introduction....78

4.3 Experimental Section....81
4.3.1 Materials....81
4.3.2 Experimental Procedure....82
4.4 Results and Discussion....84
4.4.1 Effect of Reaction Time....85
4.4.2 Effect of Temperature....86
4.4.3 Effect of Glycerol Feed Concentration....87
4.4.4 Reaction Kinetics....88
4.5 Conclusions....92
4.6 Acknowledgment....92
4.7 References....93
5. Hydrogen Production from Catalytic Gasification of Switchgrass Biocrude....95
5.1 Abstract....95
5.2 Introduction....95
5.3 Experimental....98
5.3.1 Catalyst Preparation....98
5.3.2 Feedstock Preparation....99
5.3.3 Experimental Procedure....100
5.4 Results....102
5.4.1 Crystalline structure....105
5.4.2 Surface area....107
5.4.3 Particle size and morphology....109
5.4.4 Thermo-gravimetric Analysis....111
5.5 Discussion....112
5.6 Conclusions....114
5.7 References....115

6. Stability of Cerium-modified γ-Alumina Catalyst Support in Supercritical Water....118
6.1 Abstract....118
6.2. Introduction....118
6.3. Experimental....123
6.3.1 Sample Preparation....123
6.3.2 Experimental Procedure....124
6.4. Results and Discussion....126
6.4.1 XRD....126
6.4.2 BET Surface Area....133
6.4.3 ICP-AES....134
6.5 Conclusions....135
6.6 References....136
7. Stability of Binary Aluminum, Titanium, and Zirconium Oxides for Catalyst Supports in Sub- and Supercritical Water....139
7.1 Abstract....139
7.2 Introduction....139
7.3 Experimental....141
7.3.1 Sample Preparation....141
7.3.2 Experimental Procedure....142
7.3.3 Characterization....144
7.4 Results and Discussion....144
7.4.1 Crystalline structure....144
7.4.2 Surface area and pore characterization....147
7.5 Conclusions....149
7.6 References....150
8. Overall Conclusions....152
9. Directions for Future Work....156

Appendix 1: Determination of Gas Composition.....159
Appendix 2: Calculation of Gas Flow using Viscosity Correction.....161
Appendix 3: List of Publications and Presentations.....162

List of Tables

Table 1.1: Properties of Hydrogen.....3

Table 2.1: Product Distribution during Thermal and Catalytic Reforming of Glucose in Supercritical Water (T: 700°C, P: 241 bar, 1.0 wt% glucose).....34

Table 3.1: Details of Experimental Conditions.....58

Table 3.2: Values of rate constants at different temperatures.....73

Table 4.1: Details of experimental conditions.....83

Table 5.1: Oxygenated Hydrocarbons Present in Biocrude.....100

Table 5.2: Gasification Efficiencies and Carbon Balance Closure.....103

Table 5.3: Surface Area, Pore Radii and Volume for Calcined and Used Catalysts.....108

Table 5.4: Weight Loss (%) of Carbonaceous Material During TGA.....112

Table 6.1: BET Surface Area of Samples.....134

Table 7.1: Surface Area, Average Pore Size, and Pore Volume of Binary Oxides after Calcination and Subsequent Hydrothermal Treatment at 25 MPa.....148

Table A1.1: Composition of Calibration Gas in mol%.....160

List of Figures

Figure 1.1: Phase diagram for water 4

Figure 1.2: Physical properties of water at 24 MPa.....5

Figure 2.1: Schematic diagram of the experimental apparatus.....32

Figure 2.2: Effect of residence time on product gas yields during non-catalytic reforming of glucose (T: 700°C, P: 241 bar, glucose conc.: 1 wt.%).....35

Figure 2.3: Effect of residence time on product gas yields: (T: 700°C, P: 241 bar, glucose conc.: 1 wt.%, 2.0 g Ru/Al_2O_3 catalyst).....36

Figure 2.4: Effect of residence time on product gas yields. (T: 700°C, P: 241 bar, glucose conc. 5 wt. %, 2.0 g Ru/Al_2O_3 catalyst).....37

Figure 2.5: Effect of residence time on total organic carbon in liquid phase (T=700°C, P: 241 bar, residence time: 2 s).....38

Figure 2.6: Effect of temperature on product yields (P: 241 bar, glucose conc.: 4 wt.%, residence time: 2 s, 2.0 g Ru/Al_2O_3 catalyst)..... 40

Figure 2.7: Effect of glucose concentration on product yields (T: 700°C, P: 241 bar, residence time: 2 s: 2.0 g Ru/Al_2O_3 catalyst).....41

Figure 3.1: Schematic diagram of experimental apparatus.....54

Figure 3.2: SEM images of fresh Ru/Al_2O_3 catalyst. (a) 5500x magnification (b) 33,000x magnification.....60

Figure 3.3: SEM images of used Ru/Al_2O_3 catalyst. (a) 600x magnification (b) 30,000x magnification.....61

Figure 3.4: X-ray diffraction spectra for fresh and spent Ru/Al_2O_3 catalyst.....62

Figure 3.5: Effect of residence time on product gas yields (T, 600 °C; P, 221 bar; feed conc., 10 wt% EtOH; 1.922g Ru/Al_2O_3 W/F_{Ao}, 5 s:14,200g cat*s/g-mol EtOH, 10 s: 25,200 cat*s/g-mol EtOH).....63

Figure 3.6: Effect of residence time on product yields (T, 700°C; P, 221 bar; feed conc., 10 wt% EtOH; 1.922g Ru/Al_2O_3).....64

Figure 3.7: Effect of residence time on product yields (T, 800°C; P, 221 bar; feed conc., 10 wt% EtOH; 1.922g Ru/Al_2O_3).....64

Figure 3.8: Effect of reactor pressure (T, 700°C; feed conc., 2 s in Ru/Al_2O_3 bed; 10wt% EtOH; 1.922 g Ru/Al_2O_3).....65

Figure 3.9: Effect of reactor temperature (P, 221 bar; 2 s residence time in Ru/Al_2O_3 bed; feed conc., 10wt% EtOH; 1.922 g Ru/Al_2O_3).....66

Figure 3.10: Effect of feed concentration of product gas yields (T, 800°C; P, 221 bar; residence time 4 s in Ru/Al_2O_3 bed, feed conc., 10 wt% EtOH; 1.922 g Ru/Al_2O_3).....68

Figure 4.1: Schematic of SCW hydrogen production apparatus.....83

Figure 4.2: Effect of residence time on product gas yields. T: 800°C, P: 241 bar, feed conc.:5 wt% glycerol, 2.0 g Ru/Al_2O_3 catalyst.....86

Figure 4.3: Effect of temperature on product gas yields. P: 241 bar, 1 s residence time, feed conc.: 5 wt%, 2.0 g Ru/Al_2O_3.....87

Figure 4.4: Effect of glycerol feed concentration on product gas yields. T: 800°C, P: 241 bar, 1 s residence time, 2.0 g Ru/Al_2O_3 catalyst.....88

Figure 4.5: SEM images of fresh (a) and used (b) Ru/Al_2O_3 catalysts.....91

Figure 5.1: Schematic of experimental apparatus.....101

Figure 5.2: Product gas yields for TiO_2 and ZrO_2 supported catalysts.....104

Figure 5.3: XRD spectra of ZrO_2 supported catalysts before and after SCW exposure. (a) fresh and (b) used Ni/ZrO_2; (c) fresh and (d) used Ru/ZrO_2; (e) fresh and (f) used Co/ZrO_2.....105

Figure 5.4: XRD spectra of TiO_2 supported catalysts before and after SCW exposure. (a) fresh and (b) used Ni/TiO_2; (c) fresh and (d) used Ru/TiO_2; (e) fresh and (f) used Co/TiO_2.....106

Figure 5.5: XRD spectra of $MgAl_2O_4$ supported catalysts before and after SCW exposure. (a) fresh and (b) used Ni/ $MgAl_2O_4$; (c) fresh and (d) used Ru/ $MgAl_2O_4$; (e) fresh and (f) used Co/ $MgAl_2O_4$.....107

Figure 5.6: SEM of used Ni/ZrO_2 catalyst taken from the reactor entrance.....109

Figure 5.7: SEM of used Ni/ZrO_2 catalyst taken from the reactor exit.....110

Figure 5.8: SEM of used Ni/TiO_2 catalyst taken from the reactor entrance.....110

Figure 5.9: SEM of used Ni/TiO_2 catalyst taken from the reactor exit.....111

Figure 6.1: Dehydration sequence of selected alumina hydrates in air at ambient pressure. Path a favored by $d_p < 10$ μm; Path b favored by alkalinity and $d_p > 100$ μm. Open areas indicate transitional zones. Adapted from reference [3].....120

Figure 6.2: Model of alumina surface dehydroxylation resulting in loss of surface area. Adapted from reference [4]..... 121

Figure 6.3: Experimental Apparatus.....125

Figure 6.4: XRD spectra of (a) γ-Al_2O_3 as received; freshly calcined (b) 1CeAl, (c) 2CeAl, (d) 4CeAl, (e) 6CeAl, (f) 10CeAl. ■ corresponds to CeO_2.....127

Figure 6.5: XRD spectra of unmodified Al_2O_3 after 3h exposure to supercritical water at (a) 500°C, (b) 600°C, and (c) 700°C. Labels correspond to (○) α-Al_2O_3, (□) κ-Al_2O_3, and (◊) Boehmite.....128

Figure 6.6: XRD spectra of CeAl samples after exposure to SCW at 500°C (a) 2CeAl (b) 6CeAl (c) 10CeAl. Labels correspond to (○) α -Al_2O_3, (□)κ -Al_2O_3, (◊) Boehmite, (■) CeO_2.....129

Figure 6.7: XRD spectra of CeAl samples after exposure to SCW at 600°C (a) 1CeAl (b) 2CeAl (c) 4CeAl (d) 6CeAl (e) 10CeAl. Labels correspond to (○)α -Al_2O_3, (□)κ -Al_2O_3, (■) CeO_2.....130

Figure 6.8: XRD spectra of CeAl samples after exposure to SCW at 700°C (a) 2CeAl (b) 4CeAl (c) 6CeAl. Labels correspond to (○)α -Al_2O_3, (□) κ-Al_2O_3, (■) CeO_2.....131

Figure 6.9: XRD spectra of 6CeAl samples after exposure to SCW at 600°C. (a) Reduced at 950°C, SCW exposure 3h (b) Reduced at 950°C, SCW exposure 6 h (c) Reduced at 750°C, SCW exposure 3h (d) Reduced at 750°C, SCW exposure 6 h.....133

Figure 7.1: Experimental apparatus for hydrothermal treatment of binary oxides.....142

Figure 7.2: XRD spectra of ZrTi (a) after calcination, and after hydrothermal treatment at 25 MPa and (b) 350°C, (c) 450°C, (d) 550°C, and (e) 650°C. all peaks correspond to $ZrTiO_4$.....145

Figure 7.3: XRD spectra of TiAl (a) after calcination, and after hydrothermal treatment at 25 MPa and (b) 350°C, (c) 450°C, (d) 550°C, and (e) 650°C. Labels correspond to (◇) AlO(OH), (◆) α-Al_2O_3, (○) anatase TiO_2, (●) rutile TiO_2.....146

Figure 7.4: XRD spectra of ZrAl (a) after calcination, and after hydrothermal treatment at 25 MPa and (b) 350°C, (c) 450°C, (d) 550°C, and (e) 650°C. Labels correspond to (□) t-ZrO_2, (■)m-ZrO_2, (◇)AlO(OH), (◆) α-Al_2O_3.....147

1. Introduction

The total energy demand of the world is growing every year with increasing population and demands for higher standards of living. Currently most of the world's energy demands are met by using non-renewable fossil fuels, be it coal, liquid hydrocarbons, or natural gas. In 2007 the nation's annual energy consumption was approximately 100 quadrillion BTU. Of that, 39% was petroleum, 23% natural gas, and 22% coal. Nuclear energy accounted for 8%, while all renewable energy technologies contributed only 7%[1] Hydrocarbon fuels are favored for their high energy density and ease of transportation, but combustion of these fuels contributes as a major source of air pollution and greenhouse gases. Moreover, the supply of fossil fuels is finite and exhaustible. Hydrogen has been considered as an environmentally friendly energy carrier for the future, although current production technologies rely on fossil resources as a feedstock. Hydrogen production from fossil fuels may represent a more efficient utilization of our reserves but still entails the use of a non-renewable resource, and in the absence of sequestration, the release of CO_2 into the atmosphere. It is also possible to produce hydrogen from renewable resources such as biomass and biomass derived materials with zero net emissions of carbon dioxide. This refers to the fact that CO_2 produced during the processing of biomass materials will be fixed by plants during photosynthesis, thus creating a closed carbon loop. The properties of water above its critical point make it an attractive reaction medium that provides good heat and mass transfer, as well as small reactor volumes. Supercritical water's non-polar nature allows it to solubilize organic compounds, thus reducing tar or coke formation. Another benefit conferred is that hydrogen is produced directly at high pressure ready for storage. For

these reasons this research explores hydrogen production from several biomass-derived materials in supercritical water.

1.1 Hydrogen Properties

Hydrogen is the simplest and smallest atom, with the most common isotope consisting of only one proton and one electron. It is the most abundant element in the universe, but owing to its high reactivity it is not found in its molecular form H_2. Most of the hydrogen on Earth exists either in its oxidized form as water with no fuel value or bound to carbon atoms. For this reason hydrogen may be considered as an energy carrier, but not an energy source. In order to obtain molecular hydrogen it must be produced from some other hydrogen-containing compound.

Hydrogen gas is colorless, odorless, tasteless, and nontoxic. It diffuses rapidly through air with a diffusion coefficient of $0.61 cm^2 s^{-1}$; however it has a wide flammability range in air of 4-75 vol%, and its ignition energy of 0.02 mJ is an order of magnitude lower than hydrocarbon fuels in air. Liquid hydrogen has the highest energy density of any fuel on mass basis, but has a relatively low energy density on a volume basis. For example, the LHV of liquid hydrogen (140.4 MJ kg^{-1}) is almost three times that of gasoline (48.6 MJ kg^{-1}) on a mass basis, which is reversed when considering energy density on a volume basis (8,491 MJ m^{-3} vs. 31,150 MJ m^{-3}).[2] Additional physical properties of hydrogen are presented in Table 1.

Table 1.1. Properties of Hydrogen[3]

Property	Value	Unit
Molecular Weight	2.01594	
Density		
gas at 0°C, 1 atm	0.08987	kg m^{-3}
liquid at -253°C	708	kg m^{-3}
solid at -259°C	858	kg m^{-3}
Melting Temperature	-259	°C
Normal Boiling Point	-253	°C
Heat of Fusion at -259°C	58	kJ kg^{-1}
Heat of Vaporization at -253°C	447	kJ kg^{-1}
Heat Capacity (Cp)		
gas at 25°C	14.3	kJ kg^{-1}°C^{-1}
liquid at -256°C	8.1	kJ kg^{-1}°C^{-1}
solid at -259.8°C	2.63	kJ kg^{-1}°C^{-1}
Critical Temperature	-240	°C
Critical Pressure	12.8	atm
Critical Density	31.2	kg m^{-3}
Viscosity at 25°C, 1 atm	0.00892	cP
Thermal Conductivity	190	W m^{-1}°C^{-1}

1.2 Supercritical Water Background and Properties

Liquid water at ambient conditions (25°C, 1 atm) is an excellent solvent for many polar compounds and inorganic salts due to the polar nature of water. Under elevated temperature and pressure, however, the nature of water as a solvent changes considerably. Above the critical point of water (T_c = 373.946°C, P_c = 22.046 MPa) the fluid exists in the supercritical phase, which is distinct from the liquid and gas phases. The supercritical region is illustrated in the phase diagram below.

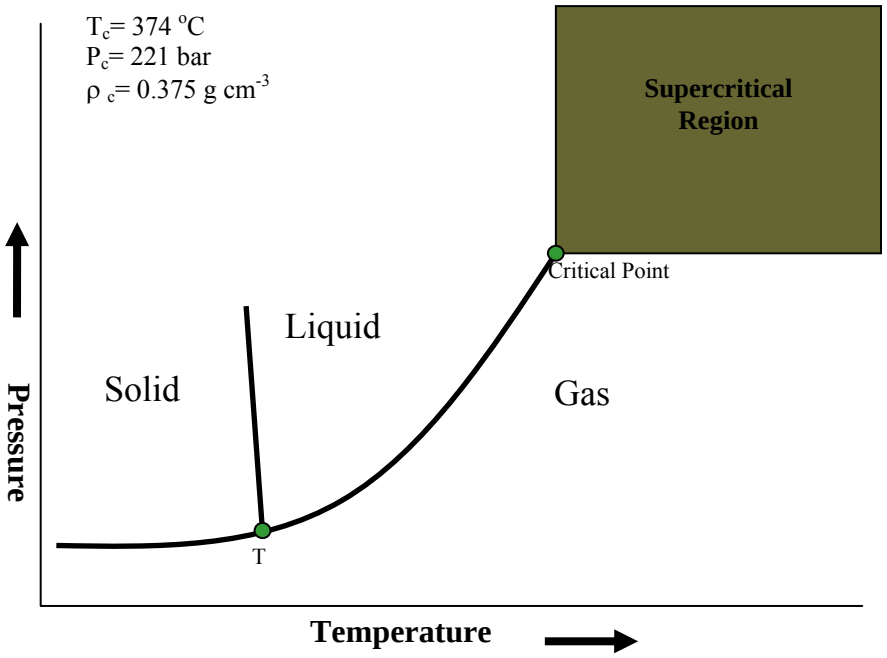

Figure. 1.1: Phase diagram for water

Above the critical point, the dielectric constant of water drops sharply from about 80 under ambient conditions to around 10, allowing it to behave like a nonpolar solvent.[4] This is associated with a decreased degree of hydrogen bonding as temperature is raised. At the critical point the degree of hydrogen bonding in water is half of what it is under ambient conditions.[5] As the temperature of water increases from ambient to 200-300°C, its ion product K_w increases three orders of magnitude[6], allowing it to participate in acid and base catalyzed chemistry;[7, 8] however, beyond the critical point the ion product falls drastically, making it a nonionic solvent.[6] The transport properties of supercritical water have some gas-like characteristics as well as some liquid-like characteristics. The viscosity of supercritical water is an order of magnitude lower than that of liquid water, greatly enhancing mass transfer and diffusion controlled reactions. Thermal conductivity

of supercritical water is also high, allowing for excellent heat transfer.[9] Several physical properties of water are presented graphically in Fig. 1.2 at 24 MPa.[10]

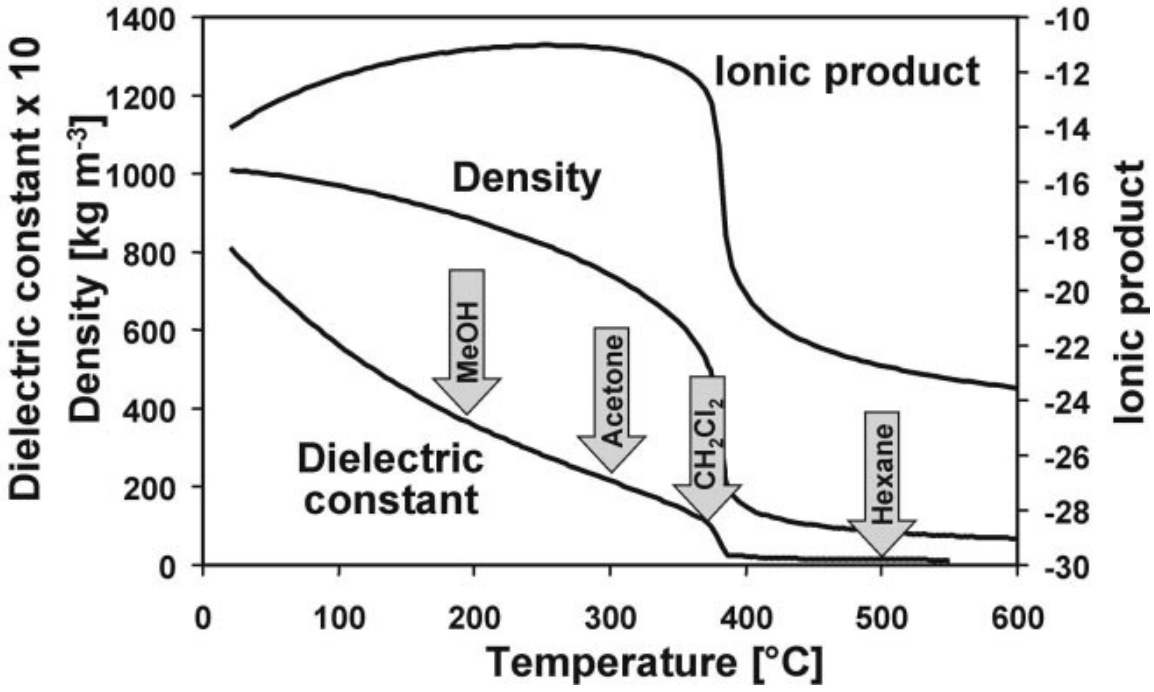

Figure 1.2: Physical properties of water at 24 MPa[10]

1.3 Hydrogen Production from Hydrocarbons

The processing of hydrocarbons, especially methane, is the most popular production strategy today in the industrial production of hydrogen. [11] Collectively called oxyforming, the three most prominent technologies in hydrocarbon reforming are steam reforming (SR), partial oxidation (POX), and autothermal reforming (ATR), each of which has advantages and disadvantages.[12] SR is most commonly used in hydrogen production as it gives the highest hydrogen yields and uses the lowest processing temperature. However, the process is highly endothermic and requires an external heat source, and also has the highest air emissions.[13] As its name implies, POX partially

oxidizes a portion of the feedstock to give a mixture of carbon monoxide and hydrogen, and can be performed without a catalyst. Accordingly the feedstock may not require desulfurization, but POX has several major disadvantages including low hydrogen yields, high operating temperatures, and the requirement of co-feeding oxygen. Partial oxidation performed with a catalyst is known as CPOX. ATR combines aspects of SR and POX, where a portion of the feed is combusted to provide heat necessary for endothermic steam reforming.[14] ATR operates at lower temperatures than POX and gives H_2/CO ratios good for Fischer-Tropsch synthesis, but has limited commercial experience and also requires co-feeding oxygen.[13]

Reactions pertinent to hydrocarbon reforming, water-gas shift, and oxidation may be summarized as follows for methane and with generalized hydrocarbon formulaes:[15-17]

Steam reforming

$$C_mH_n + mH_2O = mCO + (m+ \tfrac{1}{2}n)H_2 \quad \Delta H = \text{ endothermic, hydrocarbon dependent} \qquad (1.1)$$

$$CH_4 + H_2O = 3H_2 + CO \quad \Delta H = +205 \text{ kJ mol}^{-1} \qquad (1.2)$$

Partial oxidation

$$C_mH_n + \tfrac{1}{2}O_2 = mCO + \tfrac{1}{2}H_2 \quad \Delta H = \text{ exothermic, hydrocarbon dependent} \qquad (1.3)$$

$$CH_4 + \tfrac{1}{2}O_2 = CO + 2H_2 \quad \Delta H = -35.6 \text{ kJ mol}^{-1} \qquad (1.4)$$

Autothermal reforming

$$C_mH_n + \tfrac{1}{2}mH_2O + \tfrac{1}{4}mO_2 = mCO + (\tfrac{1}{2}m+ \tfrac{1}{2}n)H_2 \quad \Delta H = \text{thermoneutral} \qquad (1.5)$$

Water-gas shift

$$CO + H_2O = CO_2 + H_2 \quad \Delta H = - 41.1 \text{ kJ mol}^{-1} \qquad (1.6)$$

Dry reforming

$$CH_4 + CO_2 = 2CO + 2H_2 \quad \Delta H = +247.3 \text{ kJ mol}^{-1} \tag{1.7}$$

Coke formation

$$C_mH_n = xC + C_{m-x}H_{n-2x} + xH_2 \quad \Delta H = \text{hydrocarbon dependent} \tag{1.8}$$

$$2CO = C + CO_2 \quad \Delta H = +172.4 \text{ kJ mol}^{-1} \tag{1.9}$$

$$CO + H_2 = C + H_2O \quad \Delta H = -130 \text{ kJ mol}^{-1} \tag{1.10}$$

CO oxidation

$$CO + \tfrac{1}{2} O_2 = CO_2 \quad \Delta H = -283 \text{ kJ mol}^{-1} \tag{1.11}$$

H_2 oxidation

$$H_2 + \tfrac{1}{2}O_2 = H_2O \quad \Delta H = -242 \text{ kJ mol}^{-1} \tag{1.12}$$

A final version of methane reforming to be considered is the so-called dry reforming of methane, where methane is fed to the reactor with CO_2 instead of steam. Dry reforming uses two greenhouse gas feedstocks and can convert them to useful fuels, but is not well suited to hydrogen production as it is characterized by a low H_2:CO of 1:1.[17] Dry reforming methane has been studied the least out of all of the other schemes presented above.

Detailed kinetic and isotopic studies by Wei and Iglesia have shown that there is a common sequence of elementary steps in both the steam reforming and dry reforming of methane.[18] Their studies showed that in the absence of transport or thermodynamic artifacts that the only kinetically relevant step in methane reforming was activation of the C-H bond. Similar activation energies were reported for the CH_4/CO_2 and CH_4/H_2O systems, suggesting that the reactions are mechanistically equivalent.

1.4 Hydrogen Production from Biomass and Model Compounds

1.4.1 Aqueous Phase Reforming

Dumesic et al. have extensively studied the aqueous phase reforming of several oxygenated hydrocarbons including sorbitol, ethylene glycol, and glycerol in the production of hydrogen as well as alkanes.[19-21] In this work sufficient pressure is maintained to ensure a homogenous liquid phase at around 500K over supported metal catalysts. Their work with Pt/Al_2O_3 and Raney Ni/Sn catalysts highlights the importance of a catalyst active in C-C bond scission in hydrogen production, for a catalyst active in C-O cleavage leads to consumption of hydrogen through alkane production.

1.4.2 Gasification

An established process for conversion of coal or biomass to fuel gases is direct gasification. The combustion of biomass has served man as an energy source since time immemorial, although gasification represents a more efficient utilization of this resource. Gasification of coal was practiced as early as the dawn of the 18^{th} century to provide gas to light streetlamps and later homes. Gasification involves the reaction at high temperatures (1200-1400 K), moderate pressures (5-10 bar), a source of carbon, associated or not with hydrogen, with a source of hydrogen, usually steam, and/or oxygen to yield a gas product that contains CO, H_2, CO_2, CH_4, and N_2 in various proportions, as well as tars.[15] Generally, it involves several reactions including cracking, partial oxidation, steam gasification, water gas shift, and methanation.

One novel modern coal gasification technology is the so-called hydrogen production by the integrated novel gasification (HyPr-RING) method.[22-24] This method

integrates hydrocarbon reactions, water-gas shift, and CO_2 absorption into one single reactor, where CO_2 is captured by the following reaction:

$$CaO + CO_2 \rightarrow CaCO_3 \quad (1.13)$$

$CaCO_3$ is calcined in a separate regenerator to give CaO and a stream of CO_2. Heteroatoms in the coal such as chlorine and sulfur are also captured by sorbents in the reactor, resulting in a clean fuel containing ~90% hydrogen and ~10% methane with a cold gas efficiency of 77%.

Gasification of biomass has been demonstrated on a medium to large scale in several varieties of fluidized beds.[25] Gasification performed at temperatures exceeding 1000°C gives mainly syngas, and below 1000°C yields more hydrocarbons.[26] The process may be air blown or oxygen blown. The additional costs associated providing and using pure oxygen are compensated by providing a better quality fuel.[25] Gasification requires energy intensive pretreatment of biomass including drying and particle size reduction.

1.4.3 Supercritical Water Gasification

Several of the disadvantages of gasification may be obviated if the gasification is performed in supercritical water. Reduced temperatures in the range of 400°-800°C may be employed, lowering energy requirements. It is possible to utilize high moisture content biomass without additional drying. The product gases are obtained at high pressure, and very little tar and char is formed.

Some of the earliest work done in supercritical water gasification was performed by Modell et al. His work in gasification used residence times of 30 minutes near the critical point of water to form methane or syngas from biomass or coal slurries.[27, 28]

The research group of Antal has published extensively on hydrogen production in supercritical water from several feedstocks. Xu et al. investigated the activity of coconut shell activated carbon to catalyze the gasification of a wide variety of compounds, including glucose, glycerol, bagasse, and phenols. They found that a wide range of activated carbons were able to catalyst the gasification of the compounds at 600°C, 34.5 MPa, and WHSV of 0.1 to 0.5 h^{-1}. They reported that the surface area available on the catalyst did not have a large effect, which is likely the reason they were able to maintain high catalyst activity in light of the catalyst itself being slowly gasified in supercritical water.[29, 30] Further investigation by Xu and Antal used 5% corn starch mixed with 11% sawdust or 2% sewage sludge in water to form a viscous paste which was fed in a continuous manner to be gasified over activated carbon. A hydrogen-rich gas with significant methane was produced with no tar formation, however the reactors were seen to plug after several hours, especially with the high ash content sewage sludge.[31] Later studies with potato wastes and corn starch showed similar behavior, with high hydrogen yields being favored at high reaction temperatures.[32] This work also recognized the catalytic properties of the Hastelloy reactor wall, which was corroded during the reaction and deemed inappropriate for gasification in supercritical water. In another work on the steam reforming of glucose in supercritical water,[33] Antal et al. compared catalytic effects of the reactor wall by using Hastelloy and Inconel alloys. Dilute 0.1 M glucose solutions were completely gasified at 600°C, 34.5 MPa, 30 s residence time, obtaining a hydrogen yield of ~75% of the theoretical maximum with the Inconel reactor. Carbon dioxide was the other major product gas, with small amounts of methane and CO as well. With increasing feed concentrations up to 0.8 M, the hydrogen yield steadily declined to less

than 10% of the theoretical maximum and the carbon balance decreased to 68%. The Hastelloy reactor initially gave low hydrogen yields (~30% of maximum) and large amounts of CO, however as the wall was corroded its catalytic activity increased to be similar to Inconel, with H_2 yields increasing while CO decreased. From this they concluded that Inconel was active in the water-gas shift, whereas fresh Hastelloy does not catalyze the water-gas shift until sufficiently corroded.

Gasification of cellulose[34] and lignin[35] in supercritical water in the presence of ZrO_2 and NaOH catalysts has been studied by Watanabe et al. Hydrogen yields were doubled in the presence of zirconia and quadrupled in the presence of 1M NaOH. The fresh zirconia catalyst was a mixture of tetragonal and monoclinic crystal systems which was transformed almost exclusively to the more stable monoclinic form after exposure to the high temperature/pressure hydrothermal environment.

Char formation during biomass gasification can be problematic as the reactive intermediates from lignin decomposition undergo cross-linking to reform high molecular weight products.[36] Osada et al. have investigated gasification of lignin and models of its hydrolysis product alkylphenol in supercritical water over several supported noble metal catalysts.[37-39] Pipe bomb-type reactors at 400°C, water densities ranging form 0.1-0.3 g cm^{-3}, and reaction times of 15 - 60 minutes revealed an activity series of Ru/ γ-Al_2O_3 > Ru/C, Rh/C > Pt/ γ-Al_2O_3 > Pd/C > Pd/γ-Al_2O_3. Higher water density was seen to promote the gasification, however the most active catalyst only gave a gas yield of 10-15% in 15 minutes at the temperatures studied.[37] Further investigations on gasification of actual lignin showed that Ru/TiO_2 had a higher activity than Ru/ γ-Al_2O_3 in lignin

gasification. Lignin decomposition was enhanced by higher water density (i.e. higher pressure).[38]

The stability of ruthenium catalysts on various supports was also investigated in a separate study.[39] Anatase-type TiO_2 was stable at 400°C, 35 MPa for 3h, and maintained its activity for multiple uses. This is interesting to compare with earlier results from Elliott et al. who found anatase unstable in subcritical water (350°C, 25 MPa), transforming to the rutile phase.[40] Recent results have shown that a sub-critical water treatment is effective in regenerating Ru/TiO_2 poisoned by sulfur.[41] Ru/C showed high activity which gradually decreased with continued use, owing to gasification of the support itself as well as possible blocking of pores due to coking. After the first use, the activity of the Ru/ γ-Al_2O_3 catalyst was greatly decreased owing to two phenomena. The support underwent a phase change to the alpha phase sintering and a decrease in surface area. During the phase change ruthenium metals were leached and detected in the aqueous phase.

Elliott et al. have published on a mobile unit to gasify wet biomass such as dairy waste and distiller's dried grains over a Ru/C catalyst in near-critical water (350°C, 20 MPa) to a gas consisting mostly of methane and carbon dioxide.[42] Their scheme used a CSTR as preheater which also liquified a slurry which was then fed to a fixed bed catalytic reactor. In scale-up, reactor plugging was a problem, as was catalyst deactivation from components of the biomass such as calcium, magnesium, phosphorous, and sulfur.

1.5 Water Electrolysis

The ability of electricity to decompose water into its hydrogen and oxygen gases has been known for over 200 years, and the first large-scale electrolysis unit capable of producing 10,000 m^3 h^{-1} of hydrogen went into operation in 1939.[43] This process can produce clean hydrogen without contaminants such as CO or H_2S, however water does not dissociate easily; the enthalpy of the reaction $H_2O \rightarrow ½O_2 + H_2$ is +285.6 kJ mol^{-1}. Alkaline water electrolysis is the most developed commercial technology, however proton exchange and solid oxide electrolysers are expected to have higher efficiencies in the future.[44] In the long term, electrolysers can be used in conjunction with renewable energy sources such as wind or solar power to store surplus energy and alleviate problems associated with the intermittent nature of power produced from these technologies.[44]

1.6 Other Relevant Previous SCW work

1.6.1 Supercritical Water Oxidation (SCWO)

The solubilities of organic compounds and oxygen in supercritical water enable a homogenous phase in which the complete oxidation of organic species to carbon dioxide can take place in short reaction times. This is known as supercritical water oxidation (SCWO) and is one of the most studied research fields dealing with supercritical water. [45] Oxygen can be supplied by thermal decomposition of hydrogen peroxide or by dissolving oxygen into SCW; however, the same results are achieved with both methods .[46]

Some of the first work in SCWO focusing on the disposal of hazardous organic waste streams was performed by Modell et al. in the early 1980s,[47, 48], and was

commercialized in 1994.[49] The destruction of hazardous wastes such as energetic compounds and chemical warfare agents like mustard gas and VX nerve gas was explored by US Department of Defense contractors General Atomics, who reported destruction of those compounds in excess of 99.9999%.

The kinetics of SCWO of phenol and substituted phenolic compounds as model industrial pollutants has been studied extensively by several groups. Destruction of phenol is first order in phenol and sensitive to oxygen concentration.[50-53] Reaction networks and rate laws have been proposed for substituted phenols. The reactivity series of substituted phenols was found to be *ortho* > *para* > *meta*, while substituted phenols were found to have greater reactivity than unsubstituted phenols, with methoxy substitutions having greater reactivity in SCW than methyl substitutions.[30] It has also been reported that chlorinated phenols are much less reactive than other phenolic compounds.[54]

The employment of a catalyst in SCWO is often desirable for the same reasons that it is desirable in other systems: to lower reaction temperatures and increase reaction rates, thus reducing energy requirements and reducing required reactor volumes, ultimately improving process economics. Limited work has been done in heterogeneous catalysis for SCWO via transition metal salts, alkali, or polyheteroacids. These offer only modest rate increases while requiring additional processing steps to recover the catalyst. Accordingly, heterogeneous catalysis is often sought in SCWO where a catalyst is required.[55]

A number of heterogeneous catalysts have been explored for SCWO of phenols and other hazardous organic compounds. Jin et al.[56] found that use of a V_2O_5 catalyst led

to the formation of large amounts of carbonaceous char in the destruction of 1,4-dichlorobenzene. Ding et al. reported no char in the destruction of phenol over V_2O_5 catalyst, and both V_2O_5 and MnO_2/CeO gave reduced incomplete oxidation byproducts compared with homogeneous oxidation. The MnO_2/CeO catalyst was the most stable, and interestingly showed less byproducts at higher feed concentrations.[57] Krajnc and Levec used a CuO/ZnO catalyst in the SCWO of phenol, 1-methyl-2 pyrrolidone, benzoic acid and several other compounds and also found reduced concentrations of byproducts increased reaction rates compared to the noncatalytic homogenous oxidation.[58]

Commercial MnO_2-CuO/Al_2O_3 VOC oxidation catalysts were used by Zhang and Savage[59] to completely oxidize phenol at 390°C and 1 s space time, while Armbruster et al.[60] showed that catalyst to be stable for 200 h in supercritical water. Later the components of the commercial catalyst were tested individually. The ability of MnO_2 to catalyze the decomposition of phenol was evaluate by Yu and Savage[61, 62] as well as by Oshima et al.[63] The results of these studies showed significant rate increases, and that the same reaction pathway for phenol oxidation over MnO_2 was the same as for homogeneous SCWO. The role of the catalyst was to hasten the rate of production of reactive intermediates, including undesired dimers. Yu and Savage also reported on SCWO of phenol over CuO/Al_2O_3.[62] This catalyst reduced selectivity to dimers while increasing the selectivity towards CO_2, however it was unstable, with Cu and Al showing up in the reactor effluent and the surface area decreasing from 200 to 10 $m^2\ g^{-1}$.

TiO_2 was able to suppress the formation of dimers in phenol SCWO and maintained its activity for 125 h, during which time it underwent a phase transformation from anatase to rutile.[62]

Activated carbon has been evaluated for use as catalyst in phenol decomposition with varying results in the literature. Xu et al. screened phenol as part of a suite of Department of Defense wastes while studying gasification of various compounds and reported 80% conversion of phenol with benzene as byproduct at 600°C, 34.5 MPa, and WHSV of 0.1 h^{-1}. The authors consider gasification of the catalyst itself, however they determined that the rate of gasification of the catalyst was quite small under the reaction conditions and was stable over 4h.[30] Matsumura et al. later published a study specifically focusing on SCWO of phenol at 400°C and 25 MPa. In this work the activated carbon catalyst achieved similar conversions but gave a variety of undesirable dimer products in low yield. In the oxidative environment, however, activated carbon was consumed entirely within three hours on stream.[64]

Elliott et al. have published extensively on chemical processing in the high pressure aqueous environment.[40, 42, 65-70] Their research has been focused in the subcritical region at temperatures of about 350°C and 20 MPa pressure, with residence times of roughly 1-2 hours. Early works screened a wide variety of catalytic materials and supports in the destruction of phenolic compounds. Ru, Rh, and Ni were identified as active catalytic metals and ZrO_2, α-Al_2O_3 were identified as stable supports in the hot compressed water environment. Transition aluminas were hydrolyzed to AlO(OH), while tableted TiO_2 lost its physical integrity.[40] Nickel was found to have less catalytic activity than ruthenium as well as having a higher propensity for sintering.[40, 67] A recent publication from Elliott et al. examines catalytic activity and stability of additional materials in hot compressed water.[70] Several metals were tested on titania supports, including iridium, silver, rhenium, tin, and lead. Of these, iridium demonstrated a carbon

gasification of 1% in a 2 h reaction period, while the others gasified less than 0.1%. Ruthenium supported on titania showed high activity, with 55-94% of carbon being gasified in a 2 h reaction period. The anatase form of titania was more active, but was seen to convert to the rutile form even under the relatively mild temperatures employed. Molybdenum sulfide catalysts were tested as a sulfur tolerant catalyst, but showed low activity, with several variants all having gasification efficiencies of less than 2%. Ni/ZrO_2 prepared by the proprietary rapid thermal decomposition of solutes (RTDS) method gasified less than 4% of carbon, owing to nickel metal domains that were too large. A commercial nickel steam reforming catalyst was modified by doping with ruthenium. This gave a small increase in gasification of carbon (88 to 90%), however the doping improved the longevity of the catalyst by stabilizing nickel crystallite size and preventing sintering.

1.6.2 Corrosivity in SCW Environment

The high critical pressure of water of 221 bar along with high temperatures used in SCWO or SCW gasification make for severe processing conditions and may require exotic materials to cope with the harsh conditions. Early corrosion testing by General Atomics in the SCWO process led to their recommending titanium or platinum as candidate reactor materials in the presence of halides.[71] Foy et al. also report on SCWO of chlorinated organic compounds and reported acceptably low corrosion of a Ti-lined reactor.[72] They also proposed other novel schemes for dealing with the corrosive environment. One scheme was to neutralize the acid with sodium bicarbonate and operate at 650 bar where NaCl would remain as a separate fluid phase and not deposit on

reactor walls. Yet another scheme was to employ a ceramic reactor encased in steel to provide structural integrity.

Corrosion of 316 stainless steel has been studied at 400 bar and temperature ranging from 250-420°C. No significant variation of corrosion was seen between degassed and oxygenated water, but corrosion rates increased 10x with the addition of a 3% H_2O_2 mixture. The increased corrosion rate was due to transformation of the protective chromium (III) oxide layer to soluble Cr (VI).[73]

High nickel content alloys are known for their strength at elevated temperatures, however they also catalyze reactions such as the water-gas shift.[74] The catalytic activity of the reactor wall is also affected by its oxidation state. Antal has found Hastelloy to be inactive in promoting the water-gas shift until it has been somewhat corroded while Inconel was active immediately.[33]

The behavior of Inconel 625 (62 wt% Ni, 22 wt% Cr, 9.0 wt% Mo, 3.5 wt% Fe) is similar in the presence of the strong acids HNO_3, HCl and H_2SO_4 at concentrations of 0.2 mol kg^{-1}.[75] At 24 MPa the protective chromium (III) oxide layer is stable below 270°C. Severe corrosion was observed between 270-380°C, however above 380°C a film of NiO forms a protective layer and the corrosion rate is greatly decreased, although the higher solubility of nickel nitrate leads to a corrosion rate 10x higher than seen in the presence of hydrochloric or sulfuric acids. The stability of a variety of alloys has been evaluated during SCWO of various chlorinated compounds, and Hastelloy G-30 and the alloy HR-160 were identified as having better corrosion resistance than several Inconel alloys.[76] In the presence of phosphoric acid, however, corrosive behavior of Inconel 625 is much different.[77] Below 400°C a metal phosphate film protects the reactor. Above 400°C acid

concentrations of less than 0.1 mol kg^{-1} caused no corrosion, but concentrations greater than that resulted in severe corrosion. The stability of a variety of alloys has been evaluated during SCWO of various chlorinated compounds, and Hastelloy G-30 and the alloy HR-160 were identified as having better corrosion resistance than several Inconel alloys.[76]

More relevant to this research is corrosive behavior in a reducing supercritical water environment, where the protective oxide film may behave differently. Fujisawa et al. have investigated the corrosion behavior of 316 stainless steel and several Ni-base alloys in supercritical water at 25 MPa, 350-450°C, and H_2 partial pressures up to 6.5 MPa.[78, 79] 316SS corroded faster than any of the Ni-based alloys under all conditions, and corrosion rate increased with increasing hydrogen pressure. Alloys C-276 (59% Ni, 16% Cr, 16% Mo) and MAT21 (60% Ni, 19% Cr, 19% Mo) showed the best corrosion resistance in the reducing environment due to the high Mo content, which is thought to act as a stabilizer to the protective chromium oxide film. In a reducing supercritical water environment containing 0.01 M NaOH, corrosion rates of 316SS were again higher than Ni-based alloys. Ni-based alloys containing both Cr and Mo had better corrosion resistance than binary Ni-Cr alloys, and increasing Cr content reduced the susceptibility of stress cracking.

1.7 References

1. http://www.eia.doe.gov/fuelrenewable.html EIA Renewable & Alternative Fuel Data, Reports, Analysis, Surveys. (July 15, 2009),

2. *Hydrogen Fuel Cell Engines and Related Technologies*. College of the Desert: Palm Desert, CA, 2001.

3. Fundamentals and Use of Hydrogen as a Fuel. In *Kirk-Othmer Encyclopedia of Chemical Technology*, 3rd ed.; Wiley: New York, 1992; Vol. 4, p 631.

4. Fernandez, D. P. G., A. R. H.; Lemmon, E. W.; Sengers, J. M. H. Levelt; Williams, R. C., A formulation for the static permittivity of water and steam at temperatures from 238 K to 873 K at pressures up to 1200 MPa, including derivatives and Debye-Hueckel coefficients. *Journal of Physical and Chemical Reference Data* **1997,** 26, 1125-1166.

5. Gorbaty, Y. E. G., R.B., The Structural Features of Liquid and Supercritical Water. *Industrial and Engineering Chemistry Research* **1998,** 37, 3026-3035.

6. Bandura, A. V. L., S.N., The Ionization Constant of Water over Wide Ranges of Temperature and Density. *Journal of Physical and Chemical Reference Data* **2006,** 35, 15-30.

7. Watanabe, M. O., Mitsumasa; Inomata, Hiroshi; Arai, Kunio; Kruse, Andrea, Acidity and basicity of metal oxide catalysts for formaldehyde reaction in supercritical water at 673 K. *Applied Catalysis A: General* **2003,** 245, 333-341.

8. Ikushima, Y. H., Kiyotaka; Sato, Osamu; Yokoyama, Toshirou; Arai, Masahiko, Acceleration of Synthetic Organic Reactions Using Supercritical Water: Noncatalytic Beckmann and Pinacol Rearrangements. *Journal of the American Chemical Society* **2000,** 122, 1908-1918.

9. Weingartner, H. F., E.U., Supercritical Water as a Solvent. *Angewandte Chemie International Edition* **2005,** 44, 2672-2692.

10. Kritzer, P. D., E., An assessment of supercritical water oxidation (SCWO) Existing problems, possible solutions and new reactor concepts. *Chemical Engineering Journal* **2001,** 83, 207-214.

11. Holladay, J. D. J., J.; King, D.L.; Wang, Y., An Overview of hydrogen production technologies. *Catalysis Today* **2009,** 139, 244-260.

12. York, A. P. E., Xiao, T.C.; Green, M.L.H.; Claridge, J.B., Methand Oxyforming for Synthesis Gas Production. *Catalysis Reviews* **2007,** 49, 511-560.

13. Wilhelm, J. D. S., D.R.; Karp, A.D.; Dickenson, R.L., Syngas production for gas-to-liquids application: technologies, issues and outlook. *Fuel Processing Technology* **2001,** 71, 139-148.

14. Flytzani-Stephanopoulos, M. V., G.E., Autothermal reforming of aliphatic and aromatic hydrocarbon liquids. *International Journal of Hydrogen Energy* **1983,** 8, (7), 539-548.

15. Navarro, R. M. P., M.A.; Fierro, J.L.G., Hydrogen Production Reactions from Carbon Feedstocks: Fossil Fuels and Biomass. *Chemical Reviews* **2007,** 107, 3952-3991.

16. Wender, I., Reactions of Synthesis Gas. *Fuel Processing Technology* **1996,** 48, 189-297.

17. Verykios, X. E., Catalytic dry reforming of natural gas for the production of chemicals and hydrogen. *International Journal of Hydrogen Energy* **2003,** 28, 1045-1063.

18. Wei, J. I., E., Reaction Pathways and Site Requirements for the Activation and Chemical Conversion of

Methane on Ru-Based Catalysts. *J. Phys. Chem. B* **2004,** 108, 7253-7262.

19. Cortright, R. D. D., J.A. Low-temperature hydrogen production from oxygenated hydrocarbons 6,964,758, 2005.

20. Huber, G. W. D., J.A., An overview of aqueous-phase catalytic processes for production of hydrogen and alkanes in a biorefinery. *Catalysis Today* **2006,** 111, 119-132.

21. Shabaker, J. W. D., J.A., Kinetics of Aqueous-Phase Reforming of oxygenated Hydrocarbons: Pt/Al2O3 and Sn-Modified Ni Catalysts. *Industrial and Engineering Chemistry Research* **2004,** 43, 3105-3112.

22. Lin, S.-Y. S., Yoshizo; Hatano, Hiroyuki; Harada, Michaiki, Hydrogen Production from Hydrocarbon by Integration of Water-Carbon Reaction and Carbon Dioxide Removal (HyPr-RING Method). *Energy and Fuels* **2001,** 15, 339-343.

23. Lin, S.-Y. S., Yoshizo; Hatano, Hiroyuki; Harada, Michiaki, Developing an innovative method, HyPr-RING, to produce hydrogen from hydrocarbons. *Energy Conversion and Management* **2002,** 43, 1283-1290.

24. Lin, S.-Y. H., Michiaki; Suzuki, Yoshizo; Harada, Michaiki; Hatano, Hiroyuki, Process analysis for hydrogen production by reaction integrated novel gasification (HyPr-RING). *Energy Conversion and Management* **2005,** 46, 869-880.

25. Bridgwater, A. V., Renewable fuels and chemicals by thermal processing of biomass. *Chemical Engineering Journal* **2003,** 91, 87-201.

26. Klass, D. L., *Biomass for Renewable Energy; Fuels and Chemicals*. Academic Press: San Diego, CA, 1998.

27. Modell, M. *Reforming of glucose and wood at the critical conditions of water*; Massachussetts Institute of Technology: Cambridge, MA, 1977; p 7.

28. Modell, M. R., R.C.; Amin, S.I. Gasification Process. 4,113,446, 1978.

29. Matsumura, Y. X., X.; Antal Jr., M.J., Gasification characteristics of an activated carbon in supercritical water. *Carbon* **1997,** 35, 819-824.

30. Xu, X. M., Y.; Stengerg, J.; Antal Jr., M.J., Carbon-Catalyzed Gasification of Organic Feedstocks in Supercritical Water. *Industrial and Engineering Chemistry Research* **1996,** 35, 2522-2530.

31. Xu, X. A. J., M.J., Gasification of Sewage Sludge and Other Biomass for Hydrogen Production in Supercritical Water. *Environmental Progress* **1998,** 17, 215-220.

32. Antal Jr., M. J. A., S.G.; Schulman, D.; Xu, X.; Divilio, R.J., Biomass Gasification in Supercritical Water. *Industrial and Engineering Chemistry Research* **2000,** 39, 4040-4053.

33. Yu, D. A., M.; Antal Jr., M.J., Hydrogen Production by Steam Reforming Glucose in Supercritical Water. *Energy and Fuels* **1993,** 7, 574-577.

34. Watanabe, M. I., H.; Arai, K., Catalytic hydrogen generation from biomass (glucose and cellulose) with ZrO2 in supercritical water. *Biomass and Bioenergy* **2002,** 22, 405-410.

35. Watanabe, M. I., H.; Osada, M.; Sato, T.; Adschiri, T.; Arai, K., Catalytic effects of NaOH and ZrO2 for partial oxidative gasification of n-hexadecane and lignin in supercritical water. *Fuel* **2003,** 82, 545-552.

36. Saisu, M. S., T.; Watanabe, M.; Adschiri, T, Arai, K., Conversion of Lignin with Supercritical Water-Phenol Mixtures. *Energy and Fuels* **2003,** 17, 922-928.

37. Sato, T. O., M.; Watanabe, M.; Shirai, M.; Arai, K., Gasification of Alkylphenols with Supported Noble Metal Catalysts in Supercritical Water. *Industrial and Engineering Chemistry Research* **2003,** 42, 4277-4282.

38. Osada, M. S., O.; Watanabe, M.; Arai, K.; Shirai, M., Water Density Effect on Lignin Gasification over Supported Noble Metal Catalysts in Supercritical Water. *Energy and Fuels* **2006,** 20, 930-953.

39. Osada, M. S., O.; Arai, K.; Shirai, M., Stability of Supported Ruthenium Catalysts for Lignin Gasification in Supercritical Water. *Energy and Fuels* **2006,** 20, 2337-2343.

40. Elliott, D. C. S. J., L.J.; Baker, E.G., Chemical Processing in High-pressure Aqueous Environments. 2. Development of Catalysts for Gasification. *Industrial and Engineering Chemistry Research* **1993,** 32, 1542-1548.

41. Osada, M. Y., A.; Hiyoshi, N.; Sato, O.; Shirai, M., Regeneration of catalyst poisoned by sulfur in subcritical water. *Baiomasu Kagaku Kaigi Happyo Ronbunshu* **2009,** 4, 124-125.

42. Elliott, D. C. N., G.G.; Hart, T.R.; Butner, R.S.; Zacher, A.H.; Englehard, M.H.; Young, J.S.; McCready, D.E., Chemical Processing in High-Pressure Aqueous Environments. 7. Process Development for Catalytic Gasification of Wet Biomass Feedstocks. *Industrial and Engineering Chemistry Research* **2004,** 43, 1999-2004.

43. Kreuter, W. H., H., Electrolysis: the important energy transformer in a world of sustainable energy. *International Journal of Hydrogen Energy* **1998,** 23, 661-666.

44. Mueller-Langer, F. T., E.; Kaltschmitt, M.; Peteves, S., Techno-economic assessment of hydrogen production processes for the hydrogen economy for the short and medium term *International Journal of Hydrogen Energy* **2007,** 32, 3797-3810.

45. Savage, P. E., Organic Chemical Reactions in Supercritical Water. *Chemical Reviews* **1999,** 99, 603-622.

46. Phenix, B. D. D., Joanna L.; Tester, Jefferson W.; Howard, Jack B.; Smith, Kenneth A., The Effects of Mixing and Oxidant Choice on Laboratory-Scale Measurements of Supercritical Water Oxidation Kinetics. *Industrial and Engineering Chemistry Research* **2002,** 41, 624-631.

47. Modell, M. Processing methods for the oxidation of organics in supercritical water 4,338,199, 1982.

48. Thomason, T. B. M., M., Supercritical water destruction of aqueous wastes. *Hazardous Waste* **1984,** 1, 453-467.

49. McBrayer, R. In *Design and Operation of the First Commercial Supercritical Water Oxidation Facility*, First International Workshop on Supercritical Water Oxidation, Jacksonville, FL, 1995; Mohiuddin, J., Ed. Jacksonville, FL, 1995.

50. Gopalan, S. S., P.E., A reaction network model for phenol oxidation in supercritical water. *AIChE Journal* **1995,** 41, 1864-1873.

51. Krajnc, M. L., J., On the kinetics of phenol oxidation in supercritical water. *AIChE Journal* **1996,** 42, 1977-1984.

52. Koo, M. L., W.K.; Lee, C.H., New reactor system for supercritical water oxidation and its application on phenol destruction. *Chemical Engineering Science* **1997,** 52, 1201-1214.

53. Oshima, Y. H., K.; Toda, M.; Chommanad, T.; Koda, S., Phenol oxidation kinetics in supercritical water. *Journal of Supercritical Fluids* **1998,** 13, 241-246.

54. Lin, K. S. W., H.P.; Li, M.C., Oxidation of 2,4-dichlorophenol in supercritical water. *Chemosphere* **1998,** 36, 2075-2083.

55. Savage, P. E. D., J.B.; Yu, J., Recent advances in catalytic oxidation in supercritical water. *Combustion Science and Technology* **2006,** 178, 443-465.

56. Jin, L. S., Y.T.; Martin, A, The effect of supercritical water on the catalytic oxidation of 1,4-dichlorobenzene. *Journal of Supercritical Fluids* **1990,** 3, 233-239.

57. Ding, Z.-Y. A., Sudhir N. V. K.; Abraham, Martin A, Catalytic Supercritical Water Oxidation: Phenol Conversion and Product Selectivity. *Environmental Science and Technology* **1995,** 29, 2748-2753.

58. Krajnc, M. L., J., Catalytic oxidation of toxic organics in supercritical water. *Applied Catalysis B: Environmental* **1994,** 3, L101-L107.

59. Zhang, X. S., P.E., Fast catalytic oxidation of phenol in supercritical water. *Catalysis Today* **1998,** 40, 333-342.

60. Armbruster, U. M., A.; Krepel, A., Hydrolysis and oxidative decomposition of ethyl acetate in sub- and super-critical water. *Applied Catalysis B: Environmental* **2001,** 31, 263-273.

61. Yu, J. a. S., P.E., Catalytic oxidation of phenol over MnO2 in supercritical water. *Industrial and Engineering Chemistry Research* **1999,** 38, 3793-3801.

62. Yu, J. a. S., P.E., Catalyst activity, stability, and transformations during oxidation in supercritical water. *Applied Catalysis B: Environmental* **2001,** 31, 123-132.

63. Oshima, Y. T., K.; Koda, S., Kinetics of the catalytic oxidation of phenol over manganese oxide in supercritical water. *Industrial and Engineering Chemistry Research* **1999,** 38, 4183-4188.

64. Matsumura, Y. U., T.; Yamamoto, K.; Nunoura, T., Carbon catalyzed supercritical water oxidation of phenol. *Journal of Supercritical Fluids* **2002,** 22, 149-156.

65. Sealock, J. L. E., D.C.; Baker, E.G.; Butner, R.S., Chemical Processing in High-pressure Aqueous Environments. 1. Historical Perspective and Continuing Developments. *Industrial and Engineering Chemistry Research* **1993,** 32, 1535-1541.

66. Elliott, D. C. S. J., L.J.; Baker, E.G., Chemical Processing in High-pressure Aqueous Environments. 3. Batch Reactor Process Development Experiments for Organics Destruction. *Industrial and Engineering Chemistry Research* **1994,** 33, 558-565.

67. Elliott, D. C. P., M.R.; Sealock Jr., L.J.; Baker, E.G., Chemical Processing in High-pressure Aqueous Environments. 4. Continuous-Flow Reactor Process Development Experiments for Organics Destruction. *Industrial and Engineering Chemistry Research* **1994,** 33, 566-574.

68. Sealock, J. L. E., D.C.; Baker, E.G.; Fassbender, A.G.; Silva, L.J., Chemical Processing in High-Pressure Aqueous Environments. 5. New Processing Concepts. *Industrial and Engineering Chemistry Research* **1996,** 35, 4111-4118.

69. Elliott, D. C. N., G.G.; Phelps, M.R.; Hart, T.R.; Zacher, A.H.; Silva, L.J., Chemical Processing in High-Pressure Aqueous Environments. 6. Demonstration of Catalytic Gasification for Chemical Manufacturing Wastewater Cleanup in Industrial Plants. *Industrial and Engineering Chemistry Research* **1999,** 38, 879-883.

70. Elliott, D. C. H., T.R.; Neuenschwander, G.G., Chemical Processing in High-Pressure Aqueous Environments. 8. Improved Catalysts for Hydrothermal Gasification. *Industrial and Engineering Chemistry Research* **2006,** 45, 3776-3781.

71. Downey, K. W. S., R.H.; Hazlebeck D.A.; Roberts, A.J., Corrosion and chemical agent destruction. Research on supercritical water oxidation of hazardous military wastes. In *ACS Symposium Series 608 - Innovations in Supercritical Fluids*, Hutchenson, K. W. F., N.R., Ed. American Chemical Society: Washington, D.C., 1995; pp 313-326.

72. Foy, B. R. W., Kurt; Sedillo, Michael A.; Buelow, Steven J., Hydrothermal Processing of Chlorinated Hydrocarbons in a Titanium Reactor. *Environmental Science and Technology* **1996,** 30, 2790-2799.

73. Hayward, T. M. S., T.M.; Makhija, R.C., Stainless steel flow reactor for supercritical water oxidation: corrosion tests. *Journal of Supercritical Fluids* **2003,** 27, 275-281.

74. Bustamante, F. E., R. M.; Killmeyer, R. P.; Howard, B. H.; Rothenberger, K. S.; Cugini, A. V.; Morreale, B. D.; Ciocco, M. V., Uncatalyzed and wall-catalyzed forward water-gas shift reaction kinetics. *AIChE Journal* **2005,** 51, 1440-1454.

75. Kritzer, P. B., N.; Dinjus, E., The corrosion of nickel±base alloy 625 in sub- and supercritical aqueous solutions of HNO3 in the presence of oxygen. *Journal of Materials Science Letters* **1999,** 18, 771-773.

76. Mitton, D. B. Y., J.-H.; Cline, J.A.; Kim, H.-S.; Eliaz, N. Latanision, R.M., Corrosion Behavior of Nickel-Based Alloys in Supercritical Water Oxidation Systems. *Industrial and Engineering Chemistry Research* **2000,** 39, 4689-4696.

77. Kritzer, P. B., N.; Dinjus, E., The corrosion of alloy 625 (NiCr22Mo9Nb; 2.4856) in high-temperature, high-pressure aqueous solutions of phosphoric acid and oxygen. Corrosion at sub- and supercritical temperatures. *Materials and Corrosion* **1998,** 49, 831-839.

78. Fujisawa, R. S., M.; Kurata, Y.; Watanabe, Y., Corrosion behaviour of nickel base alloys and 316 stainless steel in supercritical water under alkaline conditions. *Corrosion Engineering, Science, and Technology* **2005,** 40, 244-248.

79. Fujisawa, R. N., K.; Nishida, T.; Sakaihara, M.; Kurata, Y.; Watanabe, Y., Corrosion Behavior of Nickel-Based Alloys and Type 316 Stainless Steel in Slightly Oxidizing or Reducing Supercritical Water. *Corrosion* **2006,** 62, 270-274.

2. Hydrogen Production from Glucose using Ru/Al_2O_3 Catalyst in Supercritical Water

2.1 Abstract

Glucose, as a model biomass compound, was catalytically reformed in supercritical water to produce hydrogen. The reforming experiments were conducted in a continuous tubular reactor with and without Ru/Al_2O_3 catalyst, and with short residence time. The addition of catalyst significantly enhanced the overall conversion and hydrogen yield, and reduced methane formation. The gaseous products contained mainly hydrogen, carbon dioxide, methane and a small amount of carbon monoxide. The effects of experimental conditions such as temperature, reaction time and weight percent of glucose in the feed water on formation of hydrogen product were investigated. Experimental hydrogen yield as high as 12 mol H_2/ mole of glucose were obtained, which is the stoichiometric limit. The gas yield was sensitive to temperature, residence time and feed concentration. High yield of H_2 with low CO and CH_4 yields were obtained at high reaction temperature and low glucose concentrations. Tar formation was observed at high glucose concentrations (> 5 wt. %). The catalytic conversion of glucose with ruthenium catalyst in supercritical water is an effective method for the hydrogen production directly at a high pressure, which can be extended to other biomass materials. The reaction mechanism for catalytic reforming in supercritical water is also discussed.

2.2 Introduction

Due to the environmental impacts of the fossil fuel, hydrogen is now considered as an excellent replacement. Hydrogen produced from biomass has no net carbon dioxide

impact on the environment. Thermochemical gasification of biomass has been identified as a possible way to produce renewable hydrogen. Several researchers have investigated hydrogen production from methanol, ethanol and biomass materials in subcritical and supercritical water.[1-8] Compared to other biomass thermochemical reforming processes, supercritical water reforming has a high efficiency and operates at a lower temperature. Supercritical water (SCW) possesses properties very different from that of liquid water at ambient conditions. The dielectric constant of SCW is much less than that of ambient water and hydrogen bonding is much weaker. Therefore SCW behaves like an organic solvent and is completely miscible with organic materials. Thus with SCW it is possible to conduct reactions with organic compounds in a single fluid phase which would otherwise occur in a multiphase system under conventional conditions.[1, 5, 8-10] Heterogeneous reactions can also be performed in supercritical fluids. The high diffusivity in SCW can significantly enhance mass transfer. SCW can reduce coke formation on the catalyst as it is a good solvent for the intermediate coke precursors. Hence, gasification of biomass in SCW has many advantages including high gasification efficiency and a high yield of hydrogen. In addition, the product hydrogen is obtained directly at a high pressure, hence further compression is not needed. Several attempts have been made in recent years for the gasification of biomass model compounds and biomass in supercritical water.[8-15] Cellulose, glucose, and phenolic compounds (e.g., phenol, guaiacol) can be gasified in subcritical and SCW in the presence of a metal catalyst (platinum, nickel, etc.) or an alkali catalyst.[16-26] Cortright et al.[16] conducted glucose gasification at 265 °C and 56 bar in water, using a platinum catalyst, and obtained high yields of CO_2 and H_2. Minowa et al.[18] investigated cellulose gasification in

near-critical water at 350 °C and 165 bar with a reduced nickel catalyst and reported that 70% of the carbon could be gasified.

One of the main problems encountered during the biomass gasification is reactor plugging. Yu et al.[12] reported that the gasification of biomass is effective only at low concentrations of biomass, as at high concentrations, polymerization of the decomposition products occurs. Kruse et al.[7,9,10] observed that the hydrogen yield can be significantly increased by adding 5 wt% KOH in SCW. Watanabe et al.[13,14] observed a two fold increase in the gasification efficiency of glucose and cellulose in a batch reactor by adding zirconia catalyst. Similarly Nickel based catalysts have also been tested. Elliott et al.[21] conducted a gasification of *p*-cresol in water at 350°C and 200 bar using various types of base and noble catalysts and reported that nickel and ruthenium were active for the reaction.

Again using a batch reactor, Osada et al.[22] reported formation of a high amount of methane in the presence of ruthenium catalyst during the gasification of cellulose and lignin in SCW. In a recent study, Lu et al.[23] studied the gasification of cellulose in the presence of metal catalyst including CeO_2, Pd/C and Ru/C in a batch reactor, and observed that the maximum hydrogen yield was obtained with Ru/C catalyst.

Most of the above studies were done in batch mode, in which the biomass/water/catalyst is loaded in a small steel tube reactor and then sealed and placed in an oven. After the reaction, the mixture is quenched and analysed. Typical reaction time varied from minutes to hours. In our recent work on methanol reforming, it was observed that high reaction time leads to the secondary reaction of methane formation.[1] To limit the methane formation reaction time needs to be limited to the order of seconds.

This work examines the reforming of glucose in SCW in a continuous reactor with a short reaction time (of the order of seconds). Ru/Al_2O_3 is selected as a catalyst. The effect of reaction time, temperature and feed concentrations is studied.

2.3 Experimental Section

2.3.1 Materials. All the chemicals used were of high purity (99.9%) and of analytical grade. Glucose and catalyst (5 wt.% Ru/amorphous Al_2O_3) were procured from Aldrich and used without any further treatment. The surface area and pore volume of the catalyst is 100 m^2/g and 0.30 cm^3/g, respectively. Distilled and deionized water was used.

2.3.2 Apparatus. The reforming of glucose was carried out in a tubular reactor (0.5 m long, 0.250" OD and 0.12" ID) made of Inconel 600 (Microgroup) having a composition of 73% Ni, 18% Cr, 9% Fe. Initially a few experiments were also carried out in empty bed reactor to study the effect of reactor wall. For the catalytic experiments, a known mass of the catalyst (2.0 g) was carefully poured into the tube reactor with gently tapping on the outside of the reactor wall to ensure no large voids in the bed. The catalyst was retained in the reactor by placing stainless steel frits with a pore diameter of 0.5 μm (Valco) at either end. The same charge of catalyst was used for all of the experiments. Glucose feed stock was prepared by dissolving a known mass of glucose in water and from the feed tank it was pumped to the reactor using an HPLC pump (Waters 590). The schematic diagram of the experimental set up is shown in Figure 2.1. The reactor and preheater assembly were placed inside a tubular furnace equipped with a temperature controller (Thermolyne 21100). The reactor temperature at the exit of the furnace was monitored using a type-K thermocouple. The ends of the tube furnace were covered properly to avoid heat loss and achieve a uniform temperature. The gaseous products

exiting the reactor were cooled using a water-cooled double pipe heat exchanger made of SS 316 tubing. The reactor pressure was constantly monitored by a pressure gauge. The pressure of the stream was reduced to ambient by means of a back pressure regulator (Straval BP00201T-SS). The gas-liquid mixture was separated in a glass phase-separator having gas tight valves to prevent the escape of gases. The gas flow rate was measured using a gas flow meter (Omega FMA-1600). A six-port injection valve (Valco) having a 100 μL sample loop was used for the online sample injection. The product gas composition was measured using a gas chromatograph (SRI 8610C) equipped with a TCD and 60-80 mesh Carboxen-1000 carbon molecular sieve column (Supelco) having dimensions of 15' x 1/8". Nitrogen was used as the carrier gas. The gas chromatograph was calibrated using a standard gas mixture of known composition. The liquid product coming out of the phase separator was collected at regular time intervals. The total organic carbon (TOC) content of the liquid was analyzed using a TOC analyzer (Shimadzu TOC-V_{CSN}). The flow meter (FMA-1600) was used in the H_2 mode and it generated 30 readings of the volumetric flow rate per second based the built-in properties of pure H_2. These instantaneous volumetric flow rates were acquired on computer via a RS-232 port and corrected for pressure and temperature. The average volumetric flow rate was found out by totalizing the flow for a period of 15 minutes. This average gas flow rate which corresponds to pure H_2 was corrected to the actual gas coming out of the phase separator by estimating the viscosity of the gas mixture by Wilke's semi-empirical formula[24] using the gas composition obtained from the GC analysis. This flow measurement method was checked and confirmed for accuracy by flowing the calibration gas consisting of H_2, CO, CH_4 and CO_2 of known composition at several flow rates and

measuring the actual flow by a soap-bubble flow meter. All the experiments were carried out under isothermal conditions.

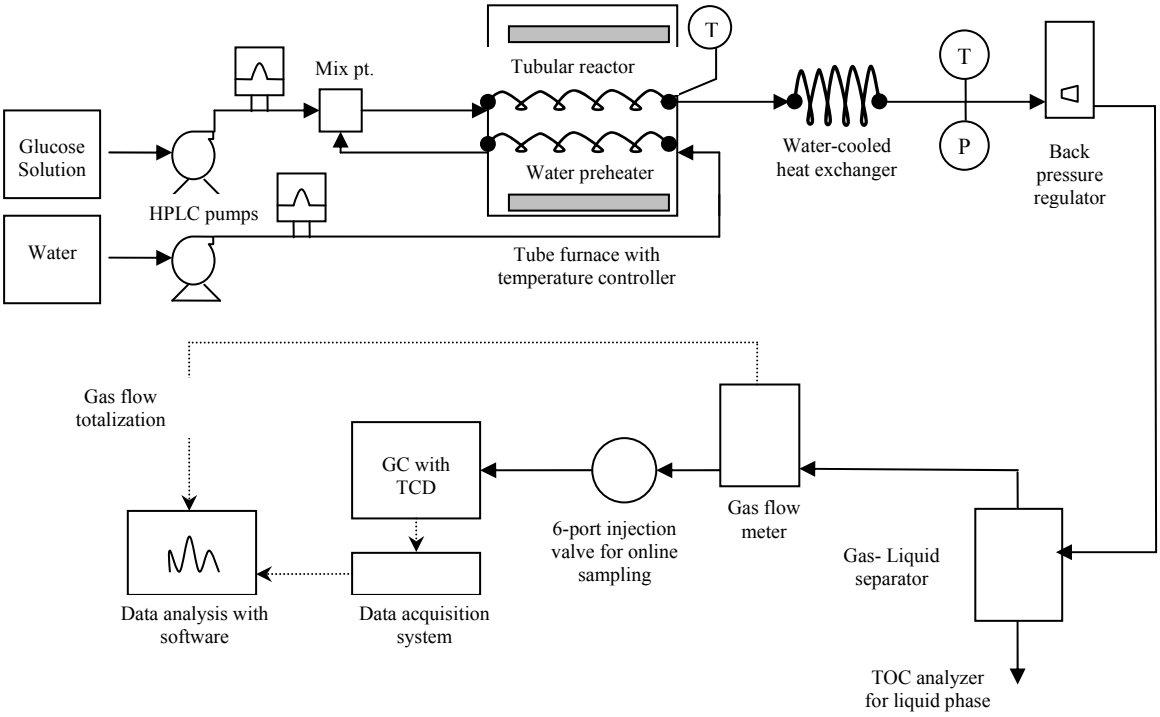

Figure 2.1: Schematic diagram of the experimental apparatus

2.3.3 Experimental Procedure. First, distilled water was pumped through the system and pressurized to the desired pressure by adjusting the backpressure regulator. After achieving a steady pressure, the tube furnace was switched on to heat the reactor. After a steady exit temperature was achieved, glucose solution was introduced into the reactor. The steady state condition was marked by a constant temperature at the exit of the reactor. The gas analysis was done at least three times to get a constant gas composition. The gas flow was totalized for a period of 15 min, and the average gas flow rate was

calculated using the method discussed before. After completion of each experiment, the feed was switched back to distilled water to flush the reactor.

All the experiments were conducted at a pressure of 241 bar (3540 psi) and at temperatures ranging from 700-800°C. Experiments were also carried out in empty bed reactor with glucose feed stock in supercritical water to study the influence of reactor wall. The effect of glucose feed concentration was studied by feeding glucose having a concentration ranging between 1.0 to 5.0 wt% calculated at the entrance of the reactor. The residence time in the catalyst bed was kept between 1 to 6 seconds.

The molar flow rates of the product gases were calculated based on the volumetric gas flow rate and dry gas composition obtained from the GC. The carbon content of the liquid stream was calculated knowing the TOC value of the liquid. All the measurements were made in triplicate. The accuracy of the run was checked by calculating the overall carbon balance for the system. The error in the overall carbon balance was found to be less than 10%. Scattering in the data of the totalized gas flow rate measured by the flow meter was less than 1%. The error in the dry gas composition obtained by the GC analysis was typically less than 2%. The overall error in the calculation of the gas yields due to the errors introduced by the individual analysis techniques and experimental error was found to be less than 5%.

2.4 Results and Discussion

2.4.1 Effect of Ru/Al_2O_3 Catalyst. To study the effect of catalyst on hydrogen yield for reforming of glucose in supercritical water, the catalytic experiments were compared to the empty reactor experiments (without catalyst) under identical conditions. The gas yield is defined as the moles of product gases divided by the moles of glucose fed to the

reactor. Typical product distributions are shown in Table 2.1 for catalytic and non catalytic experiments at 700°C with 1 wt.% glucose feed.

Table 2.1: Product Distribution during Thermal and Catalytic Reforming of Glucose in Supercritical Water (T: 700°C, P: 241 bar, 1.0 wt% glucose)

	Typical product composition (mol%)				
	H_2	CO	CH_4	CO_2	H_2 Yield
Empty bed	54.0%	1.7%	10.2%	34.1%	6.8
Catalyst (Ru/Al_2O_3)	68.9%	0.1%	1.3%	29.8%	~12

The hydrogen yield increased from 7 to 12 (moles of hydrogen formed /moles of glucose fed) upon adding the catalyst. There was also a significant reduction in carbon monoxide and methane yields in the presence of the catalyst. The main products of the reaction were hydrogen, methane, carbon dioxide and carbon monoxide. Small amounts of higher molecular weight carbon compounds such as phenols and aldehydes could be seen in the liquid product in a few experiments. Typical values of TOC in the liquid product were approximately 150 ppm. Although the detailed properties of the catalyst, such as catalyst life and strong metal- support interaction have not been reported for Ru/Al_2O_3 catalyst, the probable reason for higher gasification performance is that the intermediate agents formed during glucose decomposition, such as aldehydes and phenols, were gasified.

The gasification of hydrocarbons in supercritical water proceeds via several complex reactions such as pyrolysis, hydrolysis, steam reforming, water gas shift, and methanation. The product distribution mainly depends upon the relative extent of various

reactions. During thermal gasification (without catalyst) of glucose, the product gas contained approximately 54 mol% hydrogen along with 1.7% CO, 34.1 % CO_2 and 10.2 % methane. Due to the presence of catalyst the amount of hydrogen was significantly increased to the maximum theoretical value to approximately 69%. The yield of major products for thermal and catalytic gasification of glucose is given in Figures 2.2 and 2.3, respectively.

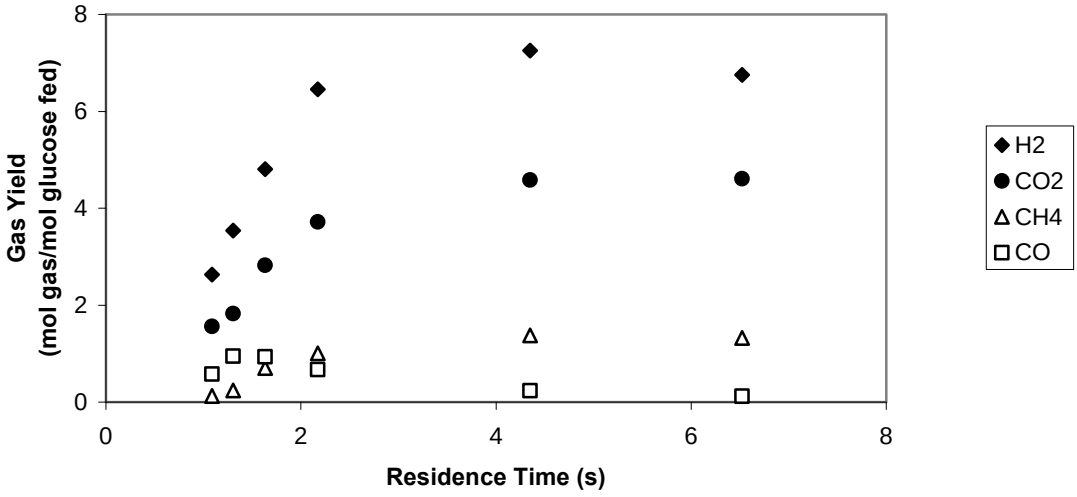

Figure 2.2: Effect of residence time on product gas yields during non-catalytic reforming of glucose (T: 700°C, P: 241 bar, glucose conc.: 1 wt.%)

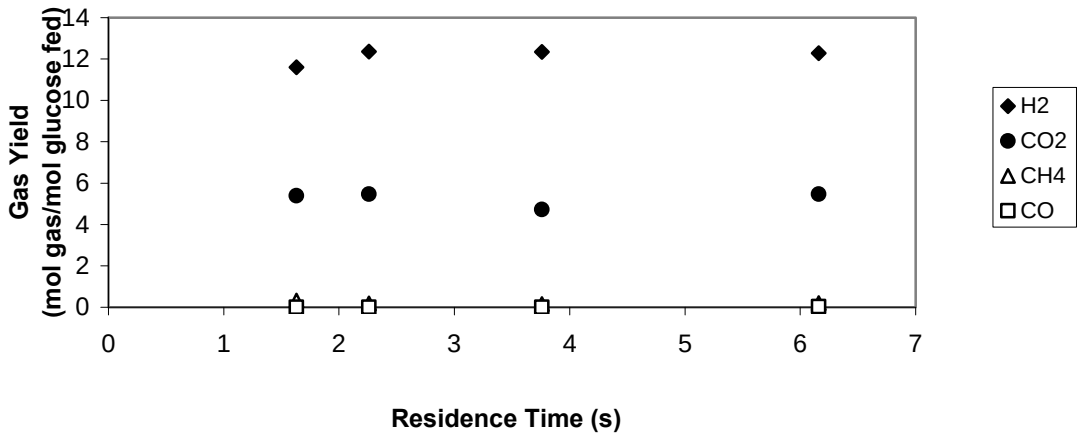

Figure 2.3: Effect of residence time on product gas yields: (T: 700°C, P: 241 bar, glucose conc.: 1 wt.%, 2.0 g Ru/Al_2O_3 catalyst)

In the catalytic experiments, there was only a negligible amount of CO in the product, and the methane concentration was also significantly reduced. Here glucose undergoes dehydrogenation on the metal surface to give adsorbed intermediates before the cleavage of C-C or C-O bonds. Subsequent cleavage of C-C bonds leads to formation of CO and H_2. CO reacts with water to form CO_2 and H_2 by the water gas shift reaction. Carbon monoxide was present only in trace amounts, probably because the Ru catalyst promotes the water gas shift reaction to form carbon dioxide and hydrogen from carbon monoxide and water. The shift reaction is initiated through interaction of CO with OH^-, which are formed by ionic dissociation of supercritical water on the metal surface, and forming the formate ion which then decomposes in to CO_2 and hydride anion. The hydride anion further interacts with water, forming H_2 and OH^- by electron transfer. [25]

$$OH^- + CO \longleftrightarrow HCOO^- \longleftrightarrow H^- + CO_2 \qquad (2.1)$$

$$H^- + H_2O \longleftrightarrow H_2 + OH^- \qquad (2.2)$$

2.4.2 Effect of Residence Time. Effect of residence time inside a catalyst bed was studied by varying the contact time from 1.6 to 6. 2 seconds. This residence time was calculated as reactor void volume in the catalyst bed divided by the volumetric flow rate at experimental conditions. The results are shown in Figure 2.4 for 5 wt.% glucose in the feed. In the range of experiments carried out, hydrogen yield increased progressively as the contact time increased. However, beyond a contact time of 4 s the increase was negligible. Effect of increasing residence time on total organic carbon in the liquid product for catalytic and non-catalytic experiments is shown in Figure 2.5. Increasing the residence time in the non-catalytic runs significantly reduced the total organic carbon in the liquid indicating that these were further converted to CO_2 and H_2 at higher residence time. In the catalytic experiments, the low TOC values correspond to near complete conversion of carbon to gaseous products. It should be noted that the residence time in these experiments are much lower than the previous batch experiments.[22]

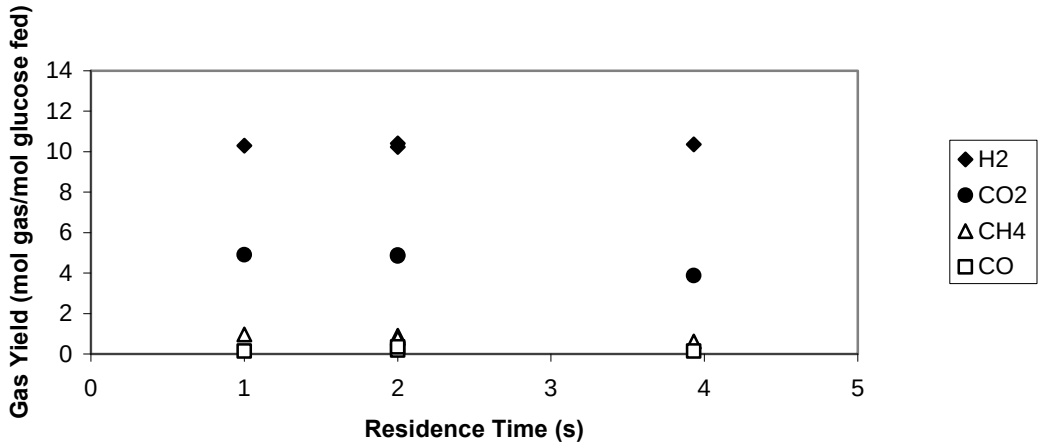

Figure 2.4: Effect of residence time on product gas yields. (T: 700°C, P: 241 bar, glucose conc. 5 wt. %, 2.0 g Ru/Al_2O_3 catalyst)

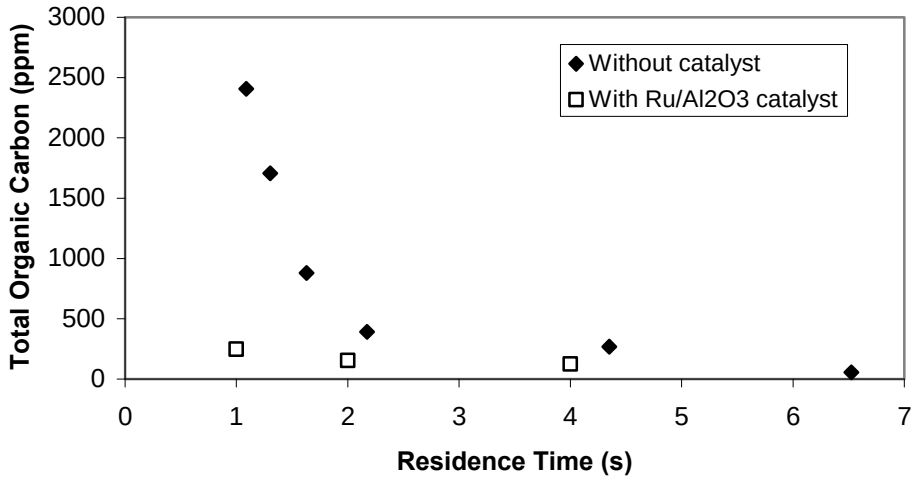

Figure 2.5: Effect of residence time on total organic carbon in liquid phase (T=700°C, P: 241 bar, residence time: 2 s)

2.4.3 Effect of Temperature. Reactor temperature has a strong influence on the gasification rate and hydrogen formation in biomass reactions. To study the influence, experiments were carried out at temperatures ranging between 700 and 800°C. The residence time inside the catalyst bed was 2 s while the glucose feed concentration was 4 wt.%. As shown in Figure 2.6, hydrogen yield was near the theoretical maximum of 12 moles H_2/mol of glucose fed. Additional experiments carried out at 650°C showed incomplete conversion of glucose to gaseous products, as witness by a strong hydrocarbon smell in the liquid product, which was further confirmed by high TOC values. Further investigation at low temperature was abandoned in the interest of preventing any tar formation on the surface of the catalyst. Compared to the thermal gasification, significantly lower temperature was effective for the hydrogen production over Ru/Al_2O_3 catalyst.

With an increase in the temperature the hydrogen and carbon dioxide yields increase while the methane yield decreases. Thermodynamically at low reaction temperatures, H_2 and CO_2 readily react to form alkanes and water. However, in the present study due to the presence of catalyst and low residence time (which avoids attainment of equilibrium), methane formation is suppressed even at low reaction temperature. The low carbon monoxide yield indicates that the water gas shift reaction approaches completion. The high water excess leads to a preference for the formation of hydrogen and carbon dioxide instead of carbon monoxide. In addition, the intermediate products such as acids and aldehydes which may otherwise form in the conventional reactions are not found in supercritical water reforming in appreciable concentrations. As compared with a typical temperature required (800– 1000°C) in conventional biomass gasification, supercritical water gasification can be carried out at a lower temperature.

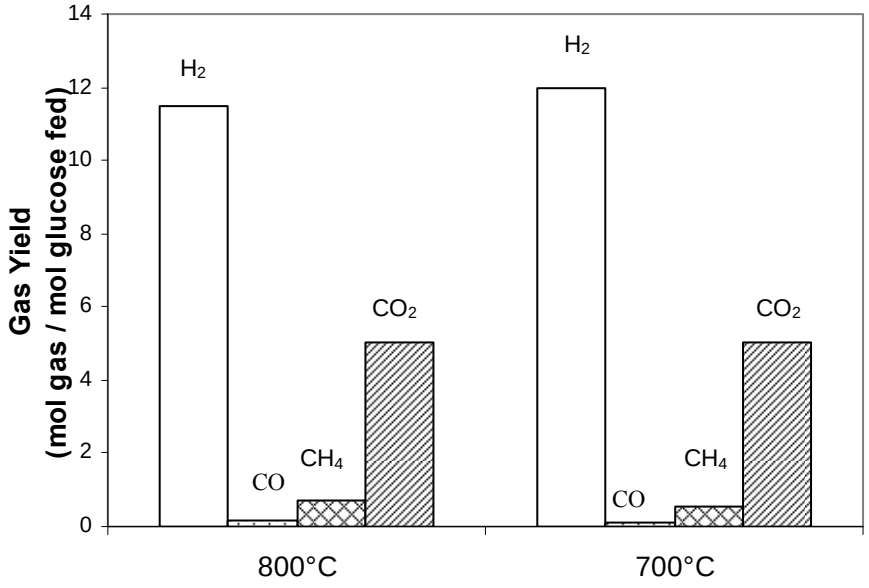

Figure 2.6: Effect of temperature on product yields (P: 241 bar, glucose conc.: 4 wt.%, residence time: 2 s, 2.0 g Ru/Al_2O_3 catalyst)

2.4.4 Effect of Glucose Concentration. Figure 2.7 shows the effect of glucose feed concentration on product gas yields at 700°C. The hydrogen yield drops by 17% as the glucose concentration in feed was increased from 1 to 5 % wt.%. Also, a decrease in the carbon dioxide yield and a small increase in methane and carbon monoxide yield were observed on increasing glucose concentration. The trends of experimental yield of hydrogen, carbon dioxide and carbon monoxide are similar to as those reported by other researchers.[28, 29, 30] Further increase in the glucose concentration results in formation of heavier molecular weight hydrocarbons and coke which often plugs the reactor. However, the heavy molecules and coke can be reduced by increasing temperature in SCW.

Figure 2.7: Effect of glucose concentration on product yields (T: 700°C, P: 241 bar, residence time: 2 s: 2.0 g Ru/Al_2O_3 catalyst)

2.4.5 Reaction Mechanism. As discussed earlier, biomass gasification proceeds via several complex reactions, such as pyrolysis, hydrolysis, steam reforming, water gas shift reaction and methanation. For glucose reforming in supercritical water, a maximum theoretical yield of hydrogen can be calculated by converting all the feed carbon to carbon dioxide with water as

$$C_6H_{12}O_6 + 6\ H_2O \longleftrightarrow 6\ CO_2 + 12\ H_2 \qquad (2.3)$$

In overall reaction scheme, CO_2 also undergoes hydrogenation reaction to form CO and CH_4 as

$$CO_2 + H_2 \longleftrightarrow CO + H_2O \qquad (2.4)$$

and

$$CO + 3\ H_2 \longleftrightarrow CH_4 + H_2O \quad (2.5)$$

However, mechanistically glucose reforming via reaction intermediates can be shown as follows[25]:

$$\text{Glucose} \longrightarrow \text{Acids / Aldehydes} \longrightarrow \text{Gases} \quad (2.6)$$

With the presence of ruthenium catalyst in supercritical water, extremely high gasification rate and a high hydrogen yield was obtained. Also, negligible coke was formed on the catalyst surface for up to 4 wt.% glucose feed, which indicates that all the solid products such as chars and aldehydes are decomposed by the supercritical water in the presence of catalyst. The dominant reactions in the gas phase are those for water gas shift and methanation reaction.

The presence of methane and some traces of liquid hydrocarbon indicate that reforming of glucose in supercritical water occurs via above reaction intermediates. Reforming of these intermediates by water gas shift reaction is highly likely since water is in high excess. Although the exact role of ruthenium is not established in supercritical water reforming, however it may be assumed that some complex is formed as a result of the reaction between adsorbed glucose and water supercritical water. The formation of adsorbed intermediates by the decomposition of this complex is assumed to be the rate determining step. The adsorbed intermediates further react with water in the gas phase to give CO_2 and H_2. Assuming *S* denotes an active site on the catalyst and *A* and *B* denote glucose and water, respectively, the overall reaction steps may be represented as follows:

$$A + S \xleftrightarrow{k_1, k_{-1}} AS \tag{2.7}$$

$$AS + B \xrightarrow{k_2} ABS \tag{2.8}$$

$$ABS \xrightarrow{k_3} \text{Intermediates} \xrightarrow{k_4} CO_2 + H_2 \tag{2.9}$$

where, Equation 2.7 denotes the reversible adsorption of glucose on the catalyst surface, and Equation 2.8 represents the reaction of adsorbed glucose molecule with water to form a complex molecule *ABS*. Assuming the steady state hypothesis for the intermediate complex *ABS* and *AS*, the dependence of the rate (r) on reactant concentration (c) can be expressed as:

$$r = \frac{k_1 k_2 c_A c_B}{k_{-1} + k_1 c_A + k_2 c_B + (k_1 k_2 c_A c_B / k_3)} \tag{2.10}$$

Since in our experiments, water concentration is significantly high, c_B is assumed constant and the above expression is simplified as:

$$r = \frac{k_R c_A}{1 + b c_A} \tag{2.11}$$

where, k_R and b are lumped parameters defined as

$$k_R = \frac{k_1 k_2 c_{Bo}}{k_{-1} + b c_{Bo}} \tag{2.12}$$

and

$$b = \frac{k_1 + (k_1 k_2 c_{Bo} / k_3)}{k_{-1} + k_2 c_{Bo}} \qquad (2.13)$$

When $(b\ c_A) << 1$, Equation 2.11 reduces to

$$r = k_R c_A \qquad (2.14)$$

The above equation was solved using a non linear regression technique on rate of hydrogen production at different glucose concentrations at a constant pressure and temperature. The value of rate constant (k_R) at 700°C was calculated to be 0.33 s^{-1}. The lowest rate of hydrogen production in the present study is more than $4x10^4$ μmoles/g. h, which is significantly higher than the maximum value of hydrogen production rate reported for glucose reforming by enzymatic route ($7x10^2$ μmoles/g. h) and also higher than the values reported for catalytic reforming of glucose over Pt/Al_2O_3 catalyst .[16]

2.5 Conclusions

The supercritical water reforming of biomass materials appears to be a suitable technique for the production of high-pressure hydrogen with short residence times. Presence of 5 wt.% Ru/Al_2O_3 catalyst significantly enhanced the conversion and hydrogen yield from glucose, while significantly reducing char and tar formation. The product gases mainly consist of hydrogen and carbon dioxide, and a small amount of methane and carbon monoxide. There are effectively no tarry products in the liquid effluent and negligible losses in catalytic activity for up to 5 wt% glucose in the feed.

However, the hydrogen yield decreases as the concentration of glucose in the feed increase beyond 5wt.%.

2.6 Acknowledgement: This research was supported by the U.S. Department of Energy through the Office of Fossil Energy (FE), National Energy Technology Laboratory (NETL), under DOE Contract DE-FC26-05424.56 via the Consortium of Fossil Fuel Science.

2.7 References

1. Gadhe, J.B.; Gupta, R.B.; "Hydrogen production by methanol reforming in supercritical water: suppression of methane formation" *Ind. Eng. Chem. Res.* **2005**, (44), 4577-4585.

2. Patel Sanjay and K.K.Pant; Production of hydrogen with low carbon monoxide formation via catalytic steam reforming of methanol, *Journal of Fuel Cell Science and Technology* **2006**, Vol. 3 / 369

3. Matsumura, Y.; Xu, X.; Antal, M. J. Gasification Characteristics of an Activated Carbon in Supercritical Water. *Carbon* **1997**, 35, 819.

4. Sahoo,D.R, Vajpai, S; Patel, S.; Pant K.K; Kinetic modeling of steam reforming of ethanol for the production of hydrogen over Co/Al2O3 catalyst *Chemical Eng Journal* **2006**,(in press) 10.1016/j.cej.2006.08.011

5. Xu, X.; Matsumura, Y.; Stenberg, J.; Antal, M. J., Jr. Carbon-catalyzed gasification of organic feedstock in supercritical water. *Ind. Eng. Chem. Res.* **1996**, 35, 2522.

6. Xu, X. D.; Antal, M. J., Jr. Gasification of sewage sludge and other biomass for hydrogen production in supercritical water. *Environ. Prog*. **1998**, 17, 215.

7. Antal, M. J., Jr; Allen, S. G.; Schulman, D.; Xu, X. D.; Divilio, R. J. Biomass gasification in supercritical water. *Ind. Eng. Chem. Res*. **2000**, 39, 4040.

8. Kruse, A.; Meier, D.; Rimbrecht, P.; Schacht, M. Gasification of pyrocatechol in supercritical water in the presence of potassium hydroxide. *Ind. Eng. Chem. Res.* **2000**, 39, 4842.

9. Kruse, A.; Gawlik, A. Biomass conversion in water at 330- 410 °C and 30-50 MPa. identification of key compounds for indicating different chemical reaction pathways. Ind. *Eng. Chem. Res*. **2003**, 42, 267.

10. Kruse, A.; Henningsen, T.; Sinag, A.; Pfeiffer, J. Biomass gasification in supercritical water: Influence of the dry matter content and the formation of phenol. Ind. Eng. Chem. Res. **2003**, 42, 3711.

11. Yoshida T., Oshima Y. "Partial Oxidative and catalytic biomass gasification in supercritical water: A promising Flow reactor system" *Ind. Eng. Chem. Res*. **2004**, 43, 4097.

12. Yu, D.; Aihara, M.; Antal, M. J., Jr. Hydrogen production by steam reforming glucose in supercritical water. *Energy Fuels* **1993**, 7, 574.

13. Watanabe, M.; Inomata, H.; Arai, K. Catalytic hydrogen generation from biomass (glucose and cellulose) with ZrO2 in supercritical water. *Biomass Bioenergy* **2002**, *22*, 405.

14. Watanabe, M.; Inomata, H.; Osada, M.; Sato, T.; Adschiri, T.; Arai, K. Catalytic effects of NaOH and ZrO2 for partial oxidative gasification of *n*-hexadecane an lignin in supercritical water. *Fuel* **2003**, *82*, 545.

15. Holgate, H. R.; Meyer, J. C.; Tester, W. J. Glucose hydrolysis and oxidation in supercritical water. *AIChE J.* **1995**, *41*, 637.

16. Cortright, R. D.; Davda, R. R.; Dumesic, J. A. Hydrogen from catalytic reforming of biomass-derived hydrocarbons in liquid water. *Nature* **2002**, 418, 964-967.

17. Minowa, T.; Ogi, T.; Yokoyama, S. Hydrogen production from wet cellulose by low temperature gasification using a reduced nickel catalyst. *Chem. Lett.* **1995**, *286*, 937.

18. Minowa, T.; Ogi, T.; Yokoyama, S. Effect of pressure on low-temperature gasification of wet cellulose into methane using reduced nickel catalyst and sodium carbonate. *Chem. Lett.* **1995**, *280*, 285.

19. Yoshida, T, Matsumura, Y. Gasification of Cellulose, Xylan, and Lignin Mixtures in Supercritical Water. *Ind. Eng. Chem. Res.* **2001**, *40*, 5469.

20. Yoshida, T.; Oshima, Y.; Matsumura, Y. Gasification of biomass model compounds and real biomass in supercritical water. *Biomass Bioenergy* **2004**, *26*, 71.

21. Elliott, D. C.; Sealock, L. J.; Backer, E. G. Chemical processing in high pressure aqueous environment: development of catalyst for gasification *Ind. Eng. Chem. Res* **1993**, *32*, 1542-1548.

22. Osada M. ; Sato, T.; Wantabe M.; Adschiri, T.; Arai, K.; Low temperature catalytic gasification of lignin and Cellulose with a Ruthenium Catalyst in Supercritical water. *Energy and Fuels* **2004**, 18 327-333.

23. Lu Y.J.; Guo l.j.; Ji, C.M. , Zhang, X.M.; Hao, X.H.; Yan Q.H.; Hydrogen production by biomass gasification in supercritical water: A parametric study *Int. J. of Hydrogen Energy* 31 **2006**, 822-831.

24. Saisu, M.; Sato, T.; Watanabe, M.; Adschiri, T.; Arai, K. Conversion of lignin with supercritical water-phenol mixtures. *Energy Fuels* **2003**, *17*, 922.

25. Penninger J. M.L; Rep. M.; Reforming of aqueous wood pyrolysis condensate in supercritical water. *Int. J. of Hydrogen Energy* 31 (**2006**) 1597-1606

26. Courson, C.; Makaga, E.; Petit, C.; Kiennemann, A. Development of Ni catalysts for gas production from biomass gasification. Reactivity in steam- and dry-reforming. *Catal. Today*. **2000**, *63*, 427.

27. Wilke, C. R. "A viscosity equation for gas mixtures" *Journal of Chemical Physics* (**1950**), 18, 517-19.

28. Sinag, A.; Kruse, A.; Schwarzkoph, V. Key compounds of the hydropyrolysis of glucose in supercritical water in the presence of K2CO3. *Ind. Eng. Chem. Res.* **2003**, *42*, 3516.

29. Yan, Q.; Guo, L. ; Lu, Y.; Thermodynamic analysis of hydrogen production from biomass gasification in supercritical water. *Energy Conversion and Management* **2006, 47,** 1515-1528.

30. Hashaikeh, R.; Butler,S.; Kozinski, J.A.; Selective promotion of catalytic Reactions during biomass gasification to hydrogen. *Energy & Fuels* **2006,** *20*, 2743-2747

3. Hydrogen Production from Ethanol by Reforming in Supercritical Water using Ru/Al_2O_3 Catalyst

3.1 Abstract

Supercritical water is a promising reforming media for the direct production of hydrogen at high pressures with a short reaction time. In addition to being a dense solvent, supercritical water also participates in reforming reaction. In this work, high pressure hydrogen is produced from ethanol by reforming over a Ru/Al_2O_3 catalyst with low methane and carbon monoxide formation. Experiments were conducted in a continuous tubular reactor to study the effects of temperature, pressure, residence time, and water-to-carbon ratio on the H_2 yield. Hydrogen formation is favored at higher temperatures and at high water-to-ethanol ratios. The formation of methane can be suppressed by operating at an optimal residence time, high reactor temperature and a low feed concentration of ethanol. Excellent conversion in reaction time as short as 4 seconds is achieved. Pressure has negligible effect on hydrogen yield above the critical pressure, and for less than 10 wt% ethanol concentration in the feed, there was negligible coke activation energy of 65.3 kJ mol^{-1} was observed.

3.2 Introduction

As the world supply of fossil fuels depletes there is a growing need for renewable energy sources. The current use of fossil fuels is responsible for pollution due to carbon dioxide, carbon monoxide, hydrocarbons, sulfur dioxide and nitrogen oxide. Every gallon of gasoline burned in an automobile produces approximately 20 pounds of the greenhouse gas CO_2, and the transportation sector is responsible for one third of all CO_2

emissions. Considerable efforts are currently under way to minimize the emissions. One promising alternative to fossil fuels is the use of hydrogen as an energy carrier, which provides zero emission of pollutants and high energy efficiency when used in polymer electrolyte membrane (PEM) fuel cell.

Hydrogen can be produced from a variety of starting materials, both renewable and nonrenewable, via several different processes. Current technologies for the commercial production of H_2 include steam reforming, partial oxidation, and electrolysis of water. Out of these, steam reforming is most commonly used, which catalytically converts hydrocarbons or oxygenated hydrocarbons to produce a mixture of H_2 and CO followed by a water gas shift reaction to produce a mixture of H_2 and CO_2 along with small amount of un-reacted CO.[1-3] Supercritical water is an environmentally friendly fluid and is gaining in popularity as a reaction medium owing to fast heat and mass transfers and adjustable density. The thermochemical properties of water at various pressures are summarized elsewhere.[4] The properties of supercritical water such as density, viscosity and hydrogen bonding are quite different from those of steam or liquid water[4,5,6]. In the supercritical region, the dielectric constant of water is much lower. Further, the number of hydrogen bonds is much smaller and their strength is considerably weaker. As a result, SCW behaves as an organic solvent and exhibits extraordinary solubility towards organic compounds containing large nonpolar groups and most permanent gases.[6-9] Another advantage of SCW reforming is that the H_2 is produced at a high pressure, which can be stored directly, thus avoiding the large energy expenditures associated with its compression. The process becomes economical as the compression work is reduced owing to the low compressibility of liquid feed compared to that of

gaseous H_2. For heterogeneous catalytic reactions in supercritical fluids, the high diffusivity of supercritical fluids can greatly reduce mass-transfer limitations and extract the coke precursors from the catalyst surface to prevent coking. Hydrocarbons are completely soluble in supercritical water, which minimizes the formation of char or slag, which may otherwise lead to catalyst deactivation. Research carried out on thermal and catalytic gasification of biomass or its model compounds in supercritical water revealed that there is lower tar or char formation as compared to conventional reforming.[8-16]. Osada et al. [10] gasified lignin and cellulose in a batch reactor at 400°C in supercritical water with a ruthenium catalyst with gas yields of 30% and 70%, respectively with methane as a major gas product and no solid product was formed.

Among the available raw materials, ethanol is an attractive option for hydrogen production because it is less toxic than methanol and it can be produced renewably from biomass with little net addition of carbon dioxide to the atmosphere. Ethanol is already being produced from corn for use as a fuel or fuel additive in automobiles. But if it were used instead to produce hydrogen for a fuel cell, the whole process would become more energy efficient. Theoretically, a bushel of corn would yield three times as much power if its energy were channeled into hydrogen fuel cells rather than burned along with gasoline, because ethanol in car engines burns with 20% efficiency, whereas ethanol reformed to hydrogen for a fuel cell has more than 60% efficiency.[17] The development of a process to produce H_2 directly at a very high pressure is attractive since it avoids compression expenses for storage. Hydrogen can be produced from ethanol and methanol feed stocks through steam reforming, partial oxidation or a combination of the two.[18-21] Steam reforming of ethanol over Ni, Co, Ni/Cu and noble metals has been

extensively used.[21] The main problem with the ethanol reforming is that besides the formation of H_2, CO, CH_4, the gaseous fuel product contains high levels of CO, which is poisonous to the Pt anode of the PEM fuel cell. Among the noble metals, Ru has been reported as the most promising catalyst having high activity in steam reforming of hydrocarbons and biomass gasification[6,10,22-24]. Liguras et al.[24] studied the steam reforming of ethanol over Ru/Al_2O_3 catalysts and reported high yield of hydrogen in subcritical water. At high Ru loading (5 wt%) the catalyst was stable and had reasonable activity and selectivity. There have been some studies to investigate the thermal H_2 production in supercritical water from a variety of organic feedstock such as methane, methanol, ethanol, glucose, and glycerol.[6-16] Most of the hydrocarbon reforming studies in supercritical water have been carried out without a catalyst (except for the catalytic effect of the reactor walls that provide very small surface area) and some studies are reported over a catalyst.[6,9 ,25-27] It has been reported that methanol reforming in supercritical water results in a hydrogen-rich product stream that has low concentrations of both carbon monoxide and methane.[25] Watanabe investigated the chemistry of carbohydrate in the presence of ZrO_2 as a catalyst.[9] Taylor et al[26] also conducted experiments to investigate the reforming of different hydrocarbons in supercritical water at 550–700°C and 27.6 MPa in a tubular Inconel 625 reactor. The results indicated that methanol can be completely converted to a product stream that is low in methane and near the equilibrium composition of hydrogen, carbon monoxide, and carbon dioxide. On the other hand ethanol and ethylene glycol resulted in less hydrogen yield and high concentrations of methane and carbon monoxide. The yield of hydrogen produced in these experiments was significantly less and high yield of methane and CO has been

reported in the product stream. Further, Boukis et al have studied methanol reforming in supercritical water catalyzed by an Inconel 625 reactor wall at both the lab scale and pilot plant scale.[28-36] In conventional reforming processes, including partial oxidation and autothermal reforming, higher pressures disturb the equilibrium conversion. However, the equilibrium limitations in SCW reforming can be avoided if the reaction time is limited to a very short period.[4]

The present work focuses on hydrogen production from ethanol in supercritical water over Ru/Al_2O_3 catalyst with minimal CO and methane in the product stream. In our recent study[6], significantly high yield of hydrogen was obtained during the reforming of glucose in supercritical water over this catalyst. Effect of reactor temperature, residence time and concentration of ethanol in water on yield of hydrogen has been studied. Finally, a reaction mechanism has been proposed and the kinetics for the catalyst is determined.

3.3 Experimental Section

All the chemicals used were of high purity (99.9% pure) and of analytical grade. The commercial 5 wt% Ru/Al_2O_3 was purchased from Aldrich. The catalyst had the following characteristics: Crystalline structure: amorphous, total BET surface area: 100 m^2/g, specific pore volume: 0.30 mL/g; density: 0.95 g/cm^3. Deionized ultra filtered water and HPLC grade ethanol were used as received from Fisher Scientific. The schematic diagram of the experimental apparatus is shown in Figure 3.1. The details of the experimental procedure are discussed elsewhere,[6] and is briefly discussed here. Experiments were conducted in supercritical water in a fixed bed tubular reactor (0.5 m long, 0.25" OD and 0.12" ID) made of Inconel 600 (Microgroup) having a composition

of 73% Ni, 18% Cr, and 9% Fe, which was placed inside a temperature controlled furnace (Thermolyne 21100).

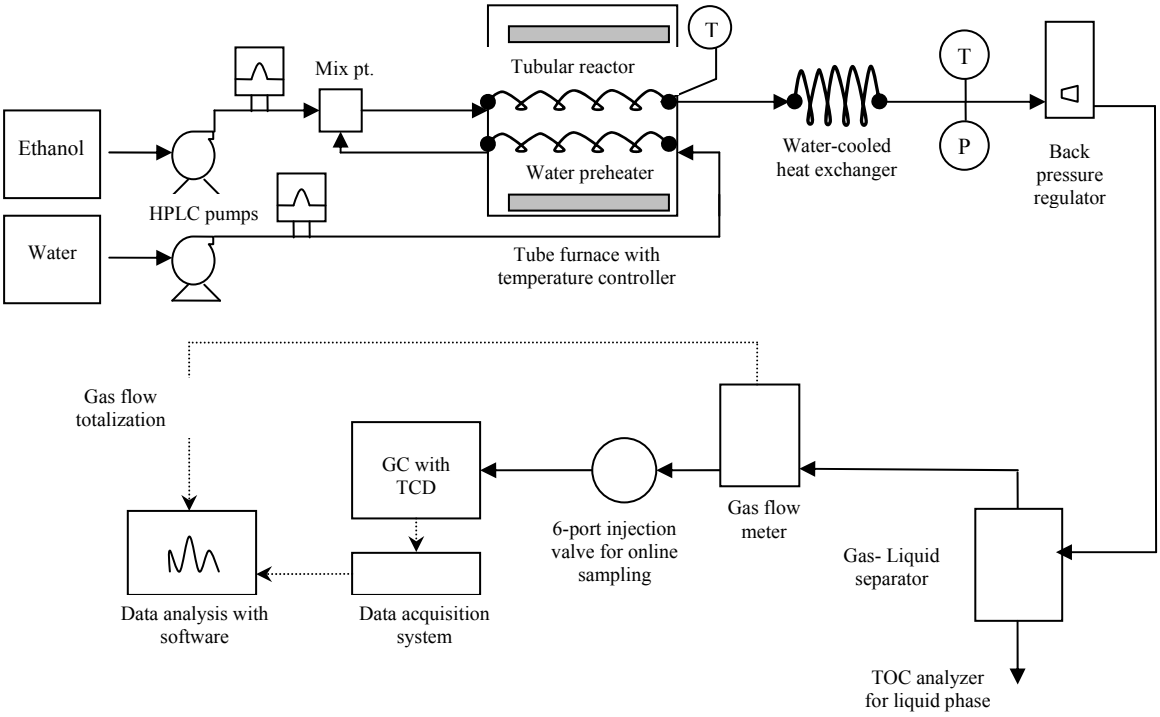

Figure 3.1: Schematic diagram of experimental apparatus

A known mass of the catalyst, 1.92 g, was packed in the reactor. Ethanol from the feed tank was pumped to the reactor using an HPLC pump (Waters 590). The feed tank was covered on top to avoid the loss of ethanol by evaporation. The reactor temperature at the exit of the furnace was measured by using a type-K thermocouple with a tee arrangement. Both ends of the tube furnace were covered properly to avoid heat loss and achieve uniform temperature. The gas mixture exiting the reactor was cooled using a water-cooled double pipe heat exchanger made of SS 316 tubing. Pressure was measured by a pressure gauge. The pressure was let down to the ambient by means of a back pressure regulator (Straval). The gas-liquid mixture was separated in a glass phase-

separator having gas-tight valves to prevent the escape of gases. The flow rate of the gases was measured using a gas flow meter (Omega FMA-1600). A six-port injection valve (Valco) having a 100 μL sample loop was used for the online sample injection. The gas composition was measured using a gas chromatograph (SRI 8610C) equipped with a TCD and 60/80 Carboxen-1000 carbon molecular sieve column (Supelco) having dimensions of 15' x 1/8". Nitrogen was used as the carrier gas. The total organic carbon (TOC) content of the liquid was analyzed using a TOC analyzer (Shimazdu TOC-V_{CSN}). Characterization of the catalyst was performed before and after use by SEM (JEOL 7000F) and X-ray diffraction (Rigaku diffractometer equipped with $Cu_{K\alpha 1}$ radiation source, graphite monochrometer, and miniflex goniometer. The diffractometer was ran at 40 kV voltage and 40 mA current, and scanned at 5°/min with 0.05° step size.

The total running time for each experiment was approximately three hours to collect necessary data. All measurements were taken at least in triplicate to ensure accuracy. Preliminary experiments were also carried out in an empty bed reactor with ethanol feed stock in supercritical water to study the influence of reactor wall. The accuracy of the run was checked by calculating the overall carbon balance for the system. The experiments with an error in the overall carbon balance greater than 5% were either repeated to check for carbon deposition or rejected. Scattering in the data of the totalized gas flow rate measured by the flow meter was less than 1%. The error in the dry gas composition obtained by the GC analysis was typically less than 2%. The overall error in the calculation of the gas yields due to the errors introduced by the individual analysis techniques and experimental error was found to be less than 5%.

3.4 Results and Discussion

The desired reaction for the reforming of ethanol is the complete conversion to hydrogen and carbon dioxide as

$$C_2H_5OH + 3H_2O \leftrightarrow 6H_2 + 2CO_2 \qquad (\Delta H°_{298} = 174 \text{ kJ/mol}) \qquad (3.1)$$

3.4.1 Effect of Ru/Al_2O_3 Catalyst. To study the effect of the Ru/Al_2O_3 catalyst on hydrogen yield for reforming of ethanol in supercritical water, catalytic experiments were compared to the empty reactor experiments under identical conditions. The gas yield is defined as the moles of product gases divided by the moles of ethanol fed to the reactor. The use of catalyst increases the hydrogen yield significantly compared to a process without Ru/Al_2O_3 catalyst. The main products of the catalytic reforming of ethanol were hydrogen and carbon dioxide, with small amounts of methane, carbon monoxide, and ethylene. Experimental conditions, product gas composition, and hydrogen yield are reported in Table 1 with and without Ru/Al_2O_3 catalyst. The hydrogen yield increased from 3 to 4.5 (moles of hydrogen formed /moles of ethanol fed) upon addition of the catalyst. The hydrogen yield obtained in the SCW in the present study is significantly higher than the hydrogen yield reported for stream reforming of ethanol in subcritical water.[18,24] There was also a significant reduction in carbon monoxide and methane yields in the presence of the catalyst. A typical value of total organic carbon in the liquid product was approximately 120 ppm in most of the experiments, indicating conversion to gaseous products greater than 99%. Only two experiments conducted at 600 °C showed higher levels of organic carbon in the liquid effluent. Although the detailed properties of the catalyst, such as catalyst life and strong metal-support interaction have not been

reported for Ru/Al_2O_3 catalyst, the probable reason for higher gasification performance is that the intermediate agents formed during ethanol decomposition such as dimethyl ether and acetaldehyde were also gasified in presence of supercritical water. The generation of H_2 by the steam reforming of ethanol in sub-critical water leads to the formation of significant amounts carbon, which limits the yield of H_2, and the reaction product contains higher hydrocarbons such as acetaldehyde, diethyl ether, ethane and ethylene in addition to the desired hydrogen. However in supercritical water, water becomes a strong oxidant, and oxygen in water can be transferred to the carbon atoms of the ethanol. As a result of the high density, carbon is preferentially oxidized into CO_2 but also low concentrations of CO were formed. In the present investigation, the reaction process can be operated continuously with the same catalyst. To study the effect of time on stream on catalyst performance, some experiments were repeated. There was no appreciable productivity change indicating that the catalyst activity does not decrease appreciably during the run. The gasification of hydrocarbons in supercritical water proceeds via several complex reactions such as ethanol decomposition, steam reforming, water gas shift, and methanation. The product distribution strongly depends upon the relative extent of these reactions. It is assumed that during the reaction, ethanol undergoes dehydrogenation on the metal surface to give adsorbed intermediates before the cleavage of C-C or C-O bonds. Subsequent cleavage of C-C bonds leads to formation of CO and H_2. CO reacts with water to form CO_2 and H_2 by the water gas shift reaction. Carbon monoxide was present only in trace amounts, probably because the Ru catalyst promotes the water gas shift reaction to form carbon dioxide and hydrogen from carbon monoxide and water.

Table 3.1: Details of Experimental Conditions

T (°C)	P (bar)	Feed Conc. (wt%)	Residence time (s)	W/F_{Ao} (g-cat*s/mol EtOH)	Product Gas Composition (mol%) H_2	CO	CH_4	CO_2	H_2 Yield
800	221	10	4	empty bed	62.8	3.5	10.8	22.9	3.0
600	221	10	5	142449	63.1	5.6	12.0	19.3	2.1
600	221	10	10	252433	57.5	0.5	15.3	26.8	2.6
700	221	10	5	181515	56.5	0.2	15.6	27.6	2.4
700	221	10	2	71563	55.6	0.5	16.1	27.8	2.5
700	221	10	1	37520	57.7	0.6	15.0	26.7	2.8
750	221	10	2	78297	62.0	1.1	11.9	24.9	3.3
750	221	10	4	164234	63.4	0.8	10.2	25.6	3.9
750	221	10	6	264062	67.2	0.5	8.8	23.5	3.3
800	221	10	6	251264	68.8	0.9	8.3	21.9	3.5
800	221	10	4	165517	70.4	1.0	7.5	21.1	4.5
800	221	10	2	84223	65.7	1.0	10.3	23.0	3.6
800	221	10	1	41845	64.8	1.2	11.6	22.4	3.7
800	221	10	0.5	20923	63.0	1.0	12.6	23.4	3.3
800	221	5	4	354399	73.0	0.7	2.8	23.5	5.3
800	221	15	4	112060	64.6	1.2	11.6	22.7	3.1
800	221	20	4	83815	59.5	1.3	14.9	24.3	2.4
700	243	10	2	62412	56.1	0.5	15.9	27.4	2.7
700	276	10	2	54219	53.2	0.7	18.0	28.0	2.6

SEM was used to characterize the catalyst. Figures 3.2 and 3.3 show SEM images of the fresh and used catalyst, respectively. From these images it can be seen that the support has undergone a structural change. The fresh catalyst consists of more-or-less round particles, characteristic of amorphous materials, whereas the used catalyst is clustered in aggregates of sharp-edged crystals. Looking at the higher magnification images, it can be seen that particle size has also increased. X-ray diffraction was used to further characterize the catalyst, and XRD spectra can be seen in Figure 3.4. The spectra of the used catalyst show sharp narrow peaks characteristic of a crystalline compound.

Also it is evident from the width of the peaks that particle size has increased, as peak width is inversely proportional to particle size. The composition of the new crystalline phase was not determined.

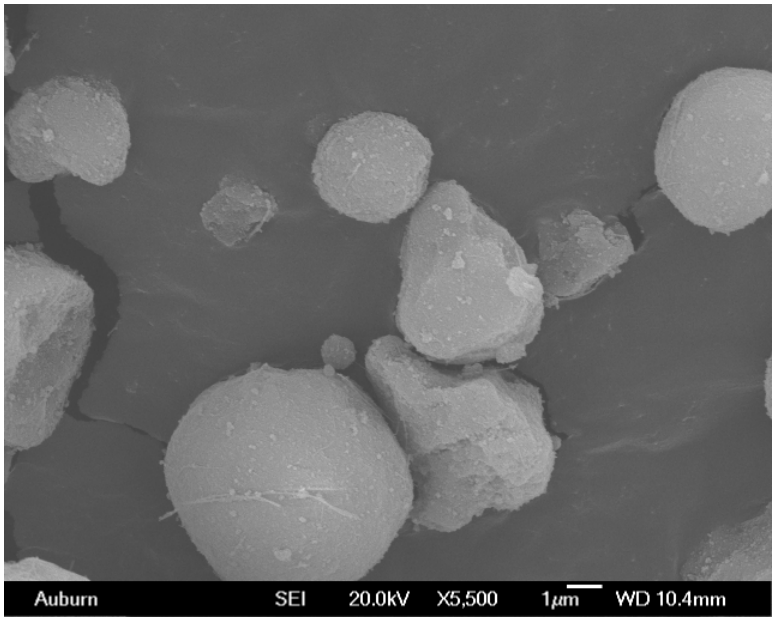

(a)

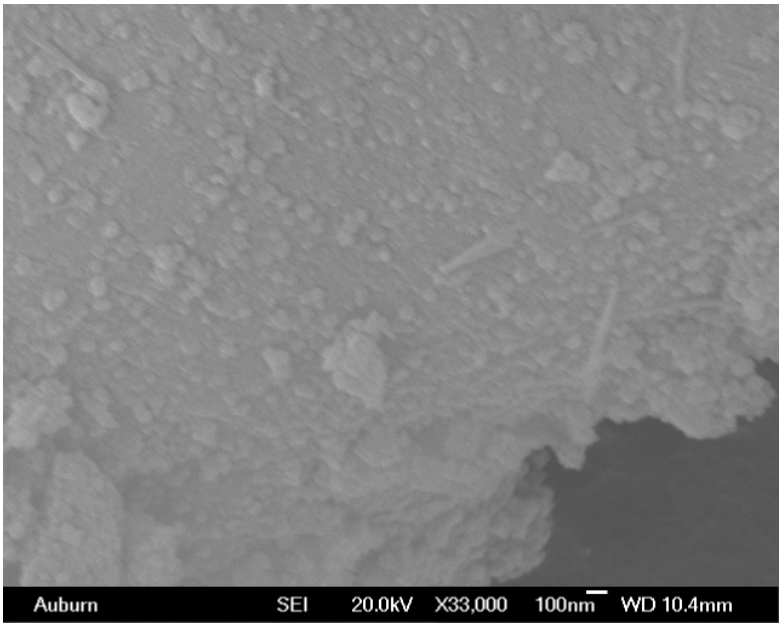

(b)

Figure 3.2: SEM images of fresh Ru/Al_2O_3 catalyst. (a) 5500x magnification (b) 33,000x magnification

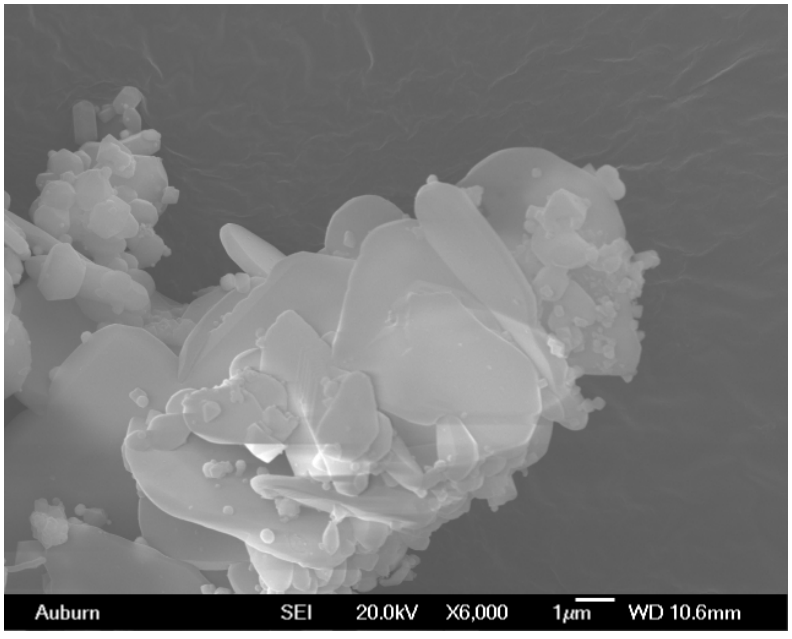

(a)

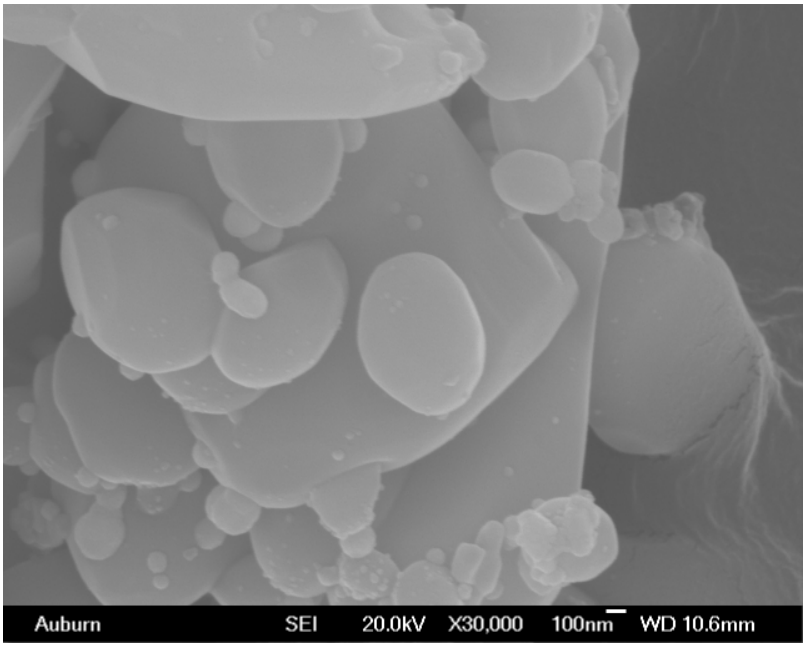

(b)

Figure 3.3: SEM images of used Ru/Al_2O_3 catalyst. (a) 6000x magnification (b) 30,000x magnification

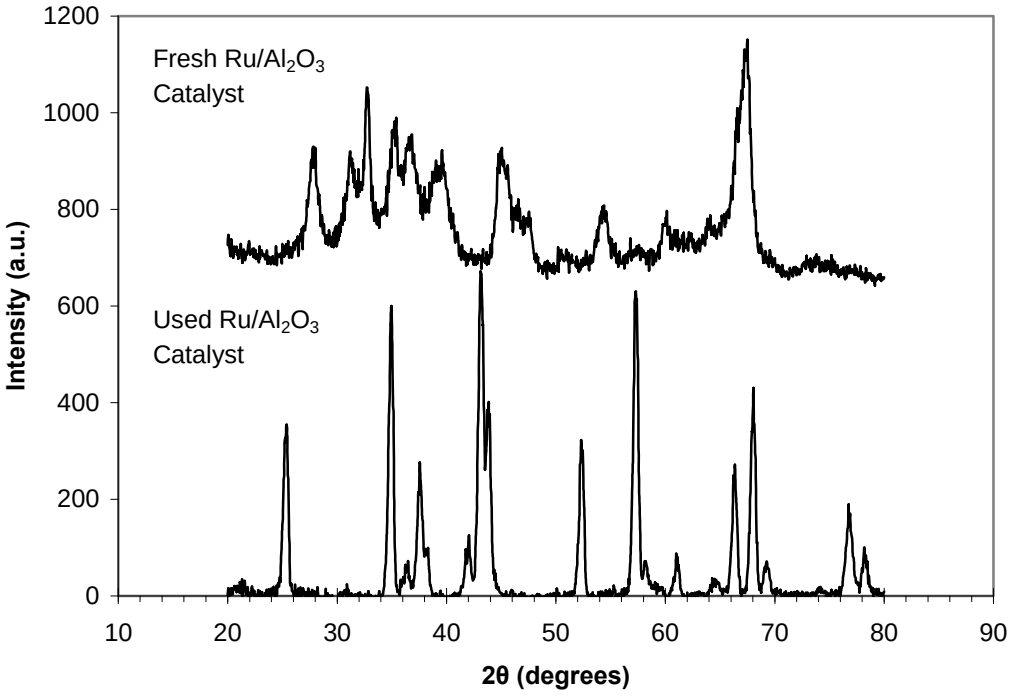

Figure 3.4: X-ray diffraction spectra for fresh and spent Ru/Al_2O_3 catalyst

3.4.2 Effect of Residence Time. The residence time in the catalyst bed was studied by changing the inlet flow rate. The product yields (moles of product/ mole of ethanol fed) are given in Figures 3.5 - 3.7, at three different temperatures. No ethanol was seen in the liquid effluent indicating that it reacted completely in supercritical water. At 800 °C, the hydrogen yield varied from 2 to 4.5 as the residence time changed from 1 to 4 seconds and decreased thereafter. In contrast, at the lower temperature of 600 °C, high levels of organic carbon were seen in the liquid product at low residence time and higher hydrogen yields were obtained at relatively high residence time. The ethylene yield was also higher at the low temperature. Specifically at high temperatures, the low residence time can prevent the methanation reactions from reaching equilibrium. This makes it possible to

significantly limit the extent of methanation and H_2 loss by operating at a low residence time.

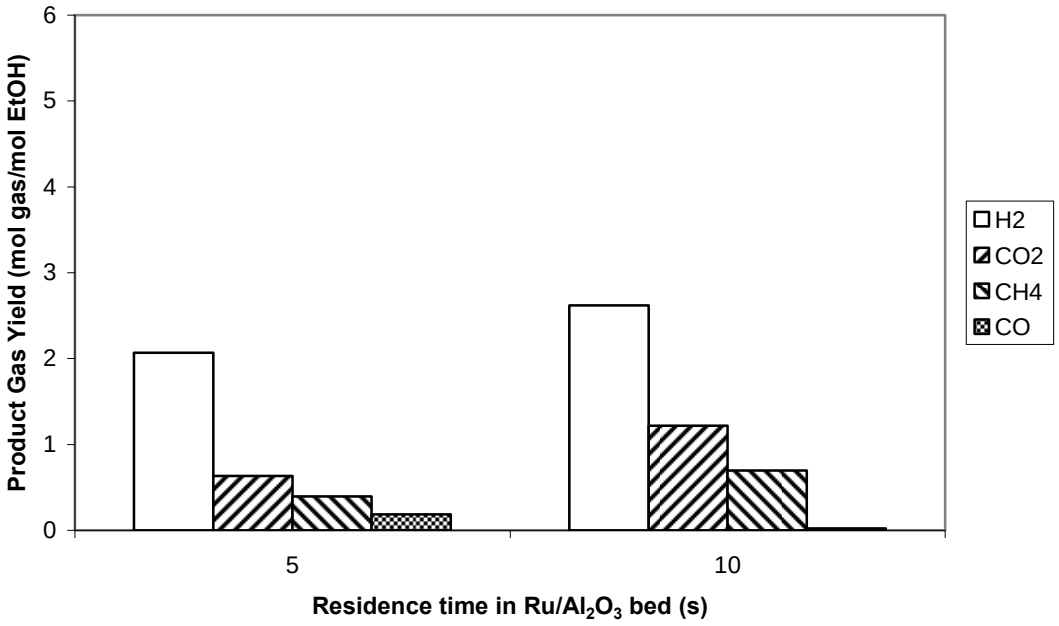

Figure 3.5: Effect of residence time on product gas yields (T, 600 °C; P, 221 bar; feed conc., 10 wt% EtOH; 1.922g Ru/Al_2O_3 W/F_{Ao}, 5 s:14,200g cat*s/g-mol EtOH, 10 s: 25,200 cat*s/g-mol EtOH)

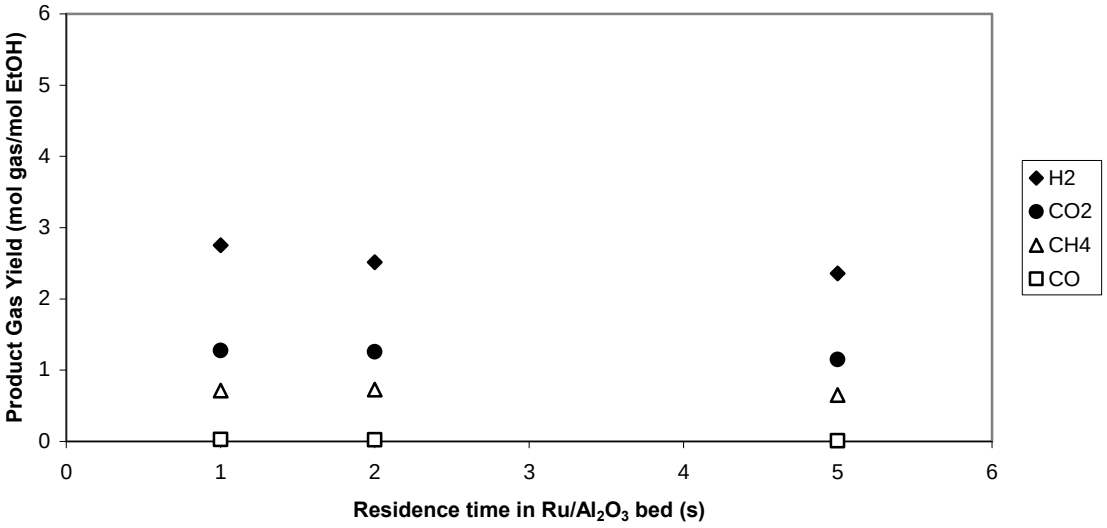

Figure 3.6: Effect of residence time on product yields (T, 700°C; P, 221 bar; feed conc., 10 wt% EtOH; 1.922g Ru/Al_2O_3)

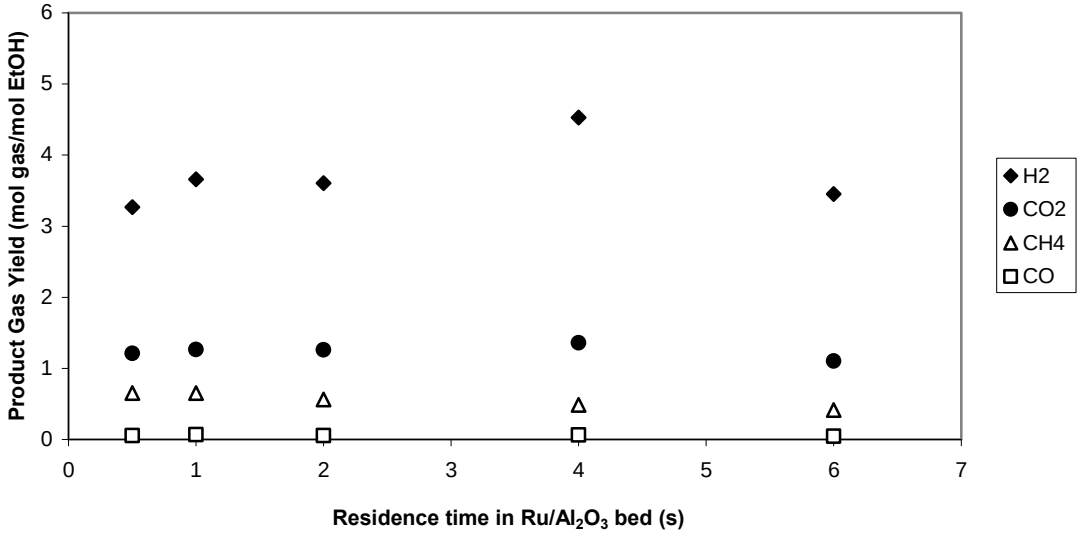

Figure 3.7: Effect of residence time on product yields (T, 800°C; P, 221 bar; feed conc., 10 wt% EtOH; 1.922g Ru/Al_2O_3)

3.4.3 Effect of Pressure. The effect of pressure on the hydrogen yield was studied at 700 °C, 10 wt% EtOH in the feed with a residence time of 2 s in the catalytic bed. As the pressure was raised from 221 bar to 276 bar, hydrogen yield was nearly constant, whereas CH_4, CO, and CO_2 yields increased from 0.73 to 0.88, 0.02 to 0.04, and 1.20 to 1.37, respectively. This trend is illustrated in Figure 3.8. These results suggest that methanation reaction of CO and CO_2 are slightly favored at higher pressures. Similar effect of pressure was also reported by Gadhe and Gupta[4] during the SCW reforming of methanol.

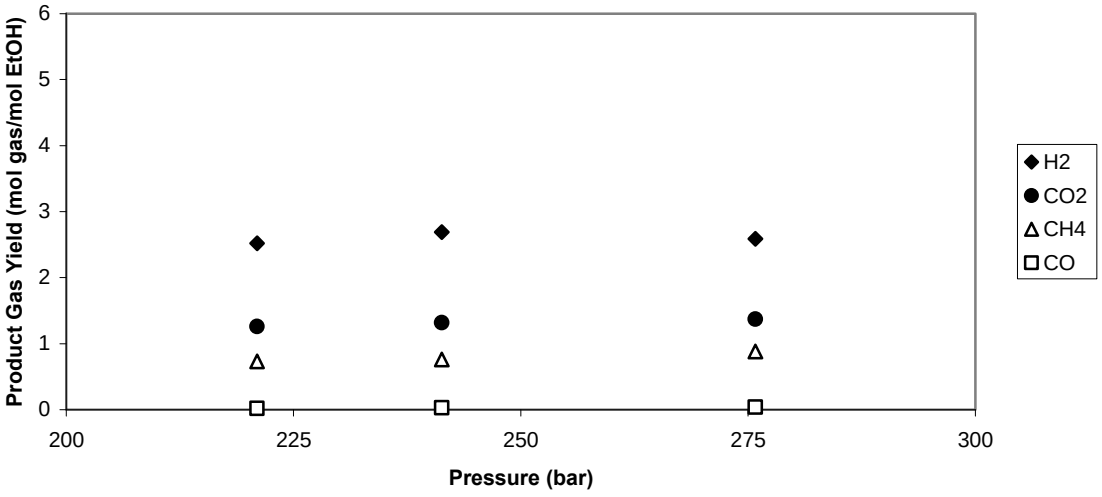

Figure 3.8: Effect of reactor pressure (T, 700°C; feed conc., 2 s in Ru/Al_2O_3 bed; 10wt% EtOH; 1.922 g Ru/Al_2O_3)

3.4.4 Effect of Temperature. Effect of temperature on H_2 yield was studied by varying the reactor temperature from 600 to 800 °C. As shown in Figure 3.9, only a small amount of hydrogen is formed at low temperatures indicating that direct reformation reaction of ethanol in SCW is favored at high temperatures (>700 °C). Two experiments

at 600 °C showed incomplete conversion of ethanol. The 5 and 10 s residence time experiments, detailed in Table 3.1, had conversions of 47.0 % and 98.4 %, respectively. With an increase in the temperature, the hydrogen and carbon dioxide yields increase, while the methane yield decreases. The yield of carbon monoxide also decreased as temperature increased and it was significantly lower than that of other species.

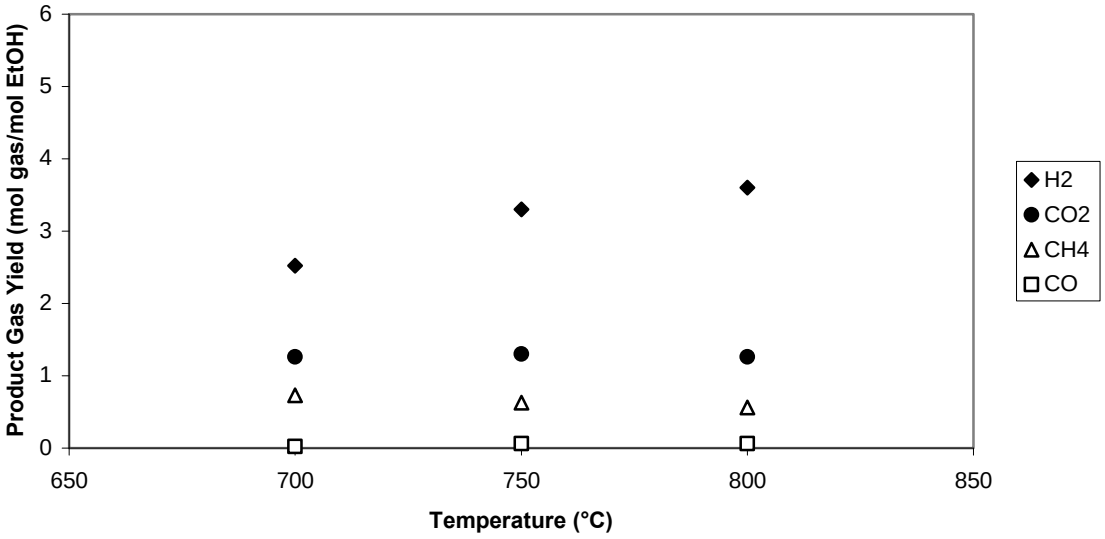

Figure 3.9: Effect of reactor temperature (P, 221 bar; 2 s residence time in Ru/Al_2O_3 bed; feed conc., 10wt% EtOH; 1.922 g Ru/Al_2O_3)

The high water excess leads to a preference for the formation of hydrogen and carbon dioxide instead of carbon monoxide. The formed intermediate carbon monoxide reacts with water via the water–gas shift reaction to hydrogen and carbon dioxide. The low carbon monoxide yield indicates that the water gas shift reaction approaches completion. The results indicate that water gas shift reaction is favorable at high temperature:

$$CO + H_2O \leftrightarrow CO_2 + H_2 \quad (3.2)$$

Due to this, the yield of H_2 increased significantly with the increase in temperature in SCW. It is also reported that the water gas shift reaction can take place non-catalytically in the supercritical reforming reactor.[37] Accordingly, the methane yield was low indicating the occurrence of methane reforming reaction.

$$CH_4 + H_2O \leftrightarrow CO + 3\ H_2 \quad (3.3)$$

No measurable quantity of carbon on the catalyst was observed during the course of the experiments up to an ethanol concentration of 10 wt%. This is probably due to the high water-to-carbon ratios and relatively higher gasification activity of the catalyst.

3.4.5 Effect of the Ethanol Concentration. The water-to-ethanol ratio is an important parameter for the economy of the process, which depends on the concentration of ethanol in the feed. To study the effect of the ethanol concentration on the H_2 yield, experiments were conducted by varying mass percent of ethanol from 5 to 20 wt%. The results, shown in Figure 3.10, show that there is a continuous decrease in the H_2 and CO_2 yields coupled with an increase in the CH_4 yield as the ethanol concentration in the feed was increased.

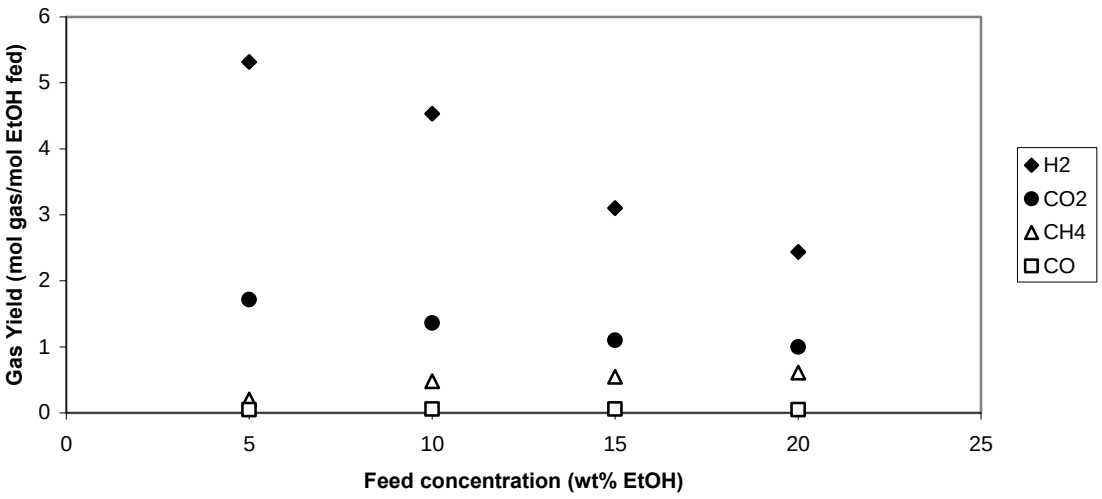

Figure 3.10: Effect of feed concentration of product gas yields (T, 800°C; P, 221 bar; residence time 4 s in Ru/Al_2O_3 bed, feed conc., 10 wt% EtOH; 1.922 g Ru/Al_2O_3)

It is well known that the methanation reaction is favored at high feed concentrations. The high water-to-ethanol ratio shifts the equilibrium of reactions backward, leading to a decrease in the CH_4 yield. Alternately, the higher amounts of water shifts the equilibrium of the water gas shift reaction to the right to produce more H_2 and CO_2. Probably at higher ethanol concentrations the active sites of the catalyst become saturated with adsorbed ethanol or derivative molecules. These adsorbed molecules prevent other next feed molecules from reaching the surface and reacting to form products. Dissociation of CO and H_2 takes place to form the intermediates, which combine in steps to form CH_4 (i.e., CO methanation reaction). At low water-to-ethanol ratios, the reaction shown below is suppressed due to low availability of water.

$$C_2H_5OH + H_2O \quad \leftrightarrow \quad 4H_2 + 2CO \qquad (3.4)$$

Another reaction which is largely responsible for formation of lighter hydrocarbon such as methane, ethylene, and ethane is decomposition and dehydration of ethanol.

$$C_2H_5OH \leftrightarrow CH_4+CO+H_2 \quad (3.5)$$

The pyrolysis of lighter hydrocarbons such as CH_4 and C_2H_6 occurs if the reaction is not properly controlled or if the residual molecules are not further reacted via an alternative chemical reaction. The repeated pyrolytic fragmentations of these may ultimately form coke via a variety of cyclization reactions. At high concentrations of ethanol (> 10 wt%) in SCW, there was some formation of carbon inside the reactor. Hence, low concentration of ethanol (<10 wt%) is favorable for improved hydrogen yield and for suppressing the CO concentration in the product stream.

3.4.6 Reaction Mechanism and Kinetics. Ideally, one mole of ethanol fed to the reactor would produce 6 moles of H_2 and 2 moles of CO_2. However, the presence of other species in the product stream indicates that reforming of ethanol in SCW occurs via several pathways. The following are the main possible reactions describing the overall ethanol reforming reaction in presence of Ru/Al_2O_3 catalyst.

$$C_2H_5OH + H_2O \leftrightarrow CO_2 + CH_4 + 2H_2 \text{ (reforming)} \quad (3.6)$$

$$CO + H_2O \leftrightarrow CO_2 + H_2 \text{ (water gas shift)} \quad (3.7)$$

$$CH_4 + H_2O \leftrightarrow CO + 3\ H_2 \text{ (reforming)} \quad (3.8)$$

Since the above reactions together represent the overall steam reforming of ethanol, it is important to consider all the three reactions simultaneously while developing the kinetic model. Additional reactions such as ethanol dehydrogenation to acetaldehyde and ethanol dehydration to ethylene may also contribute.[25,26] The elementary steps of ethanol SCW reforming reaction reveal that reforming occurs via formation of CH_3CHO, C_2H_4, C_2H_6 and CH_4 as the reaction intermediates. The initial step in the SCW reforming of ethanol is dehydrogenation, which is followed by the decomposition of CH_3CHO to CH_4 and CO, and finally CO is converted in to H_2 by the water gas shift reaction due to the presence of excess SCW and the active ruthenium catalyst. The formation of small amounts of ethylene during the reaction suggests the dehydration of ethanol.[38] However, in the presence of SCW, all these intermediates such as CH_4, C_2H_4, C_2H_6 and CH_3CHO undergo reforming to produce CO_2 and H_2. The results show that H_2 yield was higher at high temperature which happens at the expense of methane, ethylene and acetaldehyde. The mechanism of ethanol reforming is not available in presence of SCW. Based on theoretical calculations, Takahashi et al.[39] reported the direct participation of water molecules through a multi-center transition state including an ethanol molecule and several water molecules bridging the oxygen atom of ethanol and the α-hydrogen. They proposed a transition state consisting of an ethanol molecule and two water molecules. The transfer of hydrogen atoms among three molecules produces a hydrogen molecule, two water molecules and resulted in an oxidized molecule, acetaldehyde. Therefore, It can be deduced based on the experimental results that there is a formation of intermediate products (ABS) such as acetaldehyde, because of reaction between adsorbed ethanol and

SCW in gas phase.[6,18,38,39]. These adsorbed intermediates further react with water in the supercritical phase to give CO_2 and H_2. The overall reaction steps may be rewritten as[6]:

$$A + S \xleftrightarrow{k_1, k_{-1}} AS \tag{3.9}$$

$$AS + B \xrightarrow{k_2} ABS \tag{3.10}$$

$$ABS \xrightarrow{k_3} \text{Intermediates} \xrightarrow{k_4} CO_2 + H_2 \tag{3.11}$$

Where *A* and *B* denote the ethanol and water species and *S* represents an active site. Equation 3.9 represents the reversible adsorption of ethanol on the catalyst surface, and Equation 3.10 represents the reaction of adsorbed ethanol molecule with water to form a complex molecule *ABS*. The formation of adsorbed intermediates by decomposition of *ABS* was considered as the rate controlling step. Assuming the steady state hypothesis for the intermediate complex *ABS* and *AS*, the dependence of the rate (r) on reactant concentration (c) can be expressed as:

$$r = \frac{k_1 k_2 c_A c_B}{k_{-1} + k_1 c_A + k_2 c_B + (k_1 k_2 c_A c_B / k_3)} \tag{3.12}$$

Since in our experiments, water concentration is significantly high, c_B is assumed constant and the above expression is simplified as:

$$r = \frac{k_R c_A}{1 + b c_A} \tag{3.13}$$

where, k_R and b are lumped parameters defined as

$$k_R = \frac{k_1 k_2 c_{Bo}}{k_{-1} + b c_{Bo}} \tag{3.14}$$

and

$$b = \frac{k_1 + (k_1 k_2 c_{Bo} / k_3)}{k_{-1} + k_2 c_{Bo}} \tag{3.15}$$

The above equation was solved using a nonlinear regression technique on rate of hydrogen production at different ethanol partial pressures and reaction temperature. The values of rate constant k_R as calculated are reported in Table 3.2 with 95% confidence interval. From the temperature dependence of the rate constants, the activation energy of the reaction was found to be 65.3 kJ mol^{-1}. This value of activation energy is significantly lower than the values reported (96 kJ mol^{-1}) over Ru/Al_2O_3 catalyst,[18] and (82.7 kJ mol^{-1}) over Co/Al_2O_3 catalyst[21] for reforming of ethanol in subcritical water. The lower value reported here may be attributed to the nature of the reforming media, supercritical water. Low viscosity coupled with high diffusivity can overcome mass transfer limitations present in atmospheric steam reforming, resulting in faster rate of reaction and lower activation energy.

Table 3.2: Values of rate constants at different temperatures

T (°C)	k_R (μmol/g cat-s-bar)
800	5.2±1.2
750	4.5±0.9
700	2.5±0.6

3.5 Conclusions

Supercritical reforming of ethanol over Ru/Al_2O_3 catalyst is effective for the production of high pressure hydrogen with low methane and carbon monoxide. Full conversion of ethanol to gaseous products is seen above 700°C. The hydrogen yield increases with increasing temperatures, and is unaffected by pressure changes in the supercritical region studied. The methanation reaction can be reduced by keeping low residence times and a high water-to-ethanol ratio in the feed. The product composition is affected by the reactor temperature, residence time and water-to-ethanol ratio in the feed and contained mainly hydrogen, carbon dioxide, methane, and carbon monoxide. The complete conversion of ethanol is possible during supercritical water reforming over Ru/Al_2O_3 catalyst for producing high hydrogen yield with low concentrations of methane and carbon monoxide in product. Carbon formation was negligible for ethanol concentrations below 10 wt%. The activation energy for the reaction was found to be 65.3 kJ mol^{-1}.

3.6 Acknowledgment

This research was partially supported by the U.S. Department of Energy through the Office of Fossil Energy (FE), National Energy Technology Laboratory (NETL), under DOE Contract DE-FC26-05424.56 via the Consortium of Fossil Fuel Science.

3.7 References

1. Torres, J.A.; Llorca, J.; Casanovas, A.; Domınguez, M.; Salvado J., Monta D., *Journal of Power Sources*, 2006, *169*,(1), **2007**, 158-166.

2. Freni, S.; Calogero, G.; Cavallaro, S. *J. Power Sources* **2000**, *87* (1-2), 28-38.

3. Patel, S.; Pant K.K. *J. Power Sources* **2006,** *159* (1), 139-143.

4. Gadhe, J.B.; Gupta, R.B.; *Ind. Eng. Chem. Res.* **2005**, *44*, 4577-4585.

5. Pinkwart, K.; Bayha, T.; Lutter, W.; Krausa, M. *J. Power Sources* **2004**, *136* (2), 211-214.

6. Byrd, A. J.; Pant, K. K.; Gupta, R.B. *Ind. Eng. Chem. Res.* **200**7, *46*, 3574-3579.

7. Antal, M. J., Jr.; Allen, S. G.; Schulman, D.; Xu, X.; Divilio, R. J. *Ind. Eng. Chem. Res.* **2000**, *39* (11), 4040-4053.

8. Yoshida, T.; Oshima, Y. *Ind. Eng. Chem. Res.* **2004**, *43* (15), 4097-4104.

9. Watanabe, M.; Inomata H.; Arai, K.; *Biomass and Bioenergy* **2002**, *22*, 405-410.

10. Osada, M.; Sato,T.; Watanabe, M.; Adschiri,T.; Arai, K. *Energy & Fuels* **2004,** *18*, 327-333.

11. Williams P.; Onwundili J. *Energy and Fuels*, **2006,** *20* (3), 1259-1265.

12. Cortright, R. D.; Davda, R. R.; Dumesic, J. A. *Nature* **2002**, *418*, 964-967.

13. Penninger J. M. L.; Rep, M. *Int. J. of Hydrogen Energy* **2006,** *31*, 1597-1606.

14. Kruse, A.; Henningsen, T.; Sinag, A.; Pfeiffer, J. *Ind. Eng. Chem. Res.* **2003**, *42* (16), 3711-3717.

15. Hao, X. H.; Guo, L. J.; Mao, X.; Zhang, X. M.; Chen, X. J. *Int. J. Hydrogen Energy* **2003**, *28* (1), 55-64.

16. Yu, D.; Aihara, M.; Antal, M. J., Jr. *Energy and Fuels* **1993**, *7* (5), 574-577.

17. www.sciencedaily.com/releases/2004/02/040214081412.htm, May 2007.

18. Vaidya, P.V.; Rodrigues, A.E. *Ind. Eng. Chem. Res.* **2006**, 45, 6614-6618.

19. Patel, S.; Pant, K.K. *Chemical Eng. Sci*. **2007,** 62, 5425-5435

20. Xu, J.; Froment, G. F. *AIChE J.* **1989**, *35* (1), 88-96.

21. Sahoo, D.R; Vajpai, S.; Patel, S.; Pant, K.K. *Chemical Eng. Journal* **2007,** *125*(3) 139-147.

22. Fierro, V.; Akdim, O.; Mirodatos, C. *Green Chem.* **2003,** *5*, 20-24.

23. Berman, A.; Karn, R.K.; Epstein, M. *Applied Cat. A* **2005,** *282*, 73-83.

24. Liguras, D.K.; Kondarides, D.I.; Verykios, X.E. *Applied Cat. B* **2003,** *43* 345-354.

25. Arita, T.; Nakahara, K.; Nagami, K.; Kajimoto, O. *Tetrahedron Lett.* **2003**, *44* (5), 1083-1086.

26. Taylor, J. D.; Herdman, C.M.; Wu, B.C.; Wally, K.; Rice, S.F. *Int. J. Hydrogen Energy* **2003**, *28*, 1171-1178.

27. Xu, X.; Matsumura, Y.; Stenberg, J.; Antal, M. J., Jr. *Ind. Eng. Chem. Res.* **1996**, *35* (8), 2522-2530.

28. Boukis, N.; Diem, V.; Galla, U.; Dinjus,E. *Combust. Sci. and Tech.* **2006**, *178*, 467-485.

29. Boukis, N.; Galla, U.; D'Jesus, P.; Müller,H.; Dinjus,E. *14th European Conference on Biomass for Energy, Industry and Climate Protection* 17-21 October 2005, Palais des Congrès, Paris, France, 964-967.

30. Diem, V.; Boukis, N.; Hauer, E.; Franz, G.; Dinjus, E. *7th Italian Conf. on Supercritical Fluids and their Applications* Trieste, Italy, June 13-16, 2004.

31. Boukis, N.; Galla, U.; Diem, V.; Dinjus, E. *Science in Thermal and Chemical Biomass Conversion*, 30 August to 2 September 2004, Vancouver Island, BC, Canada, *2*, 975-990.

32. Diem, V.; Boukis, N.; Hauer, E.; Dinjus,E. *Chemical Engineering Transactions* **2004,** *4*, 99-104.

33. Boukis, N.; Galla, U.; Diem, V.; D'Jesus, P.; Dinjus, E.; *2nd World Conference and Technology Exhibition on Biomass for Energy, Industry and Climate Protection* 10 - 14 May 2004, Rome, ETA-Florenz, 738-741.

34. Diem, V.; Boukis, N.; Habicht, W.; Dinjus, E. *Proceedings of the 6th International Symposium on Supercritical Fluids* 28-30 April 2003, Versailles, France, Tome 2.

35. Diem, V.; Boukis, N.; Habicht, W.; Hauer, E.; Dinjus, E. *The Sixth Italian Conference on Chemical and Process Engineering*, 8-11 June 2003, Pisa, Italy, AIDIC Conference Series, Vol. 6, 101-108.

36. Boukis, N.; Diem, V.; Habicht, W.; Dinjus, E. *Ind. Eng. Chem. Res*. **2003**, *42*, 728-735.

37. Lee, S.; Lanterman, H.B.; Wenzel, J.E.; Picou, J.; Factor, M.; Leavitt, L. *Preprints-Am. Chem. Soc. Div. Petr. Chem* **2006,** *51*, 487-490.

38. Xu X.; DeAlmedia, C.P.; Antal, M. Jr.; *Ind. Eng. Chem. Res.* **1991,** *30*, 1478-1475.

39. Takahashi, H.; Hisaoki, S.; Nitta, T. *Chem. Phys. Lett.* **2002**, *363*, 80-86.

4. Hydrogen Production from Glycerol by Reforming in Supercritical Water over Ru/Al_2O_3 Catalyst

4.1 Abstract

Supercritical water is a promising medium for the reforming of hydrocarbons and alcohols for the production of hydrogen at high pressures in a short reaction time. Water serves both as a dense solvent as well as a reactant. In this work, hydrogen is produced from glycerol by supercritical water reforming over a Ru/Al_2O_3 catalyst with low methane and carbon monoxide formation. Experiments were conducted in a tubular fixed-bed flow reactor over a temperature range of 700-800°C, feed concentrations up to 40 wt% glycerol, all at short reaction time of less than 5 seconds. Glycerol was completely gasified to hydrogen, carbon dioxide, and methane along with small amounts of carbon monoxide. At dilute feed concentrations, near theoretical yield of 7 mole of hydrogen/mol of glycerol was obtained, which decreases with an increase in the feed concentration. Based on a kinetic model for glycerol reforming, an activation energy of 55.9 kJ/mol was observed.

4.2 Introduction

Growing energy demands in a time of dwindling fossil fuel supplies has attracted much attention to hydrogen as an energy carrier. Biomass too has received significant attention as an alternate energy source because it is renewable and essentially a carbon dioxide neutral since CO_2 generated during the fuel use is subsequently fixed by growing plants during photosynthesis. Glycerol, $HOCH_2$-CHOH-CH_2OH, is obtained as a byproduct from biodiesel manufacturing by transesterification of vegetable oils.

Approximately 1 kg of glycerol is produced for every 9 kg of biodiesel. In only year 2004 to 2006, annual US biodiesel production has increased from 25 to 250 million gallons.[1] Johnston and Holloway[2] project a US biodiesel production potential of almost 850 million gallons per year. With increasing production of biodiesel, an excess of glycerol is expected to flood the market, and therefore it is essential to find new uses. Currently, glycerol is used in many applications including personal care, food, oral care, tobacco, polymers, and pharmaceuticals. Another use is the production of 1,2-propanediol and 1,3-propanediol by hydrogenation of glycerol, replacing the petroleum feedstock used presently.[3] Another emerging use is to utilize glycerol for the production of hydrogen. The topic of glycerol reforming for hydrogen production has received some attention in the literature.[4-10] Shabaker and Dumesic[6] produced hydrogen from biomass-derived oxygenated hydrocarbons including glycerol in an aqueous phase reforming process. Czernik and co-workers[7] have produced hydrogen via steam reforming of crude glycerol using a commercial nickel based naphtha reforming catalyst. Hirai et al.[8] have reported the performance of noble metal based catalysts for glycerol reforming and found ruthenium to be the most active of the Group 8-10 metals.

Recently, Adhikari[11] et al. performed a thermodynamic analysis for hydrogen production by steam reforming of glycerol. Their study revealed that the best conditions for producing hydrogen is at a temperature > 625 ^{o}C and a molar ratio of water to glycerol of 9:1. Under these conditions methane production is minimized and carbon formation is thermodynamically inhibited. Although excess water in the feed increases the hydrogen production, a significant amount of unreacted water remains in the reactor effluent. Corma et al.[12] have studied the biomass derived feeds, glycerol and sorbitol,

using fluidized catalytic cracking and reported a wide range of products including hydrogen, paraffins, olefins, aromatics, and coke.

Supercritical water (SCW) reforming of hydrocarbons and biomass materials has been paid more attention recently.[13-18] Kersten et al.[19] have reported gasification results for glycerol and other model compounds in a variety of catalytic and non-catalytic reactors in SCW and found that without addition of a catalyst, only very dilute concentrations of model biomass feeds could be completely gasified. SCW has properties entirely different from those of liquid water or steam. The dielectric constant of SCW is much lower, and the number of hydrogen bonds is much lower and their strength is weaker. Therefore SCW has high miscibility with many organic solvents and gases. The density of SCW is higher than that of steam resulting in a higher space time yield, and higher thermal conductivity and specific heat, which are helpful in carrying out the endothermic reforming reactions. Transport properties, too, are unique in that SCW has both low viscosity and high diffusivity. The formation of char and tar is also minimized because of the solubility of hydrocarbons in SCW. Importantly, hydrogen produced from SCW reforming is produced at high pressure, which can be stored directly, thus avoiding large expenses associated with compression.

Reforming of glycerol for hydrogen production can be summarized by following reactions.

First, the steam reforming of glycerol:

$$C_3H_8O_3 \xrightarrow{H_2O} 3\ CO + 4\ H_2 \qquad (4.1)$$

Followed by the water-gas shift reaction:

$$CO + H_2O \rightarrow CO_2 + H_2 \qquad (4.2)$$

The desired overall reaction is then summarized as:

$$C_3H_8O_3 + 3\ H_2O \rightarrow 7\ H_2 + 3CO_2 \quad (4.3)$$

Some hydrogen is also lost via the methanation of CO and CO_2:

$$CO + 3\ H_2 \rightarrow CH_4 + H_2O \quad (4.4)$$

$$CO_2 + 4\ H_2 \rightarrow CH_4 + 2H_2O \quad (4.5)$$

As a result, the product stream is a mixture of above gases. Furthermore, the yield of hydrogen depends on several process variables, such as system pressure, temperature, and water-to-glycerol feed ratio.

Most of the above studies were done in batch mode, in which the biomass/water/catalyst is loaded in a small steel tube reactor and then sealed and placed in an oven. After the reaction, the mixture is quenched and analyzed. Typical reaction time varied from minutes to hours. In our recent work on methanol and glucose reforming, it was observed that high reaction time leads to the secondary reaction of methane formation.[13-14] To limit the methane formation reaction time needs to be limited to the order of seconds. The aim of this study is to examine hydrogen production from glycerol in SCW in a continuous reactor with a short reaction time (of the order of seconds). Ru/Al_2O_3 is selected as a catalyst. The effects of the process variables such as temperature, contact time, and water to glycerol ratio on hydrogen yield are investigated.

4.3 Experimental Section

4.3.1 Materials. Glycerol (99.5% purity) was obtained from Fisher Scientific. The commercial 5 wt% Ru/Al_2O_3 catalyst was purchased unreduced from Aldrich, and was

subsequently reduced under hydrogen flow at 500 °C for 6 hours. The catalyst had the following characteristics: total BET surface area: 100 m^2/g; crystal structure: amorphous; specific pore volume: 0.30 mL/g; density: 0.95 g/cm^3. Deionized water was obtained from a Millipore Direct-Q 5 water purification system.

4.3.2 Experimental Procedure. The schematic diagram of the experimental apparatus is shown in Figure 4.1. The details of the experimental procedure are discussed elsewhere[14], and are briefly provided here. Experiments were conducted in supercritical water in a fixed bed tubular flow reactor (0.5 m long, 0.25" OD and 0.12" ID) made of Inconel 600 (Microgroup) having a composition of 73% Ni, 18% Cr, and 9% Fe, which was placed inside a temperature controlled furnace (Thermolyne 21100) covered on each end to reduce heat loss and ensure temperature uniformity. The reactor was packed with 2 g catalyst. The details of experimental conditions are given in Table 4.1.

A glycerol-water solution from a feed reservoir was pumped to a tee using a HPLC pump (Waters 590). Due to the hygroscopic nature of glycerol, batches of pure glycerol were diluted with water to 66.7 wt% and kept covered to prevent absorption of additional water from the atmosphere. The glycerol solution then mixes with a stream of supercritical water, also by HPLC pump (Alltech 301), heated to the reaction temperature. The reactor temperature at the exit of the furnace was measured using a type-K thermocouple with a tee arrangement. The gas mixture exiting the reactor was cooled using a water-cooled double pipe heat exchanger made of SS 316 tubing. The pressure was let down to the ambient by means of a back pressure regulator (Straval).

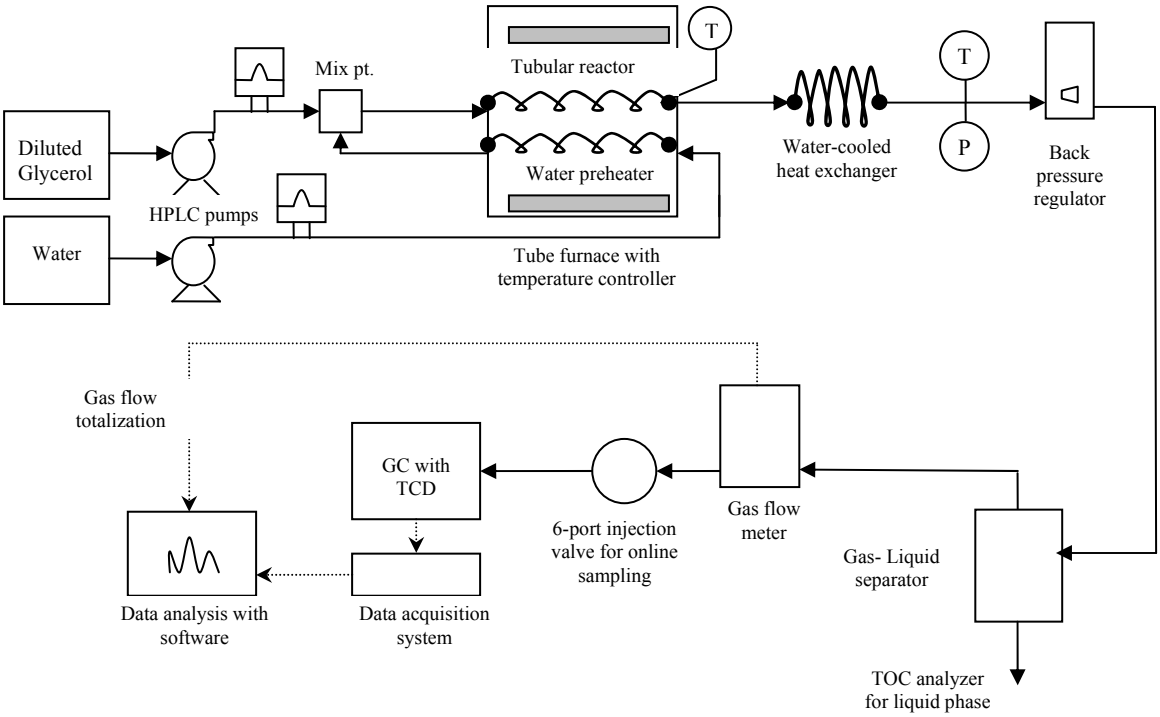

Figure 4.1: Schematic of SCW hydrogen production apparatus

Table 4.1: Details of experimental conditions

Reactor Temp.[a] °C	Reactor Pressure bar	Feed Conc. wt%	Residence Time s	W/F_{Ao} g cat-s/ μmol glycerol	Product Gas Composition (mol%) H_2	CO	CH4	CO_2	H_2 Yield mol gas/ mol glycerol fed
800	241	5	4	0.353	45.3	0.0	19.6	35.2	2.0
800	241	5	2	0.221	49.4	0.0	15.9	34.7	2.8
800	241	5	1	0.137	70.0	1.1	3.7	25.2	6.5
800	241	15	1	0.050	57.9	0.6	10.7	30.9	4.1
800	241	20	1	0.035	53.5	2.2	11.5	32.9	3.9
800	241	30	1	0.023	47.2	3.2	15.6	34.0	2.9
800	241	35	1	0.022	46.5	3.8	16.8	32.9	2.6
800	241	40	1	0.019	42.2	4.3	18.9	34.6	2.2
750	241	2.5	1	0.243	66.9	0.1	3.9	29.1	5.8
750	241	5	1	0.137	66.2	1.2	3.6	29.0	6.1
750	241	15	1	0.045	56.9	2.0	9.6	31.5	4.4
750	241	30	1	0.023	46.5	3.4	15.8	34.4	2.6
700	241	5	1	0.134	63.5	0.7	6.7	29.1	5.1

[a] Uncertainty ±3°C

The gas-liquid mixture was separated in a glass phase-separator having gas tight valves to prevent the escape of gases. The exit gas flow rate was measured using a gas flow meter (Omega FMA-1600). The gas composition was determined using a gas chromatograph (SRI 8610C) equipped with a thermal conductivity detector (TCD) and a 60/80 Carboxen-1000 carbon molecular sieve column (Supelco 15'x1/8") using nitrogen as the carrier gas. Sample injection to the gas chromatograph was done online by means of a six-port injection valve (Valco) having a 100 μL sample loop. The total organic carbon (TOC) content of the liquid effluent was measured using a TOC analyzer (Shimazdu TOC-V_{CSN}).

All measurements were taken at least in triplicate to ensure accuracy, which were further checked by calculating the overall carbon balance for the system. Scattering in the data of the totalized gas flow rate measured by the flow meter was less than 1%. The error in the dry gas composition obtained by the GC analysis was typically less than 2%. The overall error in the calculation of gas yields due to the errors introduced by the individual analysis techniques and experimental error was found to be less than 5%. Experimental results in which the carbon exiting the system was calculated to differ by more than 10% of the known amount entering were discarded.

4.4 Results and Discussion

Production of hydrogen and other compounds at different temperatures, water to glycerol feed ratios, and residence times have been analyzed. Supercritical reforming of glycerol produced a stream rich in H_2 and CO_2 with small amounts of CH_4 and CO. Over the temperature, residence times, and water to glycerol mass ratio ranges analyzed, the conversion of glycerol was always greater than 99%, and it can be considered that the

conversion was complete. Our previous study[20] showed that changing pressure has minor effect in the supercritical region, thus only one pressure was studied. Thermodynamic equilibrium calculations were done by minimizing Gibbs free energy using Peng-Robinson equation of state in CHEMCAD 5.2.0. The calculated results are shown as solid lines in Figures 4.2-4.4. The simulation did not predict coke formation for any of the experimental conditions in this paper.

4.4.1 Effect of Reaction Time. Residence time in the catalyst bed was controlled by the inlet flowrate of reactants. The product gas yields are shown as a function of residence time in Figure 4.2. The residence times of 1, 2 and 4 seconds correspond to space time (mass of catalyst in bed/molar flow rate of glycerol, W/F_{Ao}) values of 0.136, 0.221, and 0.353 g cat-s/μmol glycerol, respectively. The shortest residence time gave high hydrogen yield, however at larger residence times the hydrogen yield drops sharply with a decline in CO_2 yields as well. Considering this along with the increase in methane suggests that Equation 4.5, the methanation of carbon dioxide, becomes important at longer residence times. Hence, it is desirable to keep residence time short in order to maximize the hydrogen yield.

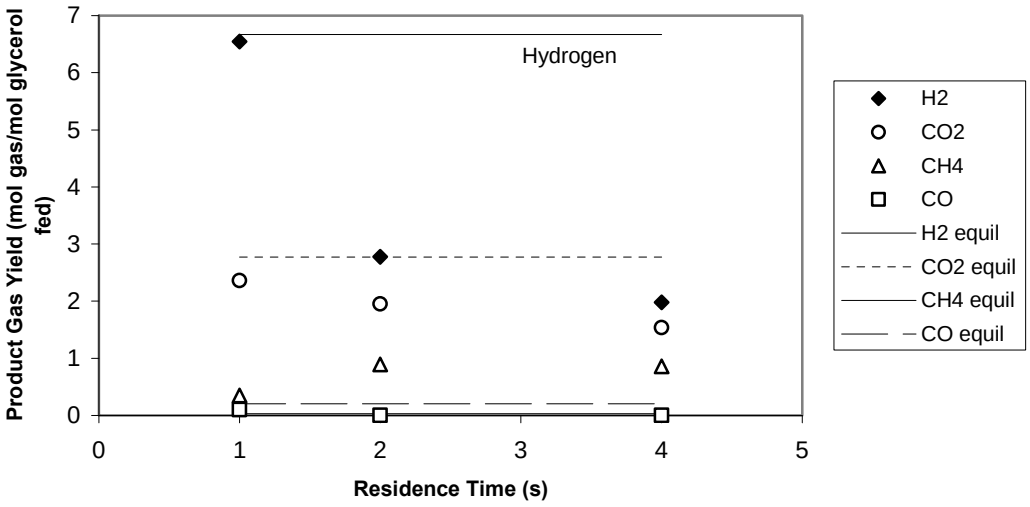

Figure 4.2: Effect of residence time on product gas yields. T: 800°C, P: 241 bar, feed conc.:5 wt% glycerol, 2.0 g Ru/Al_2O_3 catalyst

4.4.2 Effect of Temperature. The influence of temperature was studied by varying the furnace temperature from 700 to 800°C. Hydrogen yield increases with temperature as shown in Figure 4.3. It can also be seen that the methane yield is slightly higher at 700°C. The same trend is present in the calculated equilibrium concentration with slightly more methane present at lower temperatures. It should be noted that continued operation at 700 °C for feed concentrations greater than 5 wt% glycerol resulted in plugging of the reactor, however this problem was solved by operating at 800 ^{o}C. At lower temperatures, the reaction rates for reactions leading to coke formation are higher than the rates of the reforming and carbon gasification reactions.[21] At temperatures below 800°, the experimental hydrogen yield is lower than the equilibrium values, but is accompanied by higher than predicted methane yield.

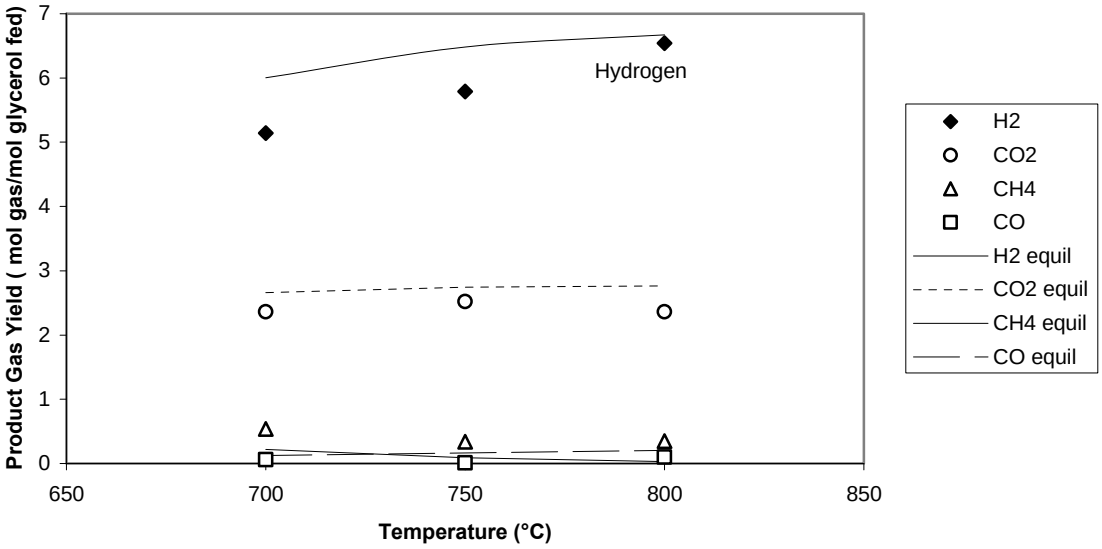

Figure 4.3: Effect of temperature on product gas yields. P: 241 bar, 1 s residence time, feed conc.: 5 wt%, 2.0 g Ru/Al_2O_3

4.4.3 Effect of Glycerol Feed Concentration. Feed concentration is an important economic consideration, it is not desirable to heat and pump more water through the system than is necessary. To study the effect of feed concentration, the glycerol concentration was varied from 5 – 40 wt% glycerol. Figure 4.4 shows that increasing the feed concentration was coupled with a decrease in the yield of hydrogen and an accompanying increase in the methane yield. This can be explained by considering that less water is present at the higher concentrations, and it is known that at low steam/carbon ratios CO is more likely to produce methane by consuming hydrogen.[22] The carbon balance showed that complete conversion of glycerol to gaseous products was realized even for the highest feed concentrations tested. It can be seen that the experimental gas yields closely mirror the equilibrium concentrations calculated from

simulation, indicating that the reaction is near its thermodynamic equilibrium. For higher concentrations, experimental carbon monoxide yields are smaller than predicted at equilibrium. Paired with higher than predicted hydrogen and carbon dioxide yields, this indicates the water-gas shift reaction going near completion.

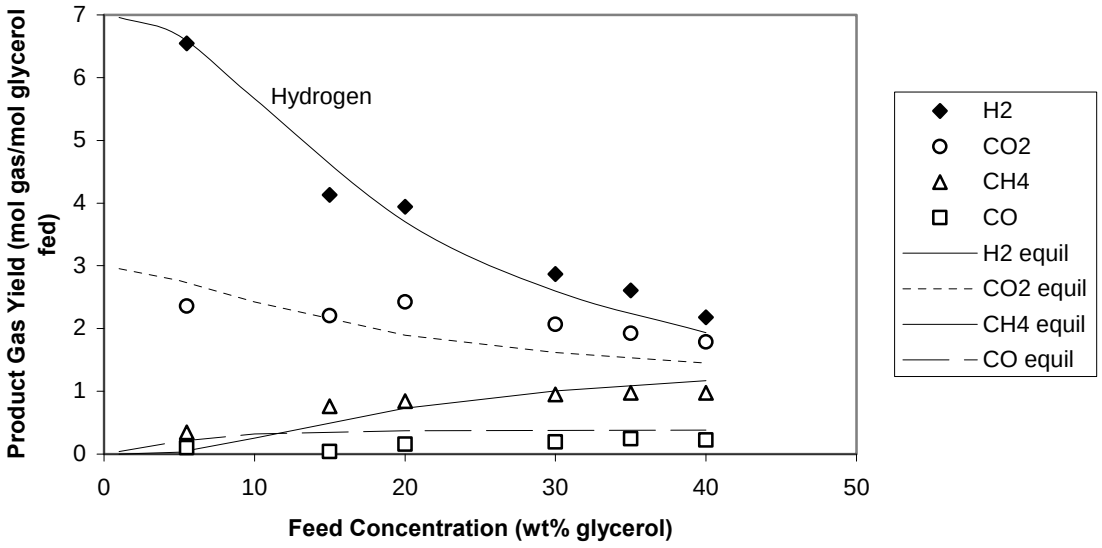

Figure 4.4: Effect of glycerol feed concentration on product gas yields. T: 800°C, P: 241 bar, 1 s residence time, 2.0 g Ru/Al_2O_3 catalyst

4.4.4 Reaction Kinetics. The reforming of oxygenated hydrocarbons entails a complex network of reactions. Adsorption and decomposition of oxygenated compounds containing hydroxyl groups such as methanol and ethylene glycol has been studied extensively on noble metal surfaces. Oxygenated compounds containing hydroxyl groups have been shown to adsorb to the catalytic Ru surface predominantly through one or more oxygen atoms. First the reactant undergoes dehydrogenation on the catalyst surface, followed by subsequent cleavage of C-C or C-O bonds. Cleavage of C-C bonds leads to synthesis gas which is subjected to the water-gas shift reaction and possible

methanation, while cleavage of C-O bonds gives organic acids and alcohols.[3] The ruthenium catalyst is known to have a high activity for C-C bond scission.[23] Very low levels of organic carbon in the liquid effluent suggests that any intermediate alcohol or organic acids formed from C-O bond breaking were further reacted to gaseous products. Hence, the following kinetic model is proposed for the reforming of glycerol in supercritical water:

$$A + S \xleftrightarrow{k_1, k_{-1}} AS \tag{4.6}$$

$$AS + B \xrightarrow{k_2} ABS \tag{4.7}$$

$$ABS \xrightarrow{k_3} \text{Intermediates} \xrightarrow{k_4} CO_2 + H_2 \tag{4.8}$$

where, *A* and *B* represent glycerol and water, respectively, and *S* represents an active site on the catalyst surface. Equation 4.6 describes the reversible adsorption of glycerol on the catalyst, and Equation 4.7 represents the reaction of the adsorbed glycerol with water to form an adsorbed complex molecule, *ABS*. Assuming steady state of adsorbed intermediates and that decomposition of *ABS* to form intermediate products is the rate-limiting step, the dependence of rate (*r*) on partial pressures (*p*) can be expressed as:

$$r = \frac{k_1 k_2 p_A p_B}{k_{-1} + k_1 P_A + k_2 p_B + (k_1 k_2 p_A p_B / k_3)} \tag{4.9}$$

Considering that water is in excess, Equation 4.9 may be simplified to:

$$r = \frac{k_R p_A}{1 + b p_A} \tag{4.10}$$

where k_R and b are lumped parameters defined as:

$$k_R = \frac{k_1 k_2 p_{Bo}}{k_{-1} + b p_{Bo}} \tag{4.11}$$

and

$$b = \frac{k_1 + (k_1 k_2 p_{Bo} / k_3)}{k_{-1} + k_2 p_{Bo}} \tag{4.12}$$

Equation 4.10 was solved using a regression on rate of hydrogen production for several values of partial pressures of glycerol at 750 and 800°C. Calculated values of k_R are 1.9 x 10^{-5} and 2.6 x 10^{-5} *μmol/g cat-s-bar* at 750°C and 800°C, respectively. Based on the temperature dependence of the rate constant, activation energy E_a for the reaction was found to be 55.9 kJ/mol. Glycerol reforming experiments were continued to evaluate the catalyst activity loss due to carbon formation. There was negligible change in reaction rate and hydrogen product yield as same catalyst was used for all the runs without any regeneration. Dispersion of Ru was not measured, but it is expected that it should decrease under the operating conditions used. Kellner and Bell[24] have reported previously that decreased dispersion can result in increased methane formation. Our recent study[18] found changes to the catalyst support after exposure to supercritical water. SEM images and XRD spectra showed that crystallinity increased in our previous study using this amorphous catalyst support, as shown in Figure 4.5. The fresh catalyst consists of more-or-less round particles, characteristic of amorphous materials, whereas the used catalyst is clustered in aggregates of sharp-edged crystals. It is expected that the catalyst support underwent similar morphological changes in the present study.

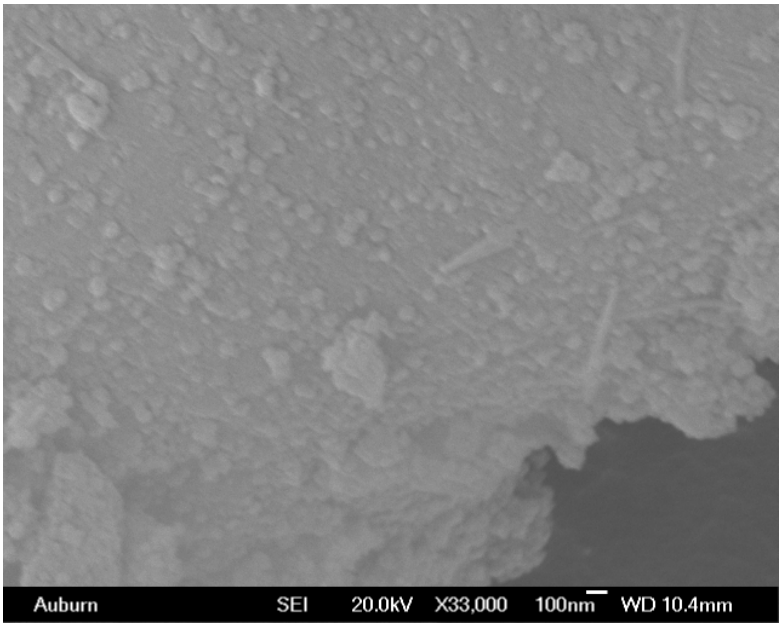

(a)

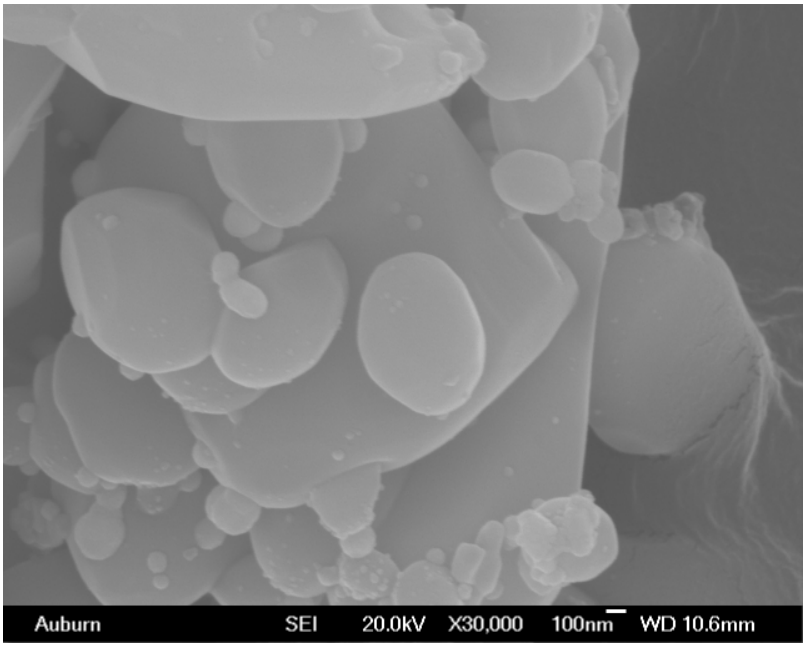

(b)

Figure 4.5: SEM images of fresh (a) and used (b) Ru/Al_2O_3 catalysts.

4.5 Conclusions

Reforming of glycerol in supercritical water over Ru/Al_2O_3 catalyst is an effective means of high pressure hydrogen production from a biomass-derived source. Although near-theoretical hydrogen yields were obtained for dilute glycerol concentrations at 800°C, it was also found to be possible to completely gasify feed containing upto 40 wt% glycerol, but with increased methane formation. Hydrogen yields were found to increase directly with temperature. Methane formation can be reduced by operating at low residence times. Values of the rate constant based upon a simplified kinetic model are reported at 750 and 800°C, and based upon those an activation energy of 55.9 kJ/mol was observed.

4.6 Acknowledgment

This research was partially supported by Alabama Center for Paper and Bioresource Engineering, and the U.S. Department of Energy through the Office of Fossil Energy (FE), National Energy Technology Laboratory (NETL), under DOE Contract DE-FC26-05424.56.

4.7 References

1. < http://www.biodiesel.org/pdf_files/fuelfactsheets/backgrounder.PDF> accessed 29 February 2008.

2. Johnston, M and Holloway, T. A Global Comparison of National Biodiesel Production Potentials. Env Sci and Tech 2007; 41: 7967-73.

3. Montassier, C, Menezo, JC, Hoang, LC, Renaud, C, Barbier, J. Aqueous polyol conversions on ruthenium and on sulfur-modified ruthenium. J. Molecular Catalysis 1991; 70: 99-110

4. Cortright RD, Davda RR, Dumesic JA. Hydrogen from catalytic reforming of biomass-derived hydrocarbons in liquid water. Nature 2002;418:964–6.

5. Davda RR, Shabker JW, Huber GW, Cortright RD, Dumesic JA. A review of catalytic issues and process conditions for renewable hydrogen and alkanes by aqueous phase reforming of oxygenated hydrocarbons over supported metal catalysts. App Cat B: Environ 2005;56: 171–86.

6. Shabaker JW, Dumesic JA. Kinetics of aqueous-phase reforming of oxygenated hydrocarbons: Pt/Al2O3 and Sn-modified Ni catalyst. Ind Eng Chem Res 2004; 43(12): 3105– 12.

7. Czernik S, French R, Feik C, Chornet E. Hydrogen by catalytic steam reforming of liquid byproducts from biomass thermoconversion process. Ind Eng Chem Res 2002;41: 4209–15.

8. Hirai, T, Ikenaga N, Miyake T, Suzuki T. Production of Hydrogen by Steam Reforming of Glycerin on Ruthenium Catalyst. Energy and Fuels 2005;19: 1761-62.

9. Zhang B, Tang X, Li, Y, Xu Y, Shen W. Hydrogen production from steam reforming of ethanol and glycerol over ceria-supported metal catalysts. Int J of Hyd Energy 2007; 32: 2367-73

10. Simonetti D A, Kunkes E L, Dumesic J A. Gas-phase conversion of glycerol to synthesis gas over carbon-supported platinum and platinum-rhenium catalysts. Journal of Catalysis 2007; 247: 298-306.

11. Adhikari S, Fernando S, Haryanto A. A Comparative Thermodynamic and Experimental Analysis on Hydrogen Production by Steam Reforming of Glycerin. Energy and Fuels 2007; 21: 2306-10

12. Corma A, Huber G, Sauvanaud L, O'Connor, P. Processing biomass-derived oxygenates in the oil refinery: Catalytic cracking (FCC) reaction pathways and role of catalyst. Journal of Catalysis 2007; 247: 307-27.

13. Gadhe JB, Gupta RB. Hydrogen Production by Methanol Reforming in Supercritical Water: Suppression of Methane Formation**.** Ind Eng Chem Res 2005; 44: 4577-85

14. Byrd AJ, Pant KK, Gupta RB. Hydrogen Production from Glucose Using Ru/Al2O3 Catalyst in Supercritical Water. Ind Eng Chem Res 2007;46: 3574-79.

15. Penninger JML, Maass GJJ, Rep M. Compressed hydrogen-rich fuel gas (CHFG) from wet biomass by reforming in supercritical water. Int J Hyd Energy 2007;32: 1472-76.

16. Penninger JML, Rep M. Reforming of aqueous wood pyrolysis condensate in supercritical water. Int J Hyd Energy 2006;31: 1597-1606.

17. Lu Y, Guo L, Zhang X, Yan Q. Thermodynamic modeling and analysis of biomass gasification for hydrogen production in supercritical water. Chem Eng J 2007;131: 233-44.

18. Lu YJ, Guo LJ, Ji CM, Zhang XM, Hao XH, Yan QH. Hydrogen production by biomass gasification in supercritical water: A parametric study. Int J Hyd Energy 2006;31: 822-31.

19. Kersten SRA, Potic B, Prins W, Van Swaaij WPM. Gasification of Model Compounds and Wood in Hot Compressed Water. Ind Eng Chem Res 2006;45: 4169-77.

20. Byrd, AJ, Pant KK, Gupta RB. Hydrogen Production from Ethanol by Reforming in Supercritical Water using Ru/Al_2O_3 Catalyst. Energy and Fuels 2007; 21: 3541-47

21. Coll, R, Salvado, J, Farriol, X, Montane, D. Steam reforming model compounds of biomass gasification tars: conversion at different operating conditions and tendency towards coke formation. Fuel Processing Tech 2001; 74: 19-31.

22. Xue, E, O'Keeffe, M, Ross, JRH. Water-gas shift conversion using a feed with a low steam to carbon monoxide ratio and containing sulfur. Cat Today 1996; 30:107-18.

23. Sinfelt, John H.; Yates, David J.C. Catalytic hydrogenolysis of ethane over the noble metals of Group VIII J. Catalysis 1967;8: 82-90.

24. Kellner, C and Bell, A. Effects of dispersion on the activity and selectivity of alumina-supported ruthenium catalysts for carbon monoxide hydrogenation. J Catal 1982; 75:251-61.

5. Hydrogen Production from Catalytic Gasification of Switchgrass Biocrude in Supercritical Water

5.1 Abstract

Biomass can be liquefied to produce biocrude for the ease of transportation and processing. Biocrude contains oxygenated hydrocarbons of varying molecular structure and molecular weights, including lignin derived products, sugars and their decomposition products. In this work several catalysts were screened for hydrogen production by gasification of switchgrass biocrude in supercritical water at 600°C and 250 bar. Nickel, cobalt, and ruthenium catalysts were prepared and tested on titania, zirconia, and magnesium aluminum spinel supports. Magnesium aluminum spinel was seen to be an inappropriate support as reactors quickly plugged. Ni/ZrO_2 gave 0.98 mol H_2/mol C, the highest hydrogen yield of all tested catalysts; however, over time, increase in pressure drop lead to reactor plugging with all zirconia supported catalysts. Titania supported catalysts gave lower conversions, however they did not plug during the course of the study. Charring of all catalysts was seen to occur at the entrance of the reactor as the biocrude was heated. All support materials suffered significant surface area loss due to sintering.

5.2 Introduction

Hydrogen has been considered as a potential energy carrier, however 95% of all hydrogen production currently relies on fossil fuel feedstocks via the thermo-catalytic and gasification processes of methane, napthas, and coal.[1] Concerns over carbon

emissions and depletion of fossil fuel reserves have led many researchers to investigate carbon neutral renewable biomass feedstocks for hydrogen production.[2-4] A recent review comparing the economic feasibility of several hydrogen production strategies found hydrogen production from the thermochemical processing of biomass to have a lower cost of hydrogen per kilogram than current wind, solar, or nuclear technologies.[5] Traditional gasification technologies require several additional steps not necessary in the supercritical water gasification scheme presented here. For example, the energy intensive grinding and drying of biomass prior to gasification is not required with sub- or supercritical water (SCW) technologies, and the amount of tarry material is greatly reduced, owing to SCW's ability to solubilize nonpolar tar precursor compounds.[6] Further, hydrogen is obtained directly at high pressure, eliminating the need for compression of the gas before storage.

In this work we use a feedstock of aqueous oxygenated hydrocarbons termed biocrude, where switchgrass was partially solubilized in sub-critical water. In the sub-critical region water has an increased ionic character and the preferred reaction pathway includes the formation of phenols and furfurals.[7] Details of the biocrude production have been published by Kumar and Gupta.[8] In the gasification of biocrude the maximum theoretical hydrogen yield would be attained by suppressing methanation and having the water-gas shift go to near completion, giving approximately 2 mol H_2/ mol C. Examples of the desired reactions are shown in Equations 1-3 for glucose, furfural, and catechol, respectively:

$$C_6H_{12}O_6 + 6\ H_2O \rightarrow 12\ H_2 + 6\ CO_2 \qquad \text{Yield: } 2\ H_2/C \qquad (5.1)$$

$$C_5H_4O_2 + 8\ H_2O \rightarrow 10\ H_2 + 5\ CO_2 \qquad \text{Yield: } 2\ H_2/C \qquad (5.2)$$

$$C_6H_6O_2 + 10\ H_2O \rightarrow 13\ H_2 + 6\ CO_2 \qquad \text{Yield: } 2.17\ H_2/C \qquad (5.3)$$

This approach of using solubilized biomass instead of whole biomass has received some attention in the literature. Matsumura et al. liquefied cellulose and cabbage at 150°C under autogeneous pressure and gasified the aqueous product with partial oxidation at 400°C and 25 MPa in a batch system over a commercial Ni catalyst and several mixed oxides from the lanthanide series. The oxides did not effectively catalyze gasification or oxidation of tars, whereas the nickel catalyst gave a 68% gasification efficiency and was active in both the water-gas shift (WGS) reaction and methanation.[13] Elliott et al. have taken a similar approach, liquefying several biomass feedstocks then gasifying them at 350°C and 20 MPa over Ru/C catalyst, obtaining a product gas composed mostly of methane and carbon dioxide. They studied continuous systems, both on the bench scale as well as a scaled up mobile reactor system. They encountered problems with reactor plugging, as well as catalyst deactivation from trace elements present in the biomass feed.[14] Recently another approach has been taken by studying the aqueous phase reforming of hydrolyzed wheat straw in a batch reactor and the results showed Raney nickel to be more active than supported noble metal catalysts.[15]

Osada et al. have previously found Ru/TiO_2 catalysts to be active and stable in the gasification of lignin in a batch reactor at 400°C and 371 bar. They achieved complete gasification in 120 minutes, obtaining a gas rich in CO_2 and CH_4. Both Ru/C and Ru/γ-Al_2O_3 were seen to lose surface area due to gasification or phase transformations of the support, respectively.[9] Yu and Savage reported that after 100 h in supercritical water oxidation service at 380°C and 250 atm a mixed rutile/anatase support had completely transformed to rutile.[10] Elliott et al. found that commercial titania tablets lost their

mechanical strength after water exposure at 350°C and 200 bar and also report all anatase titania being transformed to the rutile form, while monoclinic zirconia was reported to be stable.[11, 12]

The formation of tar and char materials from biomass components and model compounds has been investigated by several researchers. For example, Sato et al. studied the noncatalyzed alkylation of phenol by alcohols and aldehydes in SCW.[16-18] Saisu et al. later expanded on this work to include the repolymerization of lignin decomposition products by cross-linking with formaldehyde, as well as between the decomposition products themselves.[19] Chuntanapum and Matsumura have recently clarified the role of 5-HMF in tarry materials formation, finding polyaromatic char formation occurring only in the subcritical condition, resulting from polymerization of 5-HMF and it aromatic degradation products.[20, 21]

In our previous work we have gasified model and biomass derived compounds.[22-24] Here we will extend the field of knowledge on the catalytic gasification of real liquefied biomass for hydrogen production, studying nickel, cobalt, and ruthenium catalysts on titania, zirconia, and magnesium aluminum spinel supports. A focus of this work is to understand the activity of the catalyst and stability of the support materials in supercritical water.

5.3 Experimental

5.3.1 Catalyst preparation

TiO_2 and ZrO_2 supports were supplied by St. Gobain Norpro as pellets. $MgAl_2O_4$ was prepared by coprecipitation from aluminum nitrate nonahydrate (98%, Sigma

Aldrich) and magnesium nitrate hexahydrate (99%, Sigma Aldrich) following the method of Bocanegra et al.[25] All supports were crushed and sieved to particle sizes between 150 – 600 μm. Metals were loaded onto the supports by an incipient wetness technique. Precursor materials for metals were nickel nitrate hexahydrate (98%, Alfa Aesar), cobalt nitrate hexahydrate (98%, Alfa Aesar), and ruthenium (III) nitrosyl nitrate (1.5% Ru, Strem Chemicals). Following impregnation, catalyst samples were dried at 110°C overnight, followed by calcination in air at 500°C for 4 h. Prior to each experiment, a fresh 4 g portion of catalyst was reduced *in situ* at 500°C for 2 h in a stream of 5% H_2 in helium flowing at 0.2 Nl/min. All nickel and cobalt catalysts were prepared to have 10 wt% metals loading, while the ruthenium catalysts had a 1.5 wt% metals loading. A smaller metal loading was used with ruthenium catalysts due to concern over the high cost of ruthenium.

5.3.2 Feedstock preparation

Switchgrass was treated in subcritical water at 300°C and 100 bar for 30 minutes with no additional catalyst in a batch reactor to give an aqueous solution of oxygenated hydrocarbons termed biocrude. Biocrude is not extremely stable and some carbon precipitated during refrigerated storage, as has been noted by other researchers.[21] Precipitated particles were removed from the biocrude prior to a run by vacuum filtration through a 2.5 μm filter paper. Depending on the age of the biocrude it contained 1.0-1.3 wt% carbon, and an approximate composition is given in Table 5.1. For details of the experimental procedure and characterization of solid and liquid products, see Kumar and Gupta.[8]

Table 5.1: Oxygenated Hydrocarbons Present in Biocrude

Components identified by HPLC	wt.%
5 & 6 Carbon Sugars	15
5-HMF	4
Furfural	6
Organic Acids (lactic, formic, acetic)	17
Other components identified by GC-MS	57
2-furancarboxaldehyde	
1,2-benzenediol	
4-hydroxyvanillin	
2,3-dihydrobenzofuran	
2-methoxy-4-vinylphenol	
1,4-benzenediol	
2-methylphenol	
2,6-dimethoxybenzaldehyde	
homovanillyl alcohol	
4-hydroxy-3,5-dimethoxy-benzaldehyde	

5.3.3 Experimental Procedure

A schematic of the experimental apparatus used for hydrogen production is shown in Figure 5.1. After the catalyst reduction period, the reactor and apparatus were pressurized with water while the temperature of the furnace was raised such that a thermocouple at the midpoint of the 6.4 mm OD x 3.2 mm ID x 50 cm Inconel 600 reactor read 600°C. After one hour, the water feed to the reactor was replaced with biocrude fed directly to the reactor with no preheating at 0.6 ml/min, resulting in a weight hourly space velocity (WHSV) of 9 h^{-1}. Thirty minutes were allowed to elapse between the introduction of the biocrude feed and the start of product sampling. The reactor effluent was quenched by a double pipe heat exchanger with water on the shell side. Pressure control in the system was accomplished by two back pressure regulators in series, the first set at 250 bar and the second at 100 bar. This arrangement reduced pressure fluctuations in the reactor caused by two phase flow through the back pressure

regulator. Product gases were separated from the liquid effluent in a glass phase separator before online sampling by a GC equipped with TCD (SRI 8610C). The carbon content of the liquid effluent was measured by a TOC analyzer (Shimadzu TOC-V_{CSN}), and gas flow was measured by an inverted beaker type flowmeter. Gas composition and flow were measured at least five times over the course of a run. Error in the gas yields is reported as the standard deviation of the measured gas flow, all other experimentally measured quantities having very low variability.

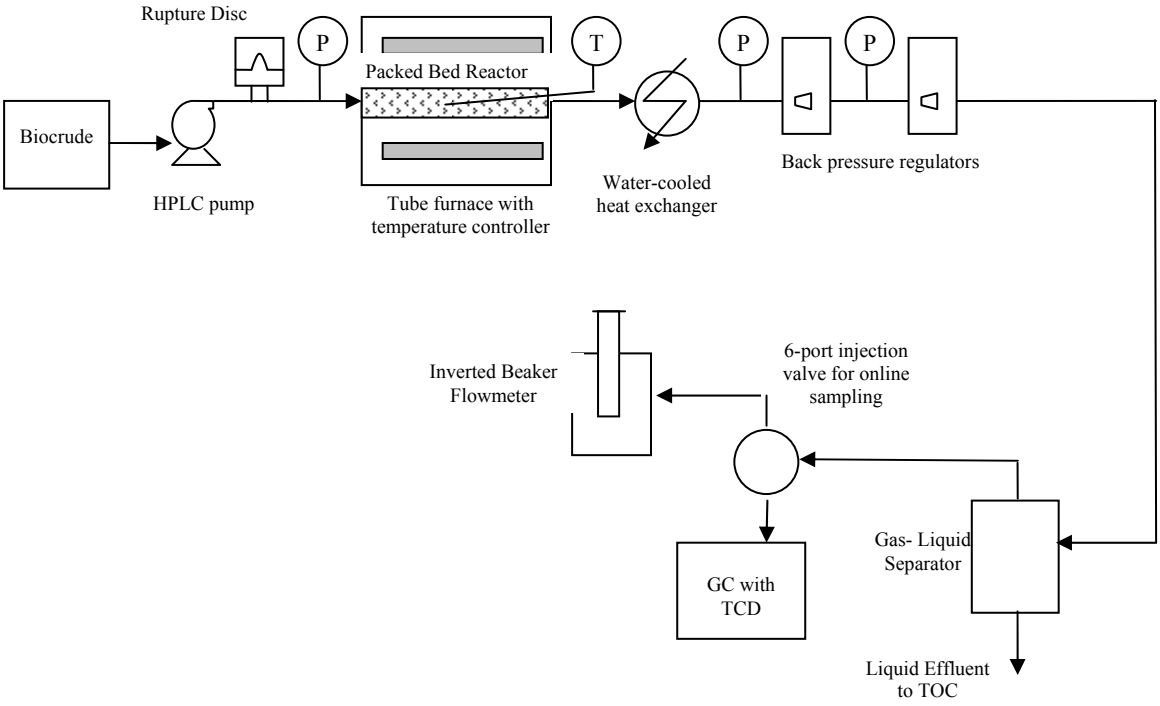

Figure 5.1: Schematic of experimental apparatus

X-ray spectra were collected on a Rigaku diffractometer equipped with a Cu $K\alpha_1$ radiation source, graphite monochromator, and miniflex goniometer. The diffractometer was run at 40 kV voltage and 40 mA current, and scanned at 5°/min with 0.05° step size. Specific surface areas and pore volume data were determined by nitrogen physisorption

at 77 K after outgassing for 3 h at 300°C on a Quantachrome NOVA 2200e. Scanning electron microscopy (SEM) was performed on a Zeiss EVO 50. The samples were scattered onto two sided adhesive carbon tape on an aluminum stub, followed by a sputter coat of gold using an Electron Microscopy Services EMS 550X sputterer. Thermogravimetric data was collected on a TA Instruments TGA Q5000 under air flow of 120 mL/min.

5.4 Results

The major product gases formed were hydrogen, methane, and carbon dioxide, with small amounts of carbon monoxide, ethane, and ethylene. Gas yields for titania and zirconia supported catalysts are shown in Figure 5.2, while gasification efficiency, carbon remaining in the aqueous effluent and closure of the carbon balance are given in Table 5.2. Gas yields are reported as moles of gas formed per mole of carbon reacted, as measured by the difference between the total organic carbon content of the biocrude feed and reactor effluent. The gasification efficiency (GE) is defined as moles of carbon in the product gases divided by the moles of carbon in the feed. Residual aqueous carbon is defined as carbon concentration of the liquid effluent divided by the feed carbon concentration. The carbon balance is defined as the carbon exiting the system in the aqueous and gaseous phases divided by the input carbon flowrate. Over the course of a typical 2 h run, the pressure drop across the reactor for zirconia supported catalysts was seen to steadily increase from approximately 5 bar at the start of the run to 100 bar when the experiment would be aborted. This large increase in pressure drop was not an issue for titania supported catalysts in the timeframe of experiments conducted. No results

are presented for gas yields from $MgAl_2O_4$ supported catalysts, as these each plugged and overpressurized the reactor before any measurements could be taken, typically within twenty minutes of operation. To ensure that the plugging of the reactor was not related to sintering during the initial water pressurization, this period was extended to three hours. Again no increase in pressure drop was seen until biocrude feed was introduced. Based on these results we find $MgAl_2O_4$ to be an inappropriate support for gasification of biocrude. However, the stability of $MgAl_2O_4$ in SCW has received no attention in the literature and will be discussed herein.

Ruthenium catalysts gave greatly differing results depending on the support. The second highest hydrogen yield was seen from Ru/TiO_2, however with Ru/ZrO_2 the product gas contains very little hydrogen, consisting almost entirely of methane and carbon dioxide. The poor closure of the carbon balance along with the lack of carbon in the liquid effluent stream point to extensive char formation over this catalyst formulation. Incomplete conversion of carbon in the liquid phase was seen for all of the titania supported catalysts, as can be seen from comparing the residual aqueous carbon in Table 2. Zirconia itself is known to have catalytic activity in the gasification of biomass[26, 27], and as such does not simply act as an inert support.

Table 5.2: Gasification Efficiencies, Residual Aqueous Carbon and Carbon Balance Closure

	Ru/TiO_2	Ru/ZrO_2	Ni/TiO_2	Ni/ZrO_2	Co/TiO_2	Co/ZrO_2
Gasification Efficiency (%)	78	67	74	96	83	102
Residual Aqueous Carbon (%)	12	2	16	3	17	4
Carbon Balance (%)	90	70	90	99	100	106

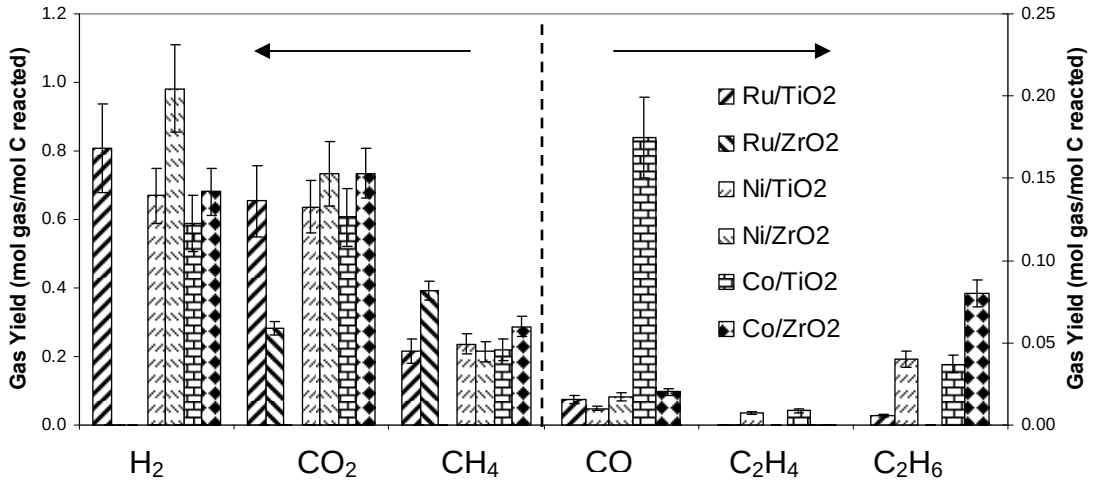

Figure 5.2: Product gas yields for TiO_2 and ZrO_2 supported catalysts

The highest observed hydrogen yield of 0.98 mol H_2 /mol C was obtained with Ni/ZrO_2, as was the lowest methane yield. A lower hydrogen yield of 0.67 was obtained with Ni/TiO_2, however the yield of methane was only slightly higher. Small amounts of ethane and ethylene were also detected in the product gas over the Ni/TiO_2 catalyst.

The third highest hydrogen yield of 0.68 was achieved with the Co/ZrO_2 catalyst. Co/TiO_2 was the only catalyst to give a significant yield of carbon monoxide, not surprising since cobalt has a low activity for the water-gas shift reaction.[28] Over Co/ZrO_2, however, little CO was detected. The increased activity of the water-gas shift may be due to strong metal support interactions between cobalt and zirconia, as has been observed for gold on zirconia.[29] Yields of hydrogen, methane, carbon dioxide, and ethane were higher for Co/ZrO_2 than Co/TiO_2, as was the overall gasification efficiency.

5.4.1 Crystalline structure

The stability of the crystalline structure of the catalyst supports was studied by XRD before and after exposure to SCW. Figure 5.3 shows X-ray spectra for zirconia supported catalysts. The diffraction patterns show that the monoclinic crystal structure of the zirconia was unchanged in the hydrothermal conditions, although in each case the peaks are more intense and have a smaller full width at half maximum after exposure to SCW, indicating a more uniform crystallinity after SCW exposure. After calcination a diffraction peak at 43.4° for NiO is present in the Ni/ZrO_2 sample, while the used catalyst instead shows a peak for Ni at 44.8°. No diffraction peaks are visible for cobalt, ruthenium, or their oxides.

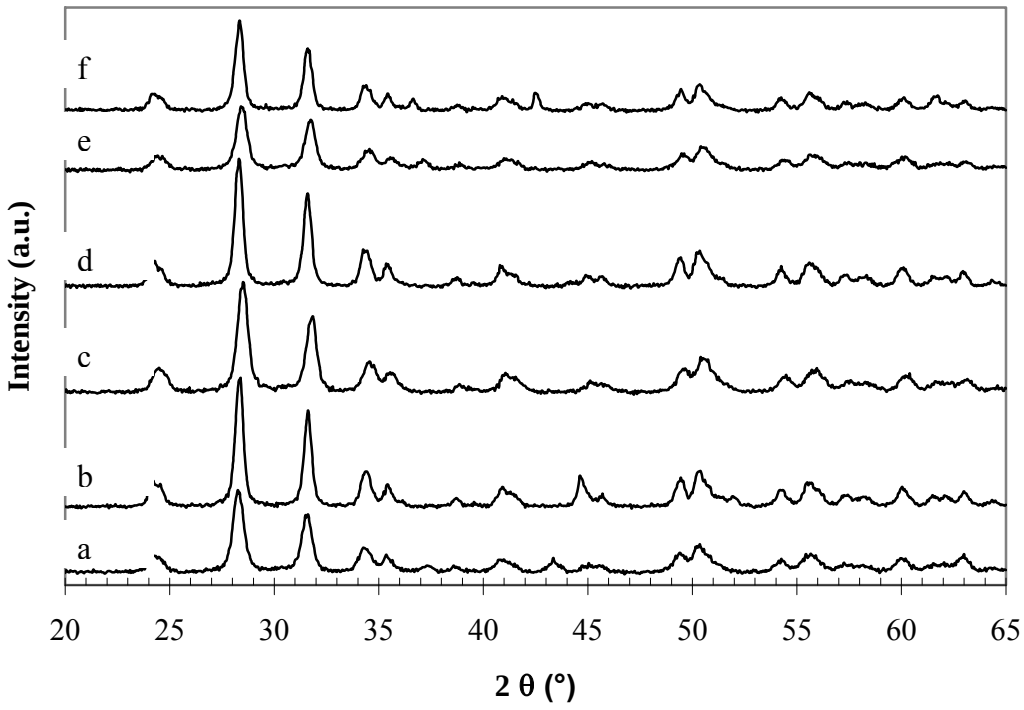

Figure 5.3: XRD spectra of ZrO_2 supported catalysts before and after SCW exposure. (a) fresh and (b) used Ni/ZrO_2; (c) fresh and (d) used Ru/ZrO_2; (e) fresh and (f) used Co/ZrO_2

The X-ray spectra of titania supported catalysts are shown in Figure 5.4. The anatase structure is still the dominant phase after being on stream; however another unidentified pattern not corresponding to rutile or brookite is apparent after SCW exposure for Ni/TiO_2 and Co/TiO_2. NiO is seen in the calcined Ni/TiO_2 sample, while no peaks corresponding to Ni or NiO are seen in the used sample.

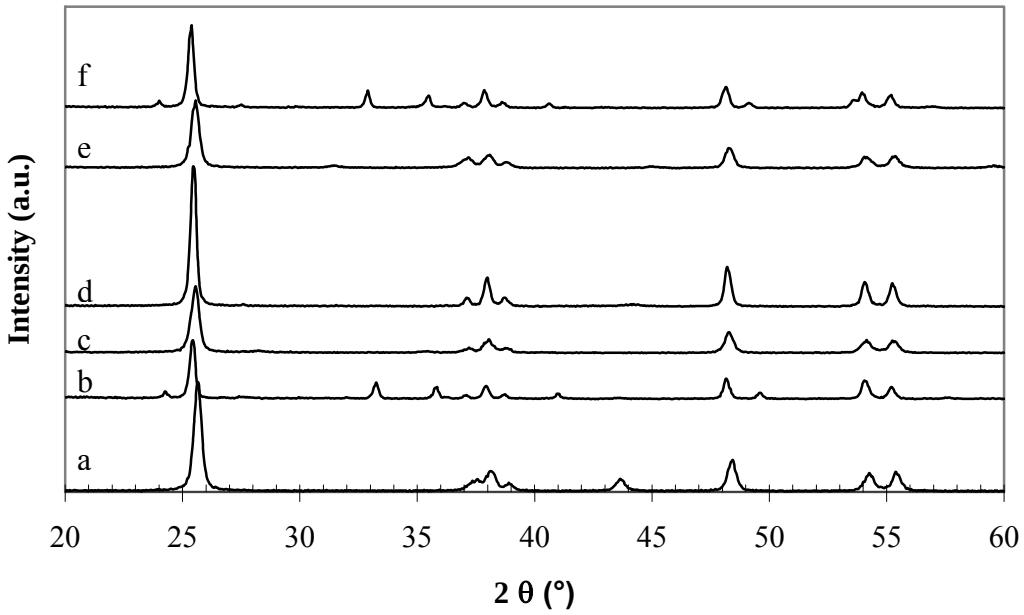

Figure 5.4: XRD spectra of TiO_2 supported catalysts before and after SCW exposure. (a) fresh and (b) used Ni/TiO_2; (c) fresh and (d) used Ru/TiO_2; (e) fresh and (f) used Co/TiO_2

Figure 5.5 shows X-ray spectra of the freshly calcined and used catalysts supported on $MgAl_2O_4$. Reflections from the $MgAl_2O_4$ structure dominate all the spectra both before and after SCW exposure with the peaks becoming narrower and more intense after SCW exposure, indicating a greater degree of crystallinity. Each $MgAl_2O_4$ supported catalyst also shows an additional phase of α-Al_2O_3 after SCW exposure, characterized by the peak at about 43.3°. Additional unidentified peaks at 2θ = 12.1°, 28.5°, 35.7°, and 54.8° are seen in the calcined $Ru/MgAl_2O_4$ sample after which are not

present after exposure to supercritical water. These may be some artifact from the preparation method.

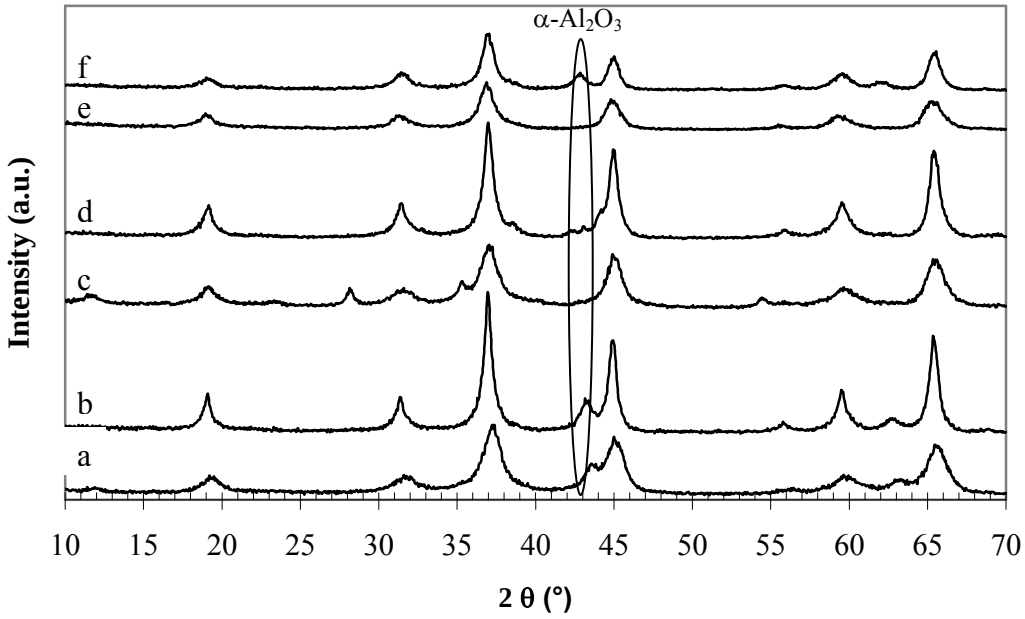

Figure 5.5: XRD spectra of $MgAl_2O_4$ supported catalysts before and after SCW exposure. (a) fresh and (b) used Ni/ $MgAl_2O_4$; (c) fresh and (d) used Ru/ $MgAl_2O_4$; (e) fresh and (f) used Co/ $MgAl_2O_4$

5.4.2 Surface area

Surface area, average pore radius, and pore volume were measured for the supports before impregnation, after new catalyst calcination, and of used catalyst from near the entrance and exit of the reactor. These results are given in Table 5.3. The surface area of each catalyst was decreased after metals impregnation and calcination. The ruthenium catalysts, which had a 1.5 wt% metals loading, showed a smaller loss of surface area than the nickel or cobalt catalysts, both of which had a 10 wt% metals loading. A similar trend is seen in the pore volume, where each ruthenium catalyst had a small decrease in pore volume and a larger decrease for the nickel and cobalt catalysts.

This indicates that metals blocked access to some of the smallest pores, decreasing the total accessible volume and correspondingly the available surface area.

Table 5.3: Surface Area, Pore Radii and Volume for Calcined and Used Catalysts

	Surface Area (m^2/g)			Average Pore radius (Å)			Pore Volume (cc/g)		
	New Calcined	Used Entrance	Used Exit	New Calcined	Used Entrance	Used Exit	New Calcined	Used Entrance	Used Exit
ZrO_2	50.4	-	-	102.0	-	-	0.256	-	-
Ru/ZrO_2	51.1	51.7	28.4	98.0	89.1	159.1	0.250	0.230	0.226
Ni/ZrO_2	43.0	56.3	24.3	96.3	65.1	161.6	0.207	0.184	0.196
Co/ZrO_2	42.0	71.8	20.7	92.9	71.8	184.0	0.195	0.228	0.190
TiO_2	39.3	-	-	79.4	-	-	0.156	-	-
Ru/TiO_2	37.0	36.1	16.9	83.8	73.8	120.1	0.155	0.133	0.101
Ni/TiO_2	31.7	55.1	9.1	83.4	54.1	117.2	0.132	0.135	0.053
Co/TiO_2	31.5	44.2	11.0	76.7	62.4	107.6	0.121	0.138	0.059
$MgAl_2O_4$	113.8	-	-	78.0	-	-	0.443	-	-
$Ru/MgAl_2O_4$	108.3	127.2	55.2	79.4	68.8	152.2	0.430	0.437	0.420
$Ni/MgAl_2O_4$	87.0	113.5	45.0	86.7	62.1	169.2	0.377	0.352	0.385
$Co/MgAl_2O_4$	86.3	124.2	46.8	84.9	58.2	105.7	0.366	0.362	0.247

Surface area of the used catalysts varied whether the catalyst sample is taken from near the entrance or the exit of the reactor. Samples taken from the reactor entrance show a marked increase in surface area, while those from near the exit show a large decrease. As the biocrude is heated in the entrance zone of the reactor it forms char particles on the catalyst surface. These carbon deposits are responsible for the apparent increase in surface area of the used catalyst. At the downstream end of the reactor the temperature is higher than the entrance zone. Little charring takes place in this zone and the surface area decrease is due to sintering in the hydrothermal environment. The pore radius data for the three supports suggests this. Smaller pore sizes are seen at the entrance as they become plugged, while the collapse of small pores at the downstream end results in larger average pore sizes.

5.4.3 Particle size and morphology

Representative SEM images of Ni/ZrO_2 taken from the entrance and exit of the catalytic bed are shown in Figures 5.6 and 5.7, respectively. The surface of the catalyst sample taken from the entrance of the reactor is covered and obstructed by char materials. The sample taken from the end of the reactor lacks much of this additional material and is charred to a lesser degree. A similar situation occurs with samples taken from the entrance and exit of the Ni/TiO_2 bed, shown in Figures 5.8 and 5.9, respectively. The surface of the Ni/TiO_2 catalyst from the entrance has a uniform covering of char particles. Larger agglomerates are seen at the downstream end, although the covering is not as thorough.

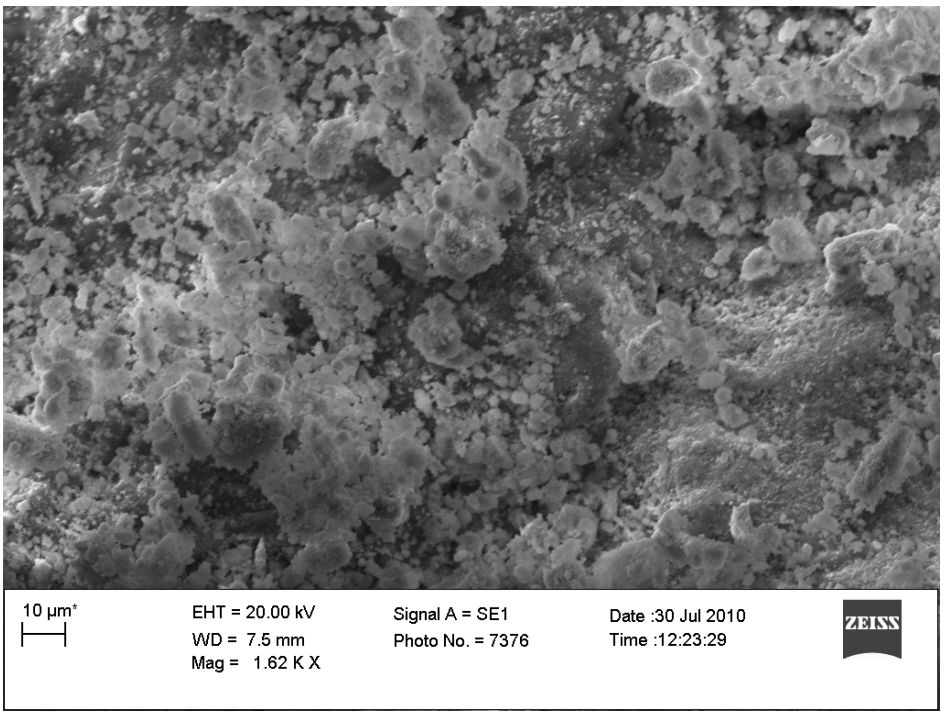

Figure 5.6: SEM of used Ni/ZrO_2 catalyst taken from the reactor entrance

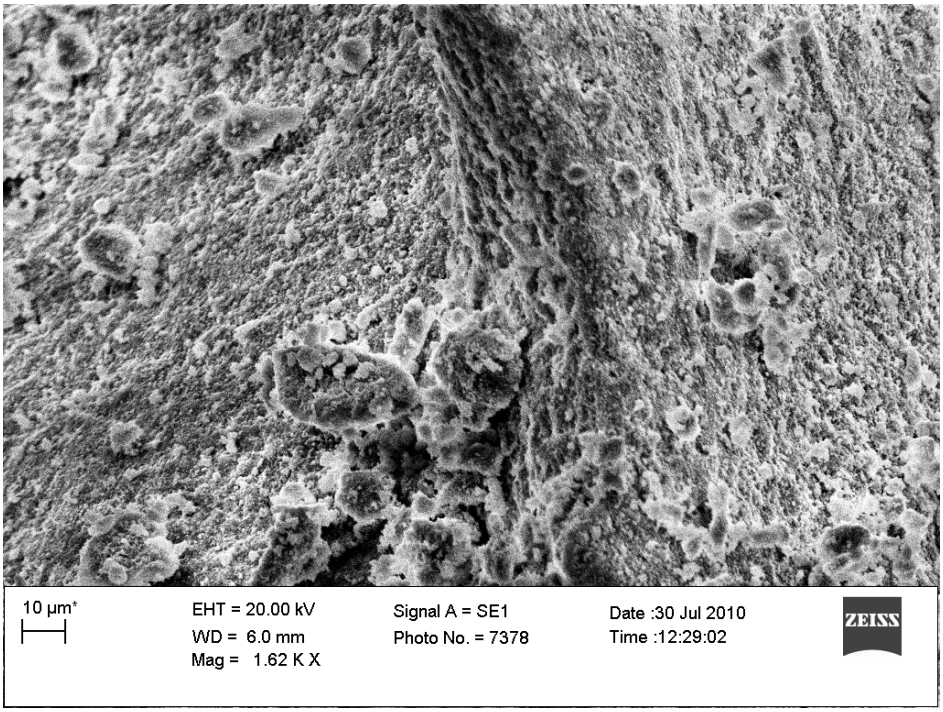

Figure 5.7: SEM of used Ni/ZrO_2 catalyst taken from the reactor exit

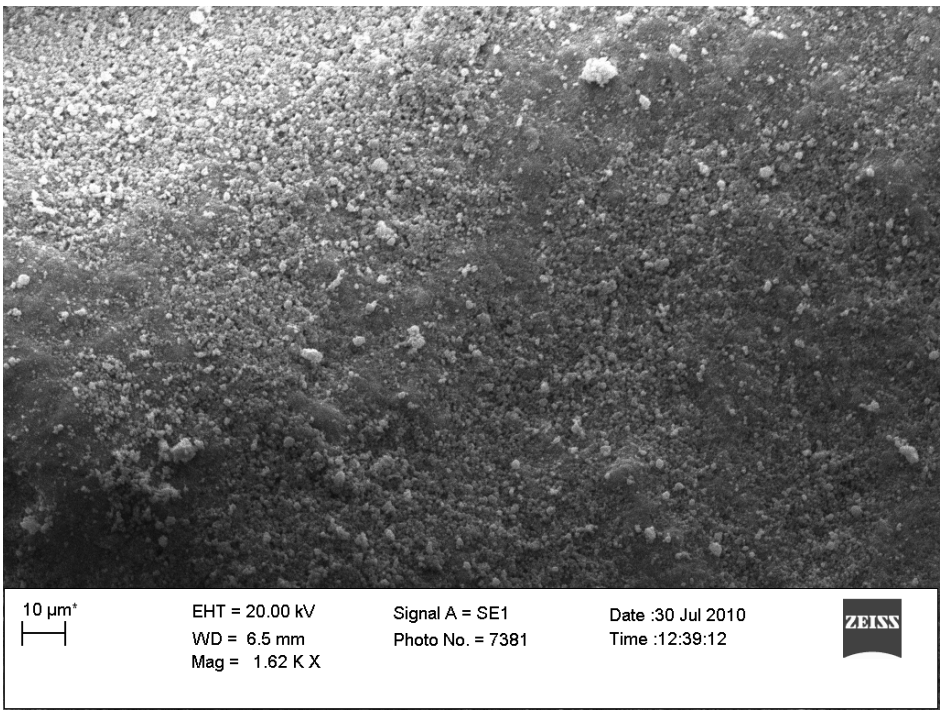

Figure 5.8: SEM of used Ni/TiO_2 catalyst taken from the reactor entrance

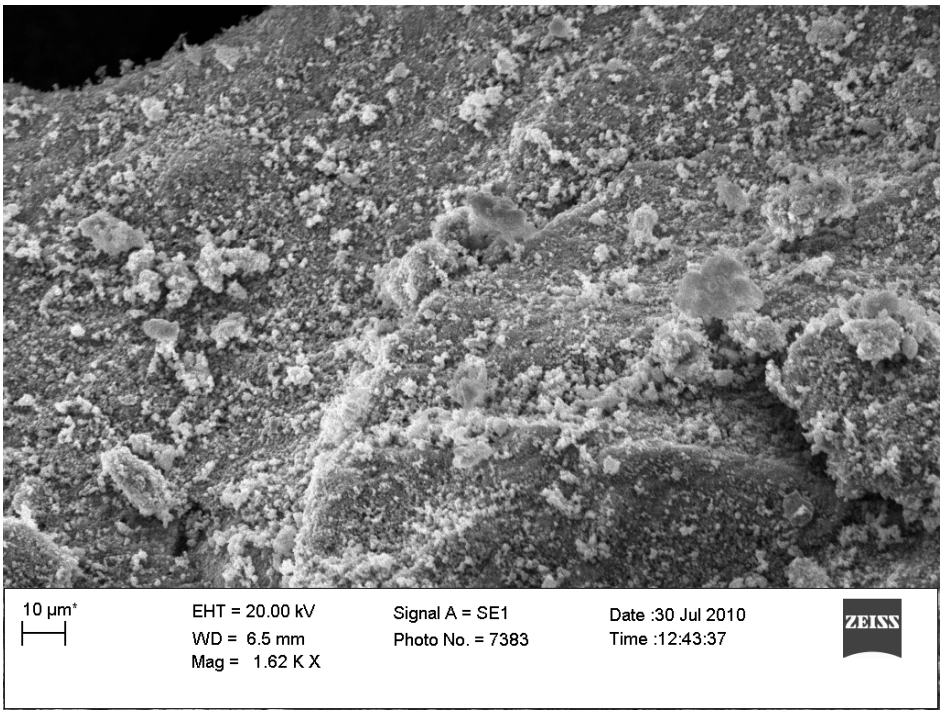

Figure 5.9: SEM of used Ni/TiO_2 catalyst taken from the reactor exit

5.4.4 Thermo-gravimetric Analysis

Used nickel catalysts were selected for further analysis by TGA. Samples of the catalyst were taken from the entrance and exit of the catalytic bed and heated at 10°C/min to 600°C in an air atmosphere. Differing weight losses were seen from catalyst samples at the entrance and exit of the reactor for each support, and are given in Table 5.4.

Weight loss associated with the burning of carbon deposits occurred over the range 200-400°C for Ni/TiO_2 and $Ni/MgAl_2O_4$, with the maximum rate of weight loss at 300°C. Ni/ZrO_2 lost weight over the range 300-500°C with the maximum rate of weight loss at 440°C. The large weight loss from $MgAl_2O_4$ after only 20 minutes on stream indicates the strong tendency for charring over this support, although no quantifiable amount was observed from the sample taken from the downstream end of the reactor. After a 2 hour

period on stream, Ni/ZrO_2 was seen to have over twice the amount of carbon as Ni/TiO_2. A small amount of weight loss was detected from the end of the bed of Ni/TiO_2, whereas none was observed from Ni/ZrO_2.

Table 5.4: Weight Loss (%) of Carbonaceous Material During TGA

	Ni/TiO_2	Ni/ZrO_2	$Ni/MgAl_2O_4$
Entrance	1.8	3.9	6.1
Exit	0.06	ND	ND

ND: None Detected

5.5 Discussion

To understand the charring behavior of the complex biocrude feedstock we examine the literature on model biomass compounds. In the supercritical water gasification of glucose, a fast heating rate is known to increase gasification efficiency[30] as well as enhance hydrogen yield[31]. Obviously with a slow heating rate the reactants will spend more time in a subcritical water environment before the critical temperature is reached. In the subcritical region furfurals and phenolic compounds can react to form higher molecular weight compounds, while direct gasification is preferred above the critical point.[7] The intermediate compound 5-hydroxymethylfurfural has been observed to form high molecular weight char in subcritical water at 25 MPa and 350°C, but is completely gasified in supercritical water at 450°C. In our system carbon deposition in the catalyst bed occurred mainly near the entrance of the reactor in each instance. This was suggested by the decrease in pore size seen in catalyst samples taken from the reactor entrance and confirmed by weight loss from TGA. The biocrude was fed to the reactor at room temperature without preheating, and it follows that the carbon deposition occurred while the reactants were being heated.

It was not expected that $MgAl_2O_4$ supported catalysts would char and plug as quickly as they did. It is generally thought that surfaces with higher acidity tend to coke more quickly in steam reforming reactions. Accordingly, basic MgO is often added to Al_2O_3 catalyst supports. The reason for the rapid charring of the $MgAl_2O_4$ supported catalysts is at this point unclear, but perhaps this points to the need for the study of the surfaces of metal oxides in the presence of supercritical water.

Crystallographically, the monoclinic zirconia support was stable in supercritical water, although BET analysis of a portion of each catalyst taken from the downstream end of the reactor lost approximately half of its surface area through sintering. As discussed above, there are varying reports on the stability of the tetragonal phase of titania in the high temperature and pressure hydrothermal environment in the literature. In this work the structure of the commercial anatase titania used was found to be stable at 250 bar and 600°C. We note that in previous studies, titania supports containing a mix of anatase and rutile transform to exclusively to rutile after exposure to hot compressed water, while pure anatase is stable under the hydrothermal conditions examined. In the case of the mixed phase titania supports it is likely that the presence of the rutile phase acts as a seed allowing anatase to transform at a lower temperature. The $MgAl_2O_4$ supported catalysts also sintered in the hydrothermal environment, each losing approximately half of their surface area after a short exposure to SCW. An α-Al_2O_3 phase was seen to appear after exposure to SCW, however the origin of this phase is unclear from X-ray analysis. The alumina could have originated from the $MgAl_2O_4$ itself, however it is also possible that some amorphous alumina, which is not detectable

by XRD, existed following the preparation of the support and crystallized during the exposure to supercritical water.

5.6 Conclusions

Liquefied switchgrass was gasified over nickel, cobalt, and ruthenium catalysts supported on TiO_2, ZrO_2, and $MgAl_2O_4$ at 600°C and 250 bar with a WHSV of 9 h^{-1}. Catalysts supported on $MgAl_2O_4$ charred immediately and were found to be an inappropriate support for biocrude reforming. A given metal supported on ZrO_2 gave a higher conversion of biocrude than those supported on TiO_2, although charring at the face of the catalyst bed led to reactor plugging within a few hours for ZrO_2 supported catalysts. Char formation occurred to the smallest degree over TiO_2 supports. The highest hydrogen yield was obtained with Ni/ZrO_2, while the lowest was with Ru/ZrO_2, which gave a product gas composed of mostly methane and CO_2. The lowest gasification efficiency was seen with Ru/ZrO_2.due to extensive char formation. Co/TiO_2 was the only catalyst to give a significant CO yield. The anatase titania and monoclinic zirconia were crystallographically stable, but both lost significant amounts of surface area through hydrothermal sintering. Following SCW exposure $MgAl_2O_4$ also sintered and was found to partially transform to α-Al_2O_3.

5.7 References

1. Balat, H.; Kirtay, E.; Hydrogen from biomass: Present scenario and future prospects. *International Journal of Hydrogen Energy* **2010,** 35, 7416-7426.

2. Matsumura, Y.; Minowa, T.; Potic, B.; Kersten, S. R. A.; Prins, W.; van Swaaij, W. P. M.; van de Beld, B.; Elliott, D. C.; Neuenschwander, G. G.; Kruse, A.; Antal, M. J., Jr., Biomass gasification in near- and super-critical water: Status and prospects. *Biomass and Bioenergy* **2005,** 29, 269-292.

3. Guo, Y.; Wang, S. Z.; Xu, D. H.; Gong, Y. M.; Ma, H. H.; Tang, X. Y., Review of catalytic supercritical water gasification for hydrogen production from biomass. *Renewable and Sustainable Energy Reviews* **2010,** 14, 334-343.

4. Gupta, R. B., *Hydrogen Fuel: Production, Transport and Storage*. CRC Press: Boca Raton, FL, 2008.

5. Bartels, J. R.; Pate, M. B.; Olson, N. K., An economic survey of hydrogen production from conventional and alternative energy sources. *International Journal of Hydrogen Energy* **2010,** 35, 8371-8384.

6. Akiya, N.; Savage, P. E., Roles of Water for Chemical Reactions in High-Temperature Water. *Chemical Reviews* **2002,** 102, 2725-2750.

7. Kruse, A.; Gawlik, A., Biomass Conversion in Water at 330-410 °C and 30-50 MPa. Identification of Key Compounds for Indicating Different Chemical Reaction Pathways. *Industrial Engineering Chemistry Research* **2003,** 42, 267-279.

8. Kumar, S.; Gupta, R. B., Biocrude Production from Switchgrass Using Subcritical Water. *Energy & Fuels* **2009,** 23, 5151-5159.

9. Osada, M.; Sato, T.; Arai, K.; Shirai, M., Stability of Supported Ruthenium Catalysts for Lignin Gasification in Supercritical Water. *Energy & Fuels* **2006,** 20, 2337-2343.

10. Yu, J.; Savage, P. E., Catalyst activity, stability, and transformations during oxidation in supercritical water. *Applied Catalysis B: Environmental* **2001,** 31, 123-132.

11. Elliott, D. C.; Sealock, J., Jr.; Baker, E. G., Chemical Processing in High-pressure Aqueous Environments. 2. Development of Catalysts for Gasification. *Industrial Engineering Chemistry Research* **1993,** 32, 1542-1548.

12. Elliott, D. C.; Hart, T. R.; Neuenschwander, G. G., Chemical Processing in High-Pressure Aqueous Environments. 8. Improved Catalysts for Hydrothermal Gasification. *Industrial Engineering Chemistry Research* **2006,** 45, 3776-3781.

13. Matsumura, Y.; Kato, A.; Sasaki, H.; Yoshida, T. In *Gasification of liquefied biomass in supercritical water using partial oxidation*, Progress in Thermochemical Biomass Conversion, Tyrol, Austria, 2000; **Bridgwater, A. V.**, Ed. Blackwell Science Ltd.: Tyrol, Austria, 2000; pp 237-251.

14. Elliott, D. C.; Neuenschwander, G. G.; Hart, T. R.; Butner, R. S.; Zacher, A. H.; Engelhard, M. H.; Young, J. S.; McCready, D. E., Chemical Processing in High-Pressure Aqueous Environments. 7. Process Development for Catalytic Gasification of Wet Biomass Feedstocks. *Industrial Engineering Chemistry Research* **2004,** 43, 1999-2004.

15. Meryemoglu, B.; Hesenov, A.; Irmak, S.; Atanur, O. M.; Erbatur, O., Aqueous phase reforming of biomass using various types of supported precious metal and raney-nickel catalysts for hydrogen production. *International Journal of Hydrogen Energy* **2010,** 35, 12580-12587.

16. Sato, T.; Sekiguchi, G.; Adschiri, T.; Arai, K., Non-catalytic and selective alkylation of phenol with propan-2-ol in supercritical water. *Chemical Communications* **2001,** 17, (1566-1567).

17. Sato, T.; Sekiguchi, G.; Adschiri, T.; Arai, K., Ortho-Selective Alkylation of Phenol with 2-Propanol without Catalyst in Supercritical Water. *Industrial Engineering Chemistry Research* **2002,** 41, 3064-3070.

18. Sato, T.; Sekiguchi, G.; Adschiri, T.; Smith, R. L., Jr; Arai, K., Regioselectivity of phenol alkylation in supercritical water. *Green Chemistry* **2002,** 4, 449-451.

19. Saisu, M.; Sato, T.; Watanabe, M.; Adschiri, T.; Arai, K., Conversion of Lignin with Supercritical Water-Phenol Mixtures. *Energy & Fuels* **2003,** 17, 922-928.

20. Chuntanapum, A.; Yont, T. L.-K.; Miyake, S.; Matsumura, Y., Behavior of 5-HMF in Subcritical and Supercritical Water. *Industrial Engineering Chemistry Research* **2008,** 47, 2956-2962.

21. Chuntanapum, A.; Matsumura, Y., Formation of Tarry Material from 5-HMF in Subcritical and Supercritical Water. *Industrial Engineering Chemistry Research* **2009,** 48, 9837-9846.

22. Byrd, A. J.; Pant, K. K.; Gupta, R. B., Hydrogen Production from Glucose Using Ru/Al2O3 Catalyst in Supercritical Water. *Industrial Engineering Chemistry Research* **2007,** 46, 3574-3579.

23. Byrd, A. J.; Pant, K. K.; Gupta, R. B., Hydrogen Production from Ethanol by Reforming in Supercritical Water Using Ru/Al2O3 Catalyst. *Energy & Fuels* **2007,** 21, 3541-3547.

24. Byrd, A. J.; Pant, K. K.; Gupta, R. B., Hydrogen production from glycerol by reforming in supercritical water over Ru/Al2O3 catalyst. *Fuel* **2008,** 87, 2956-2960.

25. Bocanegra, S. A.; Ballarini, A. D.; Scelza, O. A.; de Miguel, S. R., The influence of the synthesis routes of MgAl2O4 on its properties and bavior as support of dehydrogenation catalysts. *Materials Chemistry and Physics* **2008,** 111, 534-541.

26. Watanabe, M.; Inomata, H.; Arai, K., Catalytic hydrogen generation from biomass (glucose and cellulose) with ZrO2 in supercritical water. *Biomass and Bioenergy* **2002,** 22, 405-410.

27. Watanabe, M.; Inomata, H.; Osada, M.; Sato, T.; Adschiri, T.; Arai, K., Catalytic effects of NaOH and ZrO2 for partial oxidative gasification of n-hexadecane and lignin in supercritical water. *Fuel* **2003,** 82, 545-552.

28. Dalai, A. K.; Davis, B. H., Fischer–Tropsch synthesis: A review of water effects on the performances of unsupported and supported Co catalysts. *Applied Catalysis A: General* **2008,** 348, 1-15.

29. Menegazzo, F.; Pinna, F.; Signoretto, M.; Trevisan, V.; Boccuzzi, F.; Chiorino, A.; Manzoli, M., Highly Dispersed Gold on Zirconia: Characterization and Activity in Low-Temperature Water Gas Shift Tests. *ChemSusChem* **2008,** 1, 320-326.

30. Sinag, A.; Kruse, A.; Rathert, J., Influence of the Heating Rate and the Type of Catalyst on the Formation of Key Intermediates and on the Generation of Gases During Hydropyrolysis of Glucose in Supercritical Water in a Batch Reactor. *Industrial Engineering Chemistry Research* **2004,** 43, 502-508.

31. Watanabe, M.; Aizawa, Y.; Iida, T.; Levy, C.; Aida, T. M.; Inomata, H., Glucose reactions within the heating period and the effect of heating rate on the reactions in hot compressed water. *Carbohydrate Research* **2005,** 340, 1931-1939.

6. Stability of Cerium-modified γ-Alumina Catalyst Support in Supercritical Water

6.1 Abstract

Supercritical water (above 374.1°C and 220.6 bar) is emerging as a promising medium to carry out a variety of catalytic reactions, including reforming to produce hydrogen. However, when using a heterogeneous catalyst the support material can undergo transformations in the hydrothermal environment. In this work the stability of γ-Al_2O_3 modified with 1-10 wt% Ce in supercritical water is examined, specifically in the temperature range of 500 – 700°C at 246 bar. Transformations of the γ-phase were slowed but not prevented. Based on X-ray analysis, the transformation of γ-Al_2O_3 proceeded through the κ phase toward the stable α phase. Reduced cerium species were seen to be oxidized in the supercritical water environment, and low Ce-loading supports maintained the highest BET surface areas. The stabilization was greatest at 700°C, where Ce-modified aluminas retained significantly higher specific surface areas than unmodified alumina.

6.2. Introduction

Supercritical water (T_c = 374.1°C, P_c = 220.6 bar) is an emerging reaction medium for hydrogen production due to its desirable thermophysical properties such as high diffusivity, low viscosity, and ability to solubilize polar molecules as well as gases. As a dense reaction medium it allows for small reactor volumes, and gasification and reforming reactions may proceed homogeneously. Employment of a heterogeneous catalyst can further increase throughput by allowing even shorter reaction times as well

as lowering operating temperatures. Aluminum oxide is commonly used as a catalyst support owing to its high specific surface area, acidic nature of the surface, and low cost.[1, 2] A number of meta-stable phases (γ, δ, θ, χ, κ, η) collectively known as transition aluminas can be prepared by calcining hydrated alumina precursors such as boehmite (γ-AlO(OH)), gibbsite (γ-$Al(OH)_3$), or bayerite (α-$Al(OH)_3$) at a suitable temperature. This paper examines the stability of γ-Al_2O_3, as it generally contains the highest specific surface area of the transition aluminas. Under atmospheric pressure all of the transition aluminas transform to the thermodynamically stable alpha phase (mineralogically known as corundum) at approximately 1100°C, although the exact transition temperature is dependent on impurities and particle size.[3] γ-Al_2O_3 transforms with increasing temperature to corundum by the sequence γ → δ → θ → α. Dehydration sequences for several alumina hydrates under air at atmospheric pressure are illustrated in Figure 6.1. While the surface area decreases with each step, the final transition to the alpha phase is associated with the greatest decrease.[4]

From a crystallographic point of view, γ-Al_2O_3 can be described as a defect spinel structure with a face-centered cubic (fcc) sublattice of O atoms and a sublattice of Al^{3+} cations distributed randomly between octahedral and tetrahedral interstitial sites. During the transformation to the higher transition aluminas there is a tendency for Al^{3+} to migrate from tetrahedral sites where they are stabilized by four anions to octahedral sites which are stabilized by six anions. The final transformation to the α phase involves a complete recrystallization resulting in a hexagonally close packed (hcp) oxygen sublattice with cations at 2/3 of the octahedral sites.[5] Burtin et al.[6] describe the entire transition from

boehmite to corundum by a progressive dehydration due to loss of hydroxyl groups. This transition can be described with the following formula in Kröger-Vink notation:

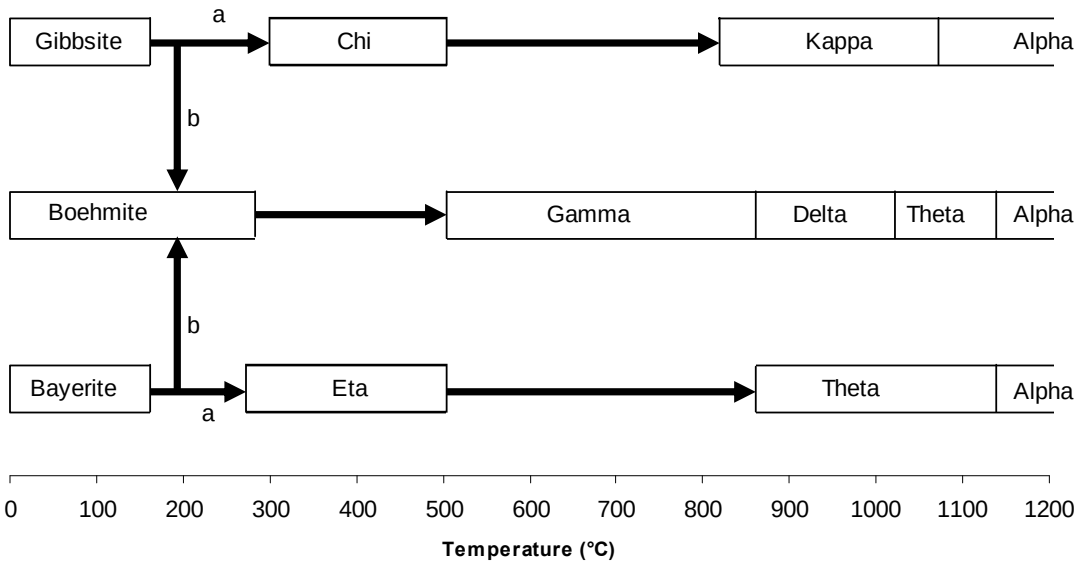

Figure 6.1: Dehydration sequence of selected alumina hydrates in air at ambient pressure. Path a favored by $d_p < 10$ μm; Path b favored by alkalinity and $d_p > 100$ μm. Open areas indicate transitional zones. Adapted from reference [3]

$$(Al_{Al}^{\times})_2 V_M^{''} (O_O^{\times})_{3-\upsilon/2} (OH_O^{\bullet})_{\upsilon} (V_O^{\bullet\bullet})_{1-\upsilon/2} \tag{6.1}$$

where $Al_{Al}^{\times}$ represents an aluminum cation in a trivalent site, $V_M^{''}$ a cationic vacancy at a divalent site, $O_O^{\times}$ an oxygen anion at an oxygen site, $OH_O^{\bullet}$ a hydroxyl substituted onto an oxygen site, and $V_O^{\bullet\bullet}$ an oxygen vacancy. Thus for $\upsilon = 2$ the formula reduces to that of boehmite, and for $\upsilon = 0$ the formula for corundum is obtained. Dehydration through dehydroxylation gives rise to the appearance of an oxygen vacancy, described in Kröger-Vink notation as:

$$2(OH_O^{\bullet}) \rightarrow H_2O + O_O + V_O^{\bullet\bullet} \tag{6.2}$$

Dehydroxylation proceeds as anionic and cationic vacancies annihilate each other, resulting in the transformation to corundum. The transformation to the alpha phase is initiated at points of contact between particles[1, 7] where necking regions contain large numbers of anion vacancies from the formation of Al-O-Al bonds during dehydroxylation according to Equation 6.2. The growth of the neck regions gives rise to sintering and thus the drastic loss of surface area associated with transformation to the alpha phase. Sintering by this mechanism is depicted in Figure 6.2.

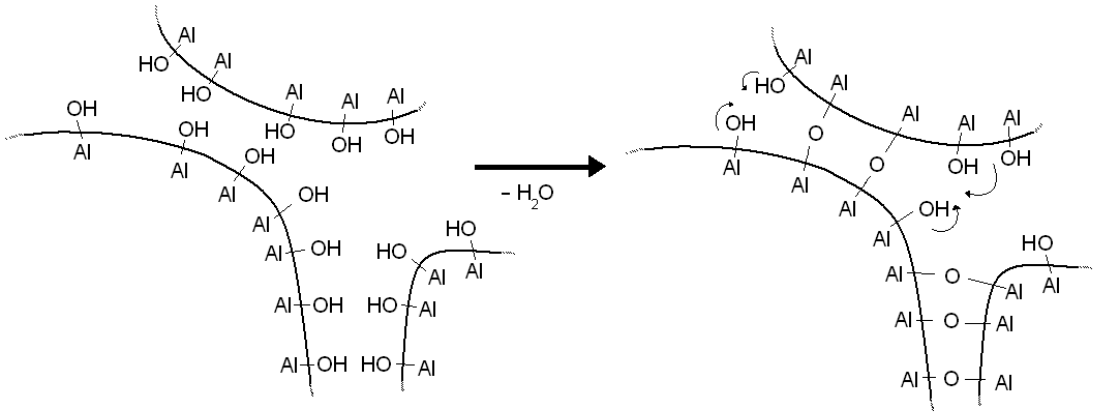

Figure 6.2: Model of alumina surface dehydroxylation resulting in loss of surface area. Adapted from reference [4]

Several groups have explored phase transitions of alumina under increased pressure. For example, Ito et al. observed that the transition to α-Al_2O_3 is accelerated by an increase in pressure, resulting in a decrease in the transition temperature.[8] Using hot isostatic pressure under an argon atmosphere, they observed that nucleation was induced by stress concentration at particle contact points. Panasyuk et al. observed that upon exposure to hydrothermal environment at 450°C and 10 MPa, gibbsite transforms first to boehmite, then to corundum; here an intermediate state between boehmite and corundum was referred but was not characterized. [9, 10] Indeed, the accelerated transformations in the

hydrothermal environment have given rise to novel syntheses of both transition[11] and alpha aluminas[12], as well as other complex oxides[13].

The suitability of alumina as a catalyst support in sub- and supercritical water has received some attention in the literature, and our group has also noted the instability of alumina in our previous work on hydrogen production in supercritical water.[14] Elliott et al. reported that after exposure to subcritical water at 350°C and 20 MPa, δ- and γ-Al_2O_3 were completely hydrolyzed to give boehmite, while η-Al_2O_3 formed a mix of boehmite and α-Al_2O_3. Corundum was the only polymorph of alumina found to be stable under conditions investigated.[15] Osada et al. evaluated ruthenium catalysts on several supports for their activity in lignin gasification at 400°C and 37 MPa. The Ru/Al_2O_3 catalyst lost most of its activity after one reaction period of 180 minutes in their batch system. This was attributed to leaching of Ru metal during a phase transition from γ- to α-Al_2O_3. In the supercritical water oxidation (SCWO) of phenol in a continuous packed bed reactor, Yu and Savage[16] saw that a CuO/γ-Al_2O_3 catalyst was unstable under the reaction conditions of 380°C and 25 MPa, finding that after exposure to SCW the dominant aluminum-containing species was boehmite.

A number of researchers have investigated the thermal stabilization of the transition aluminas by inclusion of small amounts of other materials such as Ba[17], Ca[18], Ce[17, 19, 20], Ga[18], In[18], La[17, 18, 21], Mg[17, 18], Pr[17], SrO[22] , Th[18], Zr[18, 23], and mixed oxide Ce-Zr[24, 25] systems. These studies show that most of the stabilizing agents suppress the phase transition to the alpha phase to some degree, while In^{3+}, Ga^{3+}, and Mg^{2+} accelerate the transition[6]. Oudet et al. [26-28] proposed that thermal stabilization of noble-metal automotive-exhaust catalysts supported on alumina by elements from the lanthanide

series (Ln = La, Pr, Nd) is related to the presence of $LnAlO_3$ microdomains in the corundum nucleation sites. The model was later extended to include Ce, as all of the mixed oxides are isostructural with identical lattice parameters. For example, there is a structural coherence between the $CeAlO_3$ and Al_2O_3 phases due to continuity of the anionic lattices of both compounds.[29]

The fundamental studies have focused on the thermal stability under a variety of atmospheres (reducing/oxidizing, presence of moisture), but at ambient pressure. As discussed above, exposure to a high pressure environment can accelerate phase transformations and enable them to take place at lower temperatures. This work investigates the stability of Ce-modified alumina in a supercritical water environment at both high temperature and pressure. Cerium was chosen over other stabilizing agents because in addition to its known ability to suppress phase transformations in alumina, it also gives other benefits to catalyst formulations including water-gas shift activity, increased oxygen storage capacity, as well as aiding in retaining high dispersion of supported metals.[30, 31]

6.3. Experimental

6.3.1 Sample Preparation

γ-Al_2O_3 having a specific surface area of 256 m^2 g^{-1} and a pore volume of 0.62 cm^3 g^{-1} was obtained from Alfa Aesar as 1/8" extruded pellets. The pellets were crushed and sieved to particle sizes ranging from 150-600 μm. Cerium (III) nitrate hexahydrate (99.9% Ce, metals basis) was obtained from Strem Chemicals. Deionized water was used in all catalyst preparations and hydrothermal experiments.

Cerium loading of the alumina carrier was performed by an incipient wetness impregnation technique where an appropriate amount of cerium nitrate was dissolved in water to give a solution whose volume was equivalent to the pore volume of the support. The samples were then dried overnight at 110°C and subsequently calcined in air at 500°C for 6 h, followed by reduction at 750 or 950°C in a stream of 5%H_2 in He flowing at 0.2 SLPM for 6 h. Throughout the article, the nomenclature to designate cerium loading is written as xCeAl, where x is the loading of cerium in weight percent, defined as grams of elemental cerium in 100 grams of alumina plus elemental cerium.

6.3.2 Experimental Procedure

A schematic of the experimental apparatus is shown in Figure 6.3. In each experiment, approximately 0.5 g of alumina or Ce-modified alumina was placed into a 50 cm Inconel 600 tube (OD: 6.35 mm, ID: 3.05 mm) with pressed steel frits at both ends having pore sizes of 2 μm. Additionally, there was a quantity of smaller steel frits randomly packed into the last 5 cm of the tube to serve as an inert reactor packing and to ensure that the sample did not experience any uneven heating effects from heat losses through the fittings at the end of the tube.

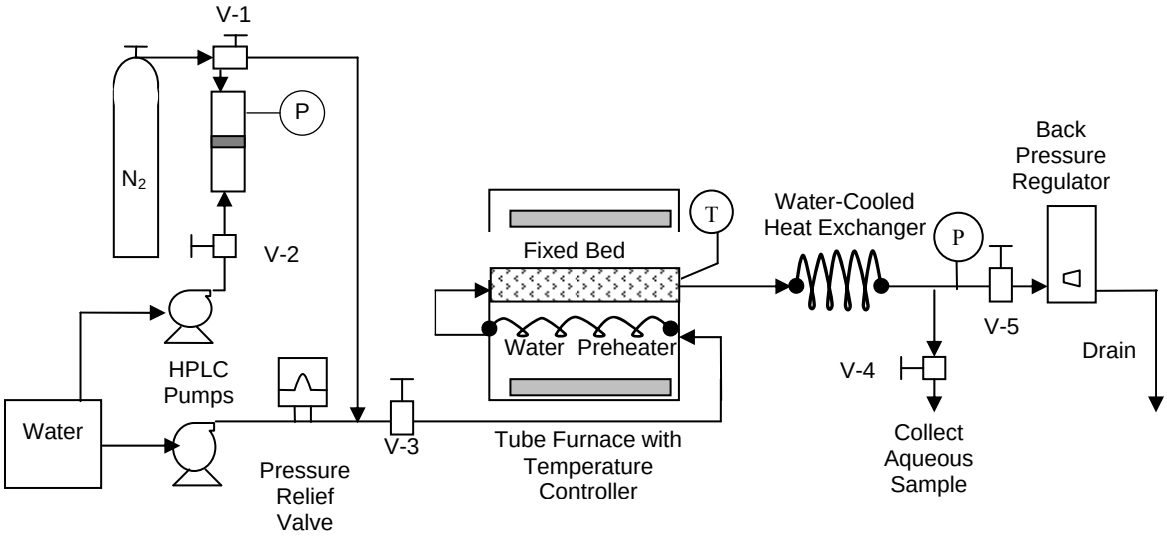

Figure 6.3: Experimental apparatus

The reactor was placed inside of a Thermolyne 21100 tubular furnace with the ends covered in ceramic insulation and additional insulation was placed around the pressure fittings protruding from the furnace to reduce heat losses. The furnace was then brought to the desired temperature and held for ten minutes before pressurization with water. Water was supplied at 2 mL min^{-1} by an HPLC pump (Alltech 301) and pumped through a 2 m section of 1/16" tubing serving as a preheater before entering the reactor. The time at which the desired temperature and pressure were achieved was taken as t = 0 in each experiment, and the reactor was then isolated by closing valves V-3 and V-5. A fixed pressure of 246 bar was used in all experiments. After the allotted time had passed, nitrogen gas slightly above the pressure of the hydrothermal system was applied and needle valve V-4 was carefully opened to collect water from the system. In this way the sample was not exposed to subcritical water at the end of the run. High pressure nitrogen was supplied by means of a 1.5 L high pressure vessel (HiP TOC31-10-P) equipped with a close fitting piston. Prior to the start of an experiment, nitrogen gas was supplied to one

side of the piston at cylinder pressure by a high pressure regulator. The high pressure side of the piston was then isolated and water pumped to the other side to increase pressure to the desired level. The time to drain water from the hydrothermal system was 5 minutes, after which nitrogen gas was bled out for another ten minutes before fully opening valve V-4. Upon the increase in nitrogen flow, the furnace was quickly cooled by blowing compressed air into the furnace while the remaining gas from the piston passed through the bed. The total time to depressurize was approximately 30-40 minutes, during which the sample was exposed to nitrogen at high temperature and pressure.

Samples were characterized by X-ray Diffraction (XRD), Brunauer-Emmett-Teller (BET) method, and inductively coupled plasma atomic emission spectroscopy (ICP-AES). X-ray spectra were collected over the range $2\theta = 10°$- $80°$on a Rigaku diffractometer equipped with a $Cu_{K\alpha 1}$ radiation source, graphite monochrometer, and miniflex goniometer. The diffractometer was run at 40 kV voltage and 40 mA current, and scanned at 5°/min with 0.05° step size. X-ray spectra obtained were compared against JCPDS/ICDD cards 21-1307 (AlO(OH)), 04-0878 (κ-Al_2O_3), 46-1131 (δ-Al_2O_3), 35-0121 (θ-Al_2O_3), 10-173 (α-Al_2O_3), 34-394 (CeO_2), and 18-0315 ($CeAlO_3$).[32] Specific surface areas were determined by N_2 physisorption using a 5-point BET method at 77 K on an Autosorb-1 instrument (Quantachrome). Following the depressurization of the apparatus, water that was in contact with the Ce-modified alumina samples was checked for presence of cerium species by ICP-AES (Varian Vista-MPX ICP AES).

6.4. Results and Discussion

6.4.1 XRD

X-ray spectra of the freshly calcined CeAl samples and γ-Al_2O_3 are shown in Fig 6.4. Diffraction peaks appear at $2\theta = 29.2°$, 48.4°, and 57.1° corresponding to CeO_2 for 4 wt% (i.e., 4CeAl) and greater Ce loading, while no additional diffraction peaks were seen on the lower loading samples. CeO_2 on the lower loading samples is expected to be undetectable by XRD due to small crystallite size and/or weak signal.[31] After a reducing treatment at 750°C, diffraction peaks from CeO_2 in the 4CeAl sample were absent but still persisted on 6CeAl samples. Following reduction at 950°C, however, 6CeAl and 10CeAl showed no diffraction peaks from CeO_2. No additional diffraction peaks assignable to $CeAlO_3$ or Ce_2O_3 were seen in the X-ray spectra of any samples following reduction.

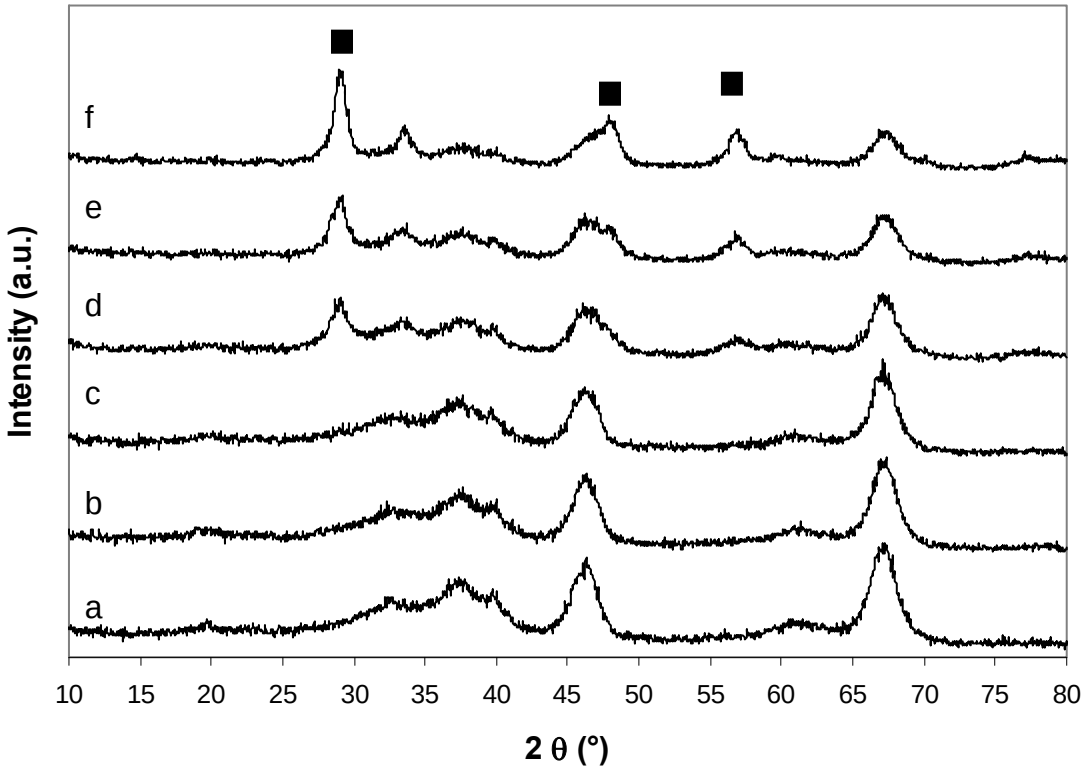

Figure 6.4:. XRD spectra of (a) γ-Al2O3 as received; freshly calcined (b) 1CeAl, (c) 2CeAl, (d) 4CeAl, (e) 6CeAl, (f) 10CeAl. ■ corresponds to CeO_2.

XRD spectra of unmodified alumina before and after exposure to supercritical water between 500-700°C at 246 bar for three hours are shown in Fig. 6.5. After exposure to SCW at 500°C the dominant phase present is boehmite, indicating extensive hydrolysis of the support. Weaker reflections are also present corresponding to the alpha and kappa phases. After SCW exposure at 600°C boehmite is not present. Instead, the alpha phase shows the strongest reflections, while kappa is also visible. Broad diffraction peaks appearing at 32°-34° and 45-47° are not easily assignable to a particular phase, as δ-, θ-, and κ-Al_2O_3 all contain multiple reflections in this region with very similar positions. All peaks present on the spectrum after SCW exposure at 700° can be indexed as a well-crystallized alpha phase.

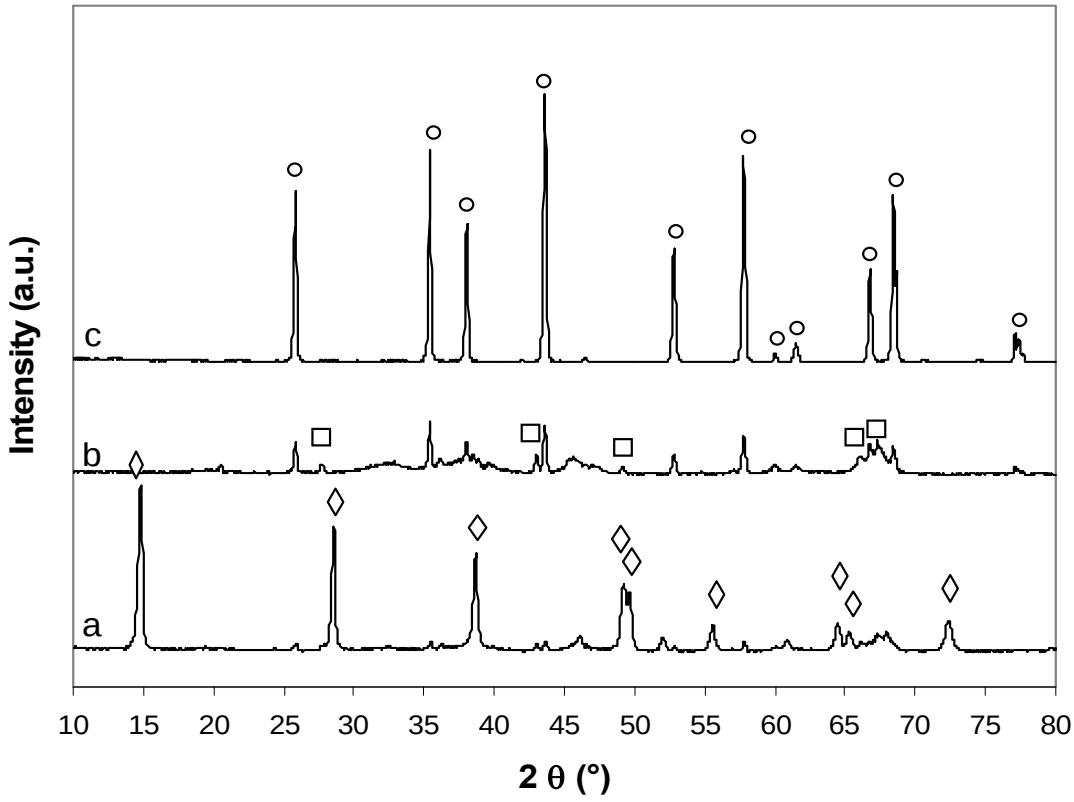

Figure 6.5: XRD spectra of unmodified Al_2O_3 after 3h exposure to supercritical water at (a) 500°C, (b) 600°C, and (c) 700°C. Labels correspond to (○) α-Al_2O_3, (□) κ-Al_2O_3, and (◊) Boehmite

Examining the X-ray spectra from Ce-modified alumina after exposure to 500°C SCW in Fig. 6.6, it is apparent that the intensity of the reflections associated with boehmite are greatly reduced in all three spectra compared with plain γ-Al_2O_3 after SCW exposure. The degree of recrystallization to the κ or α phase varies with Ce loading. The 2CeAl sample shows intense reflections from the alpha phase which are much smaller in the higher loading CeAl samples. The most intense reflection from the alpha phase ((113) at 43.65°) is only discernable as a weak shoulder to the intense peak from the kappa phase at 43.1° in the 6CeAl sample, but is distinct in the highest Ce loading sample.

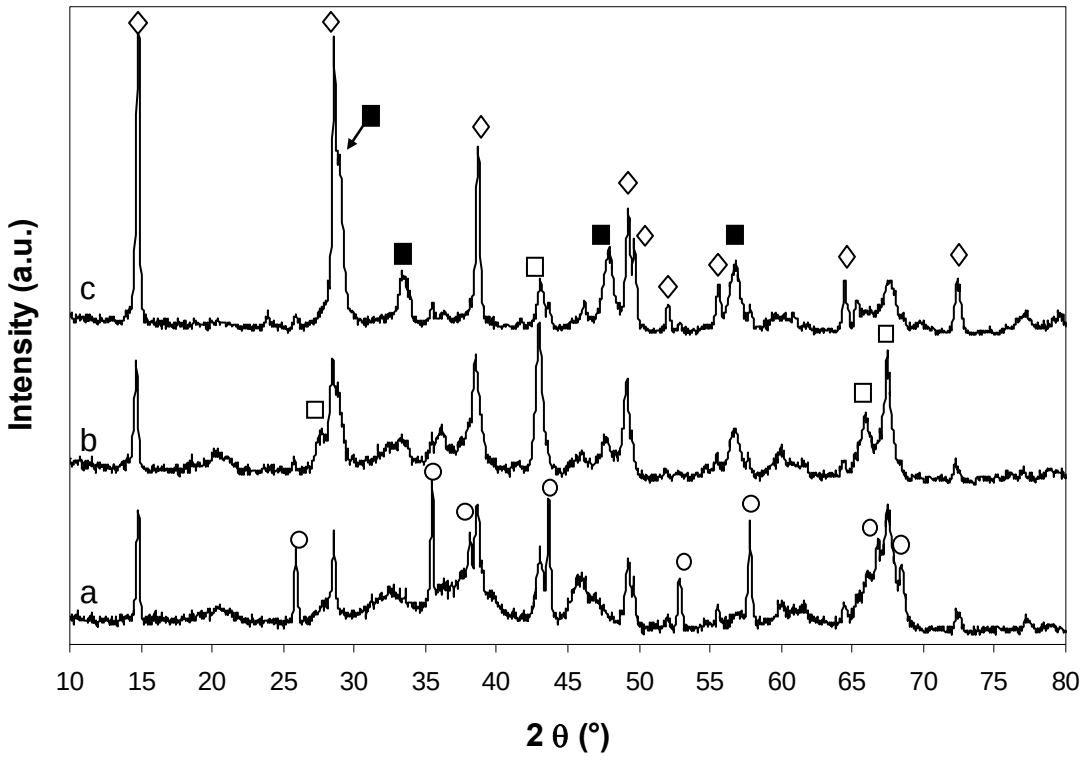

Figure 6.6: XRD spectra of CeAl samples after exposure to SCW at 500°C (a) 2CeAl (b) 6CeAl (c) 10CeAl. Labels correspond to (○) α-Al_2O_3, (□) κ-Al_2O_3, (◊) Boehmite, (■) CeO_2

As was the case with plain γ-Al_2O_3, Ce-modified aluminas exposed to SCW at 600°C do not show any evidence of boehmite formation, as seen in Fig. 6.7. The dominant alumina phases present are alpha and kappa. Again the tendency towards α or κ phase dominance after 3 h is related to the cerium loading. As the loading of cerium was increased from 1 to 4 wt%, the intensity of the α-(113) peak decreases while the neighboring peak for κ-Al_2O_3 increases. The samples with the highest cerium loading show only a broad shoulder at the position of the α-(113) peak.

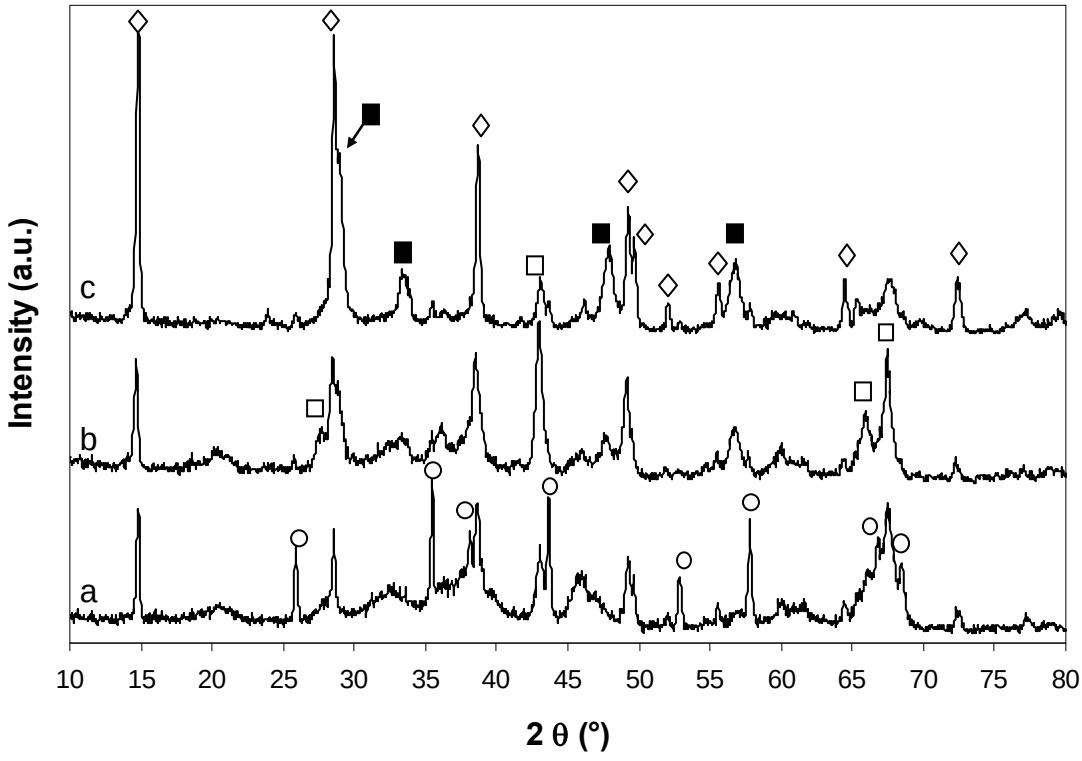

Figure 6.7: XRD spectra of CeAl samples after exposure to SCW at 600°C (a) 1CeAl (b) 2CeAl (c) 4CeAl (d) 6CeAl (e) 10CeAl. Labels correspond to (○) α-Al_2O_3, (□) κ-Al_2O_3, (■) CeO_2

X-ray spectra from samples exposed to SCW at 700°C are shown in Fig 6.8. The 2, 4, and 6 wt% Ce-modified alumina samples all exhibit mixed alpha and kappa phases, in contrast to plain alumina that was completely converted to the alpha phase under identical conditions. The intensity of reflections from the alpha phase overshadows the kappa phase for the 2 and 4 wt% samples, however the 6 wt% Ce sample shows higher intensity diffraction peaks for the kappa phase.

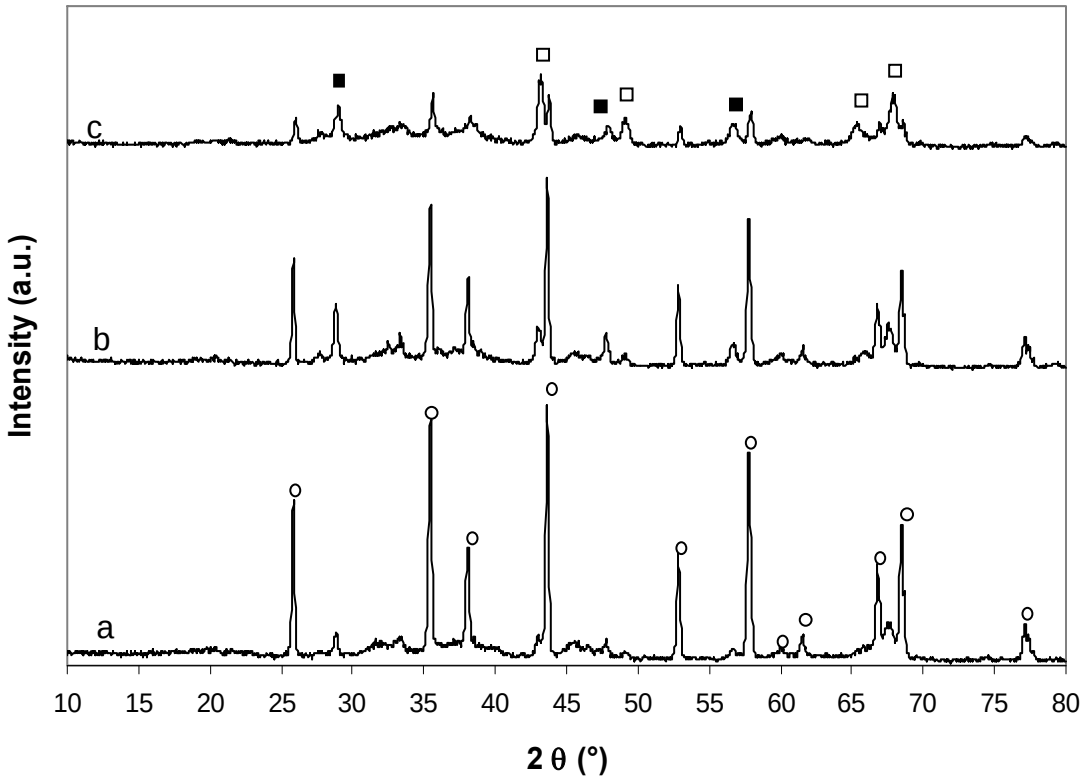

Figure 6.8: XRD spectra of CeAl samples after exposure to SCW at 700°C (a) 2CeAl (b) 4CeAl (c) 6CeAl. Labels correspond to (○) α-Al_2O_3, (□) κ-Al_2O_3, (■) CeO_2

The presence of diffraction peaks assignable to CeO_2 after exposure to SCW indicates the oxidation of $CeAlO_3$ to some degree. The reappearance of diffraction peaks for ceria after exposure to SCW occurred at all temperatures explored in the present study. Further, there is evidence for sintering of ceria after exposure to SCW. Whereas freshly calcined 2CeAl showed no diffraction peaks for CeO_2, small reflections at the positions expected for ceria can be seen post-SCW treatment, indicating that ceria domains below the size detection limits for XRD have coalesced to observable sizes.

Additional experiments were performed with time extended to 6 h as well as with 6CeAl reduced at 950°C for hours. Figures 6.9a and 6.9c show the X-ray spectra of 6CeAl samples reduced at 950° and 750°C, respectively, and exposed to SCW for three hours. In both cases the kappa phase is the only clearly visible phase of alumina, although the (113) reflection from the alpha phase is present as a shoulder in both cases. Reflections from the sample reduced at 750°C have a higher intensity. Spectra shown in Figures 6.9b and 6.9d were obtained after exposure to SCW for six hours. Examining Fig. 6.9b, it can be seen that for the sample reduced at 950°C that the kappa phase reflections have increased in intensity, while (113) reflection from the alpha phase still remains as a shoulder. This contrasts with Fig. 6.9d, reduced at 750°C, where reflections from the alpha phase are clearly identifiable. There are several differences in the reflections from ceria in these samples as well. The most intense peak associated with ceria is at 29°, corresponding to the (111) plane. This peak has a greater intensity in both samples reduced at 750°. The diffraction peak from the ceria (111) plane is narrower and more intense in Fig. 6.9d than the freshly calcined sample, indicating a greater degree of crystallinity and the sintering of ceria. This effect is not noticeable in the 6CeAl sample

reduced at 950°C. Additionally, in Fig. 6.9d a weak reflection for boehmite is present at 14.8° which may be due brief period of exposure to subcritical water during the course of the experiment caused by a leak in the system.

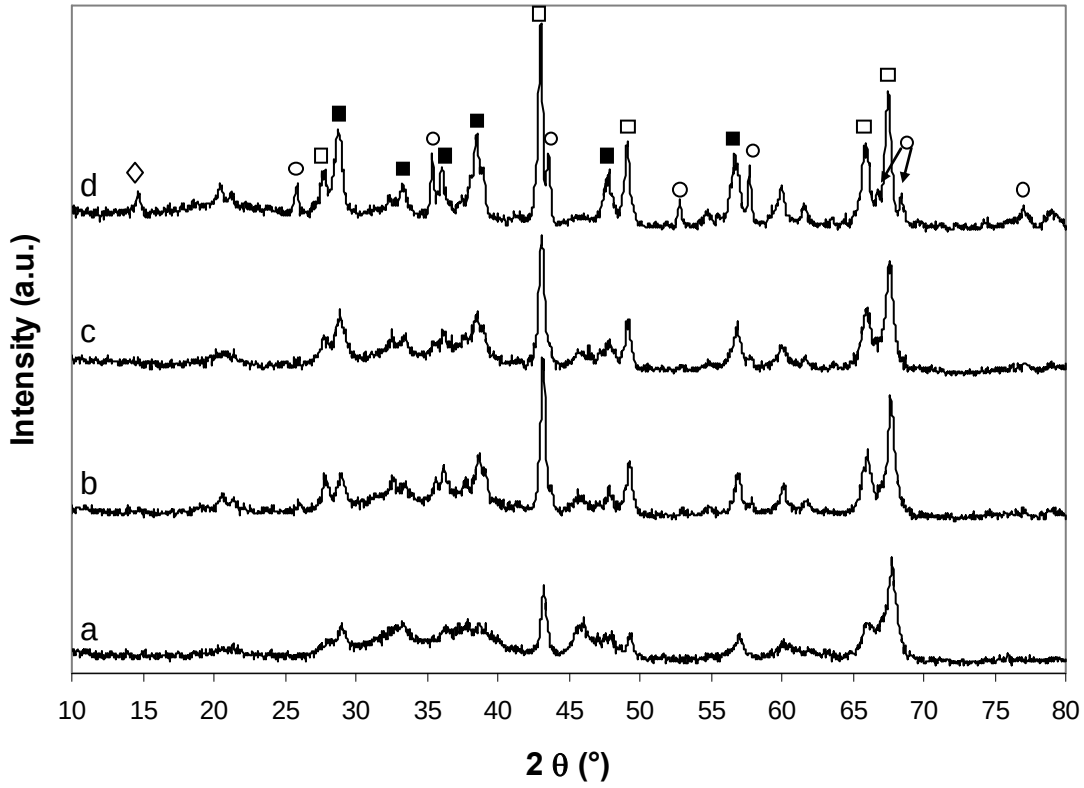

Figure 6.9: XRD spectra of 6CeAl samples after exposure to SCW at 600°C. (a) Reduced at 950°C, SCW exposure 3h (b) Reduced at 950°C, SCW exposure 6 h (c) Reduced at 750°C, SCW exposure 3h (d) Reduced at 750°C, SCW exposure 6 h. Labels correspond to (○) α-Al_2O_3, (□) κ-Al_2O_3, (■) CeO_2, (◊) Boehmite

6.4.2 BET Surface Area

Surface areas measured by N_2 physisorption for as received γ-Al_2O_3, CeAl samples following calcination and reduction (indicated by C&R), and after exposure to SCW at 500-700°C, 246 bar for 3h are shown in Table 6.1. Generally, all CeAl samples

experienced some loss of surface area after calcination and reduction, with losses increasing with higher Ce loading. At 500° and 600°C, samples loaded with 1-2% Ce retained both the highest specific surface area as well as the largest percentage of original surface area. After exposure to SCW at 700°C all of the Ce-modified aluminas reduced at 750°C retained approximately 30-40 m^2 g^{-1}, significantly more than the 2 m^2 g^{-1} exhibited by the unmodified sample under the same conditions. Comparing the specific surface areas of 6CeAl samples reduced at 750 and 950°C, the samples reduced at 950°C have a lower initial surface area, however each retained a higher overall surface area as well as a higher percentage of the specific area before exposure to SCW.

Table 6.1: BET Surface Area of Samples

		SCW Exposure Temperature		
Ce loading (wt%)	C&R[a]	700°C	600°C	500°C
10	164.4	37.4	30.1	39.1
6	215.5	42.3	57.2	50.6
6[b]	143.3	56.9	70.0	91.3
4	172.7	37.1	56.0	90.2
2	187.0	42.0	63.7	101
1	197.0	27.7	105	71.4
0	256.5[c]	2.4	97.2	49.1

[a] Surface area after calcination at 500°C and reduction at 750°C
[b] Reduction performed at 950°C
[c] Surface area of alumina as received

6.4.3 **ICP-AES**

Inductively coupled plasma atomic emission spectroscopy was used to detect cerium species present in the water after depressurizing the experimental apparatus.

Concentrations of cerium corresponding to ~1% of the original loading were seen after exposure to SCW at 500° and 600°C in the effluent from 4CeAl samples calcined at 500°C and receiving no reductive treatment. Analysis of a 4CeAl sample which was calcined at 800°C and exposed to identical SCW treatments did not show the presence of detectable Ce in the effluent water. No cerium was detected in samples which were subjected to reductive treatments at 750°C.

6.5 Conclusions

The stability of cerium-modified γ-Al_2O_3 was evaluated in supercritical water. XRD and BET studies showed that the inclusion of cerium slowed phase transformations in the supercritical water environment; however, the γ-phase was transformed in all cases and was accompanied by the loss of a large percentage of surface area. Ce-modified alumina samples showed reduced boehmite formation at 500°C, while at higher temperatures the transformation towards the thermodynamically stable α-Al_2O_3 was slowed. Formation of κ-Al_2O_3 was observed in the transformation sequence towards corundum, and reduced cerium species were oxidized after exposure to SCW. Low cerium loadings (1-2 wt%) maintained the highest BET surface areas at 500-600°C, while at 700°C all loadings retained approximately 30-40 $m^2\ g^{-1}$, compared to 2 $m^2\ g^{-1}$ for unmodified alumina.

6.6 References

1. Johnson, M. F. L., Surface area stability of aluminas. *Journal of Catalysis* **1990,** 123, 245-249.

2. Jun-Cheng, L.; Lan, X.; Feng, X.; Zhan-Wen, W.; Fei, W., Effect of hydrothermal treatment on the acidity distribution of γ-Al2O3 support. *Applied Surface Science* **2006,** 253, 766-770.

3. Gitzen, W. H., *Alumina as a Ceramic Material*. The American Ceramic Society, Inc.: Columbus, Ohio, 1970.

4. Arai, H.; Machida, M., Thermal stabilization of catalyst supports and their application to high-temperature catalytic combustion. *Applied Catalysis A: General* **1996,** 138, 161-176.

5. Levin, I.; Brandon, D., Metastable Alumina Polymorphs: Crystal Structures and Transition Sequences. *Journal of the American Ceramic Society* **1998,** 81, 1995-2012.

6. Burtin, P.; Brunelle, J. P.; Pijolat, M.; Soustelle, M., Influence of surface area and additives on the thermal stability of transition alumina catalyst supports. II. Kinetic model and interpretation. *Applied Catalysis* **1987,** 34, 239-254.

7. Tucker, D. S., Gamma-to-alpha transformation in spherical aluminum oxide powders. *Journal of the American Ceramic Society* **1985,** 68, C163-164.

8. Ito, S.; Umehara, N.; Takata, H.; Fujii, T., Phase transition of [gamma]-Al2O3 under hot isostatic pressure. *Solid State Ionics* **2004,** 172, (1-4), 403-406.

9. Panasyuk, G. P.; Danchevskaya, M. N.; Belan, V. N.; Voroshilov, I. L.; Ivakin, Y. D., Phenomenology of corundum crystal formation in supercritical water fluid. *Journal of Physics: Condensed Matter* **2004,** 16, S1215-S1221.

10. Panasyuk, G. P.; Belan, V. N.; Voroshilov, I. L.; Shabalin, D. G., Aluminum hydroxide transformations during thermal and vapor heat treatments *Inorganic Materials* **2008,** 44, (1), 45-50.

11. Noguchi, T.; Matsui, K.; Islam, N. M.; Hakuta, Y.; Hayashi, H., Rapid synthesis of γ-Al2O3 nanoparticles in supercritical water by continuous hydrothermal flow reaction system. *The Journal of Supercritical Fluids* **2008,** 46, (2), 129-136.

12. Liao, J.; Huang, L.; Meng, Y.; Wu, B.; Zhang, L., Phase Transition Actibity Characteristics of Nanosized AlOOH in the Hydrothermal Synthesis of nanosized alpha-Al2O3. *Key Engineering Materials* **2008,** 368-372, 675-678.

13. Danchevskaya, M. N.; Ivakin, Y. D.; Torbin, S. N.; Muravieva, G. P.; Ovchinnikova, O. G., Thermovaporous synthesis of complicated oxides. *Journal of Material Science* **2006,** 41, 1385-1390.

14. Byrd, A. J.; Pant, K. K.; Gupta, R. B., Hydrogen production from glycerol by reforming in supercritical water over Ru/Al2O3 catalyst. *Fuel* **2008,** 87, 2956-2960.

15. Elliott, D. C.; Sealock, L. J.; Baker, E. G., Chemical Procesing in High-Pressure Aqueous Environments. 2. Development of Catalysts for Gasification. *Industrial Engineering Chemistry Research* **1993,** 32, 1542-1548.

16. Yu, J.; Savage, P. E., Catalyst activity, stability, and transformations during oxidation in supercritical water. *Applied Catalysis B: Environmental* **2001,** 31, 123-132.

17. Rossignol, S.; Kappenstein, C., Effect of doping elements on the thermal stability of transition aluminas. *International Journal of Inorganic Materials* **2000,** 3, 51-58.

18. Burtin, P.; Brunelle, J. P.; Pijolat, M.; Soustelle, M., Influence of surface area and additives on the thermal stability of transition alumina catalyst supports. I: Kinetic Data. *Applied Catalysis* **1987,** 31, 225-238.

19. Piras, A.; Trovarelli, A.; Dolcetti, G., Remarkable stabilization of transition alumina operated by ceria under reducing and redox conditions. *Applied Catalysis B: Environmental* **2000,** 28, (2), L77-L81.

20. Piras, A.; Colussi, S.; Trovarelli, A.; Sergo, V.; Llorca, J.; Psaro, R.; Sordelli, L., Structural and Morphological Inverstigation of Ceria-Promoted Al2O3 under Severe Reducing/Oxidizing Conditions. *Journal of Physical Chemistry B* **2005,** 109, 11110-11118.

21. Schaper, H.; Doesburg, E. B. M.; Van Reijan, L. L., The influence of lanthanum oxide on the thermal stability of gamma alumina catalyst supports. *Applied Catalysis* **1983,** 7, (211-220).

22. Bloch, B.; Ravi, B. G.; Chaim, R., Stabilization of transition alumina and grain growth inhibition in ultrafine Al O –5 wt.% SrO alloy. *Materials Letters* **2000,** 42, 61-65.

23. Horiuchi, T.; Teshima, Y.; Osake, T.; Sugiyama, T.; Suzuki, K.; Mori, T., Improvement of thermal stability of alumina by addition of zirconia. *Catalysis Letters* **1999,** 62, 107-111.

24. Wu, X.; Yang, B.; Duan, W., Effect of Ce-Zr mixed oxides on the thermal stability of transition aluminas at elevated temperature. *Journal of Alloys and Compounds* **2004,** 376, 241-245.

25. Wei, Z.; Li, H.; Zhang, X.; Yan, S.; Lv, Z.; Chen, Y.; Gong, M., Preparation and property investigation of CeO2-ZrO2-Al2O3 oxygen-storage compounds. *Journal of Alloys and Compounds* **2008,** 455, (1-2), 322-326.

26. Oudet, F.; Bordes, E.; Courtine, P.; Lambert, C.; Guerlet, J. P., Structural consideration with respect to the thermal stability of a new platinum supported lanthanum-alumina catalyst. *Studies in Surface Science and Catalysis* **1987,** 30, 313-321.

27. Oudet, F.; Courtine, P.; Vejux, A., Thermal stabilization of transition alumina by structural coherence with lanthanide aluminum oxide (LnAlO3, Ln = lanthanum, praseodymium, neodymium). *Journal of Catalysis* **1988,** 114, 112-120.

28. Oudet, F.; Vejux, A.; Courtine, P., Evolution during thermal treatment of pure and lanthanum-doped Pt/Al/sub 2/O/sub 3/ and Pt-Rh/Al/sub 2/O/sub 3/ automotive exhaust catalysts. Transmission electron microscopy studies on model samples. *Applied Catalysis* **1989**, Medium: X; Size: Pages: 79-86.

29. Humbert, S.; Colin, A.; Monceaux, L.; Oudet, F.; Courtine, P., Simultaneous atmosphere and temperature cycling of three-way automotive exhaust catalysts. *Studies in Surface Science and Catalysis* **1995,** 96, 829-839.

30. Yao, M. H.; Baird, R. J.; Kunz, F. W.; Hoost, T. E., An XRD and TEM Investigation of the Structure of Alumina-Supported Ceria-Zirconia. *Journal of Catalysis* **1997,** 166, (1), 67-74.

31. Damyanova, S.; Perez, C. A.; Schmal, M.; Bueno, J. M. C., Characterization of ceria-coated alumina carrier. *Applied Catalysis A: General* **2002,** 234, (1-2), 271-282.

32. JCPDS-ICDD, *Powder Diffraction File*. 2001.

7. Stability of Binary Aluminum, Titanium, and Zirconium Oxides for Catalyst Supports in Sub- and Supercritical Water

7.1 Abstract

Hot compressed water is an attractive reaction medium due to its desirable tunable thermophysical properties; however, the severe conditions of water's critical point (374.1°C, 22.1 MPa) leads to extensive sintering and phase transformations of traditional support materials. In this work, binary oxides of aluminum, titanium, and zirconium with 1:1 mole ratios of the component metals were synthesized by a coprecipitation method. Their stability in sub- and supercritical water was evaluated at 25 MPa over a temperature range of 350 – 650 °C for a period of three hours by XRD and BET studies. The compound $ZrTiO_4$ was crystallographically stable at all conditions. It maintained its surface area in subcritical water, although it sintered and lost much of its pore volume in supercritical water. ZrO_2/Al_2O_3 maintained high surface area up to 450°C, but sintered above this temperature as a result of phase transformation of both ZrO_2 and Al_2O_3. The TiO_2/Al_2O_3 mixed oxide, while having the highest initial surface area, sintered extensively following all hydrothermal treatments. Alumina in the TiO_2/Al_2O_3 system hydrolyzed in subcritical water and transformed to corundum in supercritical water, while anatase titania was transformed to rutile only at 650°C.

7.2 Introduction

Supercritical water is an emerging reaction medium due to its desirable physical and chemical properties. The severity of water's critical point (371.4°C, 22.1 MPa) often leads to sintering and phase transformation of the high surface area metastable metal oxide support materials traditionally used in heterogeneous catalysis. For example,

transition aluminas are hydrolyzed in subcritical water and transform to corundum at higher temperatures.[1, 2] Pure anatase titania has been reported to be stable in supercritical water over the range of 400-600°C,[3, 4] while mixed rutile-anatase titania has been observed to transform completely to the rutile phase following exposure to hot compressed water.[2, 5] Owing to its solubility in supercritical water, silica is inappropriate as a support.[6] Activated carbons have been used as support materials in heterogeneously catalyzed reactions, however varying results have been reported. Carbon supported catalysts have been sometimes found to be stable in hot compressed water,[7] but others report that the carbon is slowly gasified.[2, 3, 8]

Titania can exist in three polymorphs: the metastable tetragonal anatase and stable tetragonal rutile phase or the orthorhombic brookite phases. At atmospheric pressure the transformation temperature from anatase to rutile is approximately 800°C, however depending on preparation conditions, precursor materials, particle size, and impurities, the transformation may take place at temperatures ranging from 400-1200°C.[9, 10] For pure zirconia, the monoclinic form is the stable polymorph at ambient temperature, while tetragonal zirconia forms at above 1170°C.[11] Alumina exhibits a number of metastable phases (γ, δ, θ, χ, κ, η) collectively known as transition aluminas, each sharing defect spinel structures. At approximately 1100°C, each of the transition aluminas will transform to α-Al_2O_3, which is the only thermodynamically stable phase of alumina.[12]

Phase transition temperatures of catalyst supports can be greatly reduced in the high pressure supercritical water environment. Ito et al. observed that the temperature for phase transformation of γ-Al_2O_3 to the stable α phase was reduced to 720°C under 50 MPa and took place at only 500°C under 200 MPa hot isostatic pressure. Nucleation of

the α phase is induced by stress concentration at the points of contact between particles and is accelerated by the presence of water.[13]

The use of a binary oxide can significantly increase the effective operating temperature over a single oxide. A 1:1.3 molar ratio of Al_2O3:TiO_2 has been seen to increase the anatase to rutile transition temperature by 200°C for supported vanadia catalysts.[14] TiO_2/ZrO_2 catalysts have been found to retain reasonably high surface areas after high temperature calcinations.[15] Mixed oxides may also be desirable as they can exhibit a larger number of acid sites than the pure component oxides.[16] In this work we examine the stability of binary oxides of aluminum, titanium, and zirconium in sub- and supercritical water to evaluate their potential as support materials for heterogeneous catalytic reactions. Nomenclature used to represent mixed oxides in this paper will be TiAl for $TiO_2 + Al_2O_3$, ZrAl for $ZrO_2 + Al_2O_3$, and ZrTi for $ZrTiO_4$.

7.3 Experimental

7.3.1 Sample Preparation

The binary oxides were prepared by a coprecipitation method from chloride salts. $AlCl_3$ (99% purity), $ZrCl_4$ (99.5% purity), and $TiCl_4$ (99.9% purity) were obtained from Sigma Aldrich. The synthesis of ZrTi was performed as follows: $ZrCl_4$ and $TiCl_4$ were added dropwise to a volume of water at 60°C with stirring to give a total metal concentration of 0.5 M. NH_4OH (29.6%) was then slowly added to the solution until the pH rose from 1 to 10. The resulting hydroxide gel was allowed to age for 1h before undergoing vacuum filtration. The gel was rinsed with deionized water until the filtrate was free of the chloride anion, as evidenced by a lack of precipitation of AgCl upon

addition of $AgNO_3$ to the filtrate. The gel was then dried at 110°C overnight, followed by a 3 hour calcination at 750°C. Syntheses of ZrAl and TiAl were analogous to the preparation of ZrTi.

7.3.2 Experimental Procedure

All hydrothermal treatments were performed in an Inconel 600 tube (OD: 6.35 mm, ID: 3.05 mm) with pressed steel frits at both ends having pore sizes of 2 μm. Approximately 1.6 g of a binary oxide was loaded into the reactor tube to fill it halfway, allowing a 0.5 g sample to be removed from the middle portion of the reactor after hydrothermal treatment. This ensured that the sample taken for analysis was not exposed to uneven heating near the ends of the reactor. A schematic of the experimental apparatus is shown in Figure 7.1.

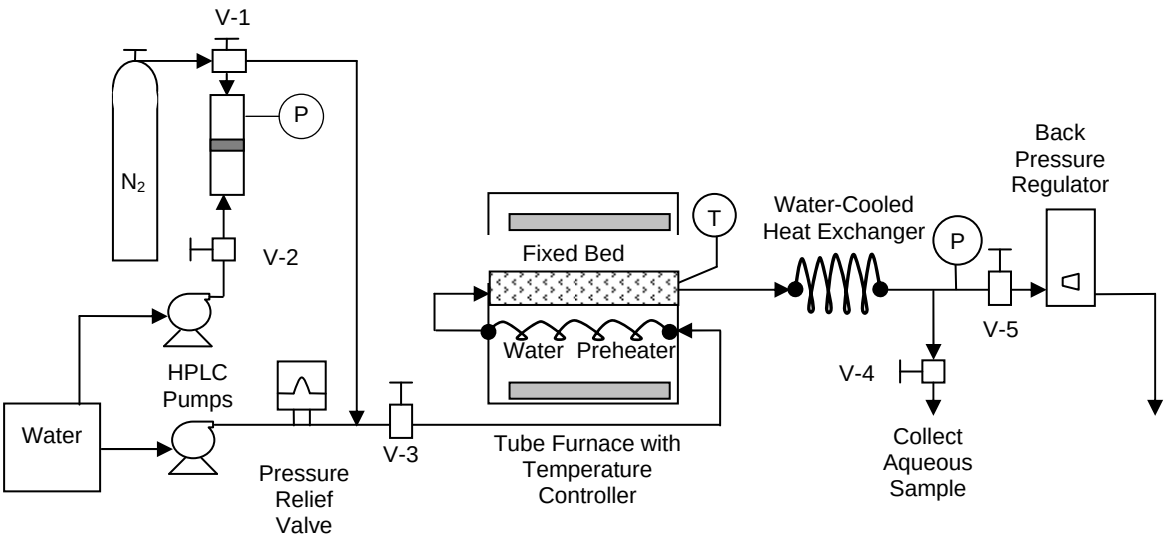

Figure 7.1: Experimental apparatus for hydrothermal treatment of binary oxides

The reactor was placed inside of a Thermolyne 21100 tubular furnace with the ends covered in ceramic insulation with additional insulation placed around the pressure

fittings protruding from the furnace to reduce heat losses. The furnace was then brought to the desired temperature and held for ten minutes before pressurization with water. A fixed pressure of 25 MPa was used in all experiments. Water was supplied at 2 mL min^{-1} by an HPLC pump (Alltech 301) and pumped through a 2 m section of 1/16" tubing serving as a preheater before entering the reactor. The time at which the desired temperature and pressure were achieved was taken as t = 0 in each experiment, and the reactor was then isolated by closing valves V-3 and V-5. After 3 h had elapsed, nitrogen gas slightly above the pressure of the hydrothermal system was applied and needle valve V-4 was slightly opened to collect water from the system. This prevented many of the samples from being exposed to subcritical water at the end of the run and also dried the samples as the system depressurized. High pressure nitrogen was supplied by means of a 1.5 L high pressure vessel (HiP TOC31-10-P) equipped with a close fitting piston. Prior to the start of an experiment, nitrogen gas was supplied to one side of the piston at cylinder pressure by a high pressure regulator. The high pressure side of the piston was then isolated and water was pumped to the other side to increase pressure to the desired level. The time to drain water from the system was 5 minutes, after which nitrogen gas was bled out for another ten minutes before fully opening valve V-4. Upon the increase in nitrogen flow, the furnace was quickly cooled by blowing compressed air into the furnace while the remaining gas from the piston passed through the bed. The total time to depressurize was approximately 30-40 minutes, during which the sample was exposed to nitrogen at high temperature and pressure.

7.3.3 Characterization

X-ray spectra were collected on a Discover D8 diffractometer equipped with a Cu $K\alpha_1$ radiation source. The diffractometer was run at 40 kV voltage and 40mA current, and scanned at 6°/min with 0.01° step size. Specific surface areas and pore volume data were determined by nitrogen physisorption at 77 K after vacuum outgassing for 3 h at 300°C on a Quantachrome NOVA 2200e.

7.4 Results and Discussion

7.4.1 Crystalline structure

X-ray diffraction spectra of the ZrTi samples after calcination and subsequent hydrothermal treatment are shown in Fig. 7.2. Freshly calcined ZrTi shows diffraction pattern from a single $ZrTiO_4$ phase, which presents an orthorhombic structure.[17] There is no evidence of TiO_2 or ZrO_2, as expected after calcination above 700°C.[15] Mechanical stresses from cold pressing $ZrTiO_4$ at 147 MPa have been seen to induce partial decomposition of $ZrTiO_4$ to monoclinic zirconia at temperatures as low as 300°C;[18] however, the crystalline structure of ZrTi remained unchanged after exposure to sub- and supercritical water.

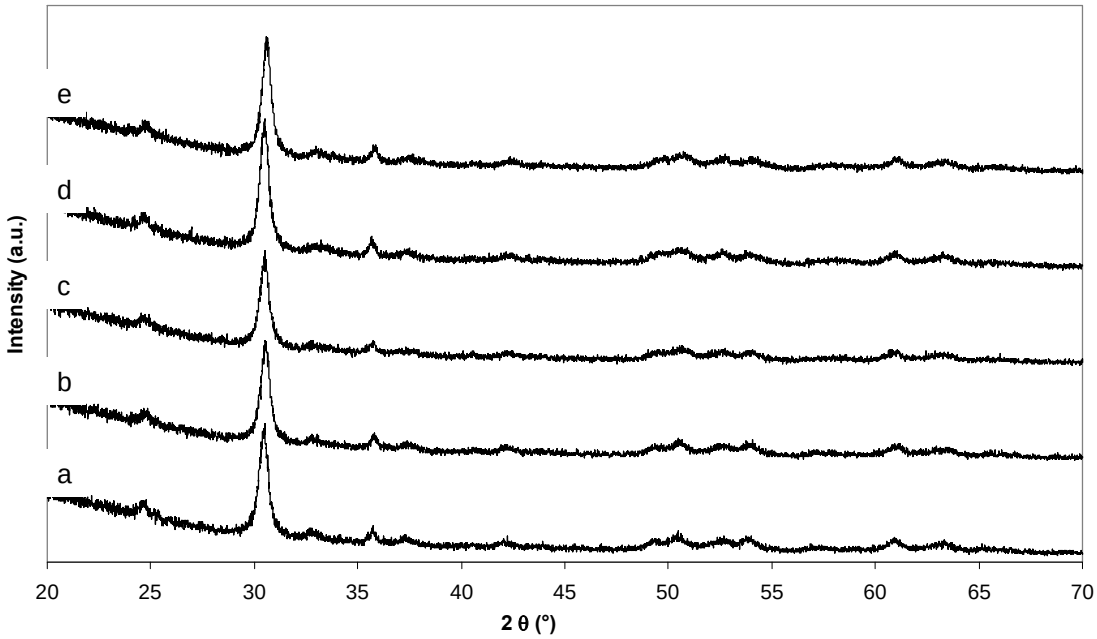

Figure 7.2: XRD spectra of ZrTi (a) after calcination, and after hydrothermal treatment at 25 MPa and (b) 350°C, (c) 450°C, (d) 550°C, and (e) 650°C. All peaks correspond to $ZrTiO_4$

XRD spectra from TiAl samples are shown in Fig. 7.3. Calcined TiAl shows only a crystalline anatase TiO_2 phase. The lack of any diffraction peaks from alumina indicates that all alumina present in the calcined sample is amorphous. Following hydrothermal treatment below 650°C only the anatase polymorph of titania is present, although as the temperature of the exposure was increased, the peaks become narrower and more intense, indicating increased crystallinity of the tetragonal phase. At 650°C, transformation from the anatase to rutile is evidenced by the appearance of the peak at 27.5°. The amorphous state of alumina was changed after each hydrothermal treatment in both sub- and supercritical water. In subcritical water at 350 °C the peak at 23.16 °C is indicative of the formation of AlO(OH) (boehmite) from the hydrolysis of alumina. In all cases after exposure to supercritical water the only phase of alumina visible from XRD is α-Al_2O_3.

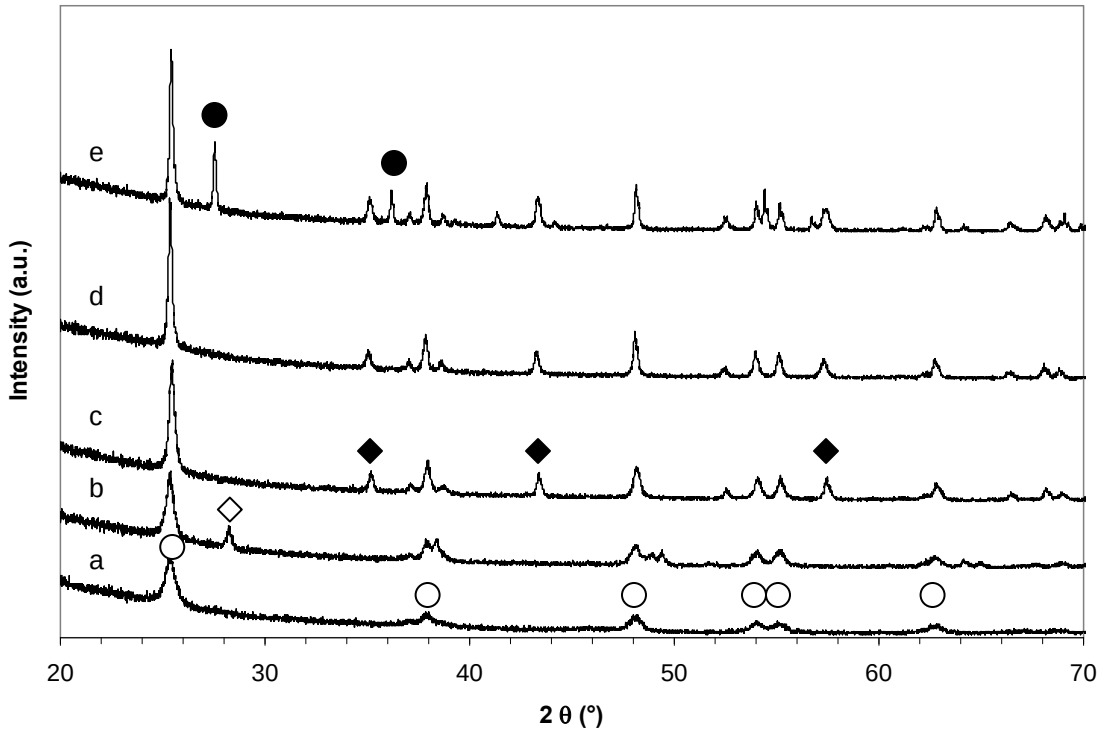

Figure 7.3: XRD spectra of TiAl (a) after calcination, and after hydrothermal treatment at 25 MPa and (b) 350°C, (c) 450°C, (d) 550°C, and (e) 650°C. Labels correspond to (◇) AlO(OH), (◆) α-Al_2O_3, (○) anatase TiO_2, (●) rutile TiO_2

The XRD spectra of calcined ZrAl also shows no evidence of a crystalline Al_2O_3 phase. The only phase detectable by XRD after calcination is tetragonal ZrO_2. Tetragonal zirconia is normally formed above 1170°C and reverts to the monoclinic form at lower temperatures.[11] The presence of alumina, however, stabilizes the tetragonal phase.[19] Depending on preparation conditions and ratios of the two metals, the exclusive formation of tetragonal zirconia in the presence of alumina may be achieved, [20, 21] however it is also possible to obtain a mixture of tetragonal, monoclinic, and cubic zirconia.[22] After exposure to subcritical water ZrAl showed a weak reflection at around 14.5° (not shown), evidencing the hydrolysis of a small amount of alumina to form boehmite. No changes in the alumina are seen at 450°C, however at 550°C and above α-

Al_2O_3 can clearly be seen by the peak at about 43.4°. After each hydrothermal treatment there is some recrystallization of zirconia to the monoclinic form, although only a small amount is transformed up to 550°C. Following hydrothermal treatment at 650°C, however, reflections for the monoclinic phase are much more intense than at lower temperatures. In the TiAl and ZrAl samples, no evidence for a transition through the κ-phase of alumina before the α-phase is observed, as has been for CeO_2 coated γ-Al_2O_3.[23]

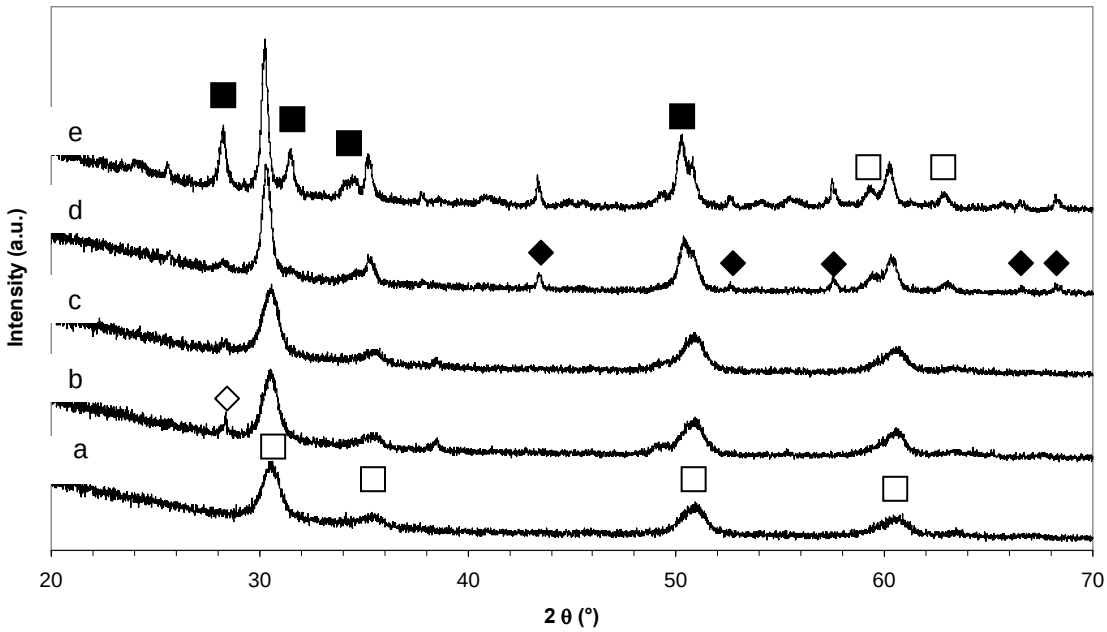

Figure 7.4: XRD spectra of ZrAl (a) after calcination, and after hydrothermal treatment at 25 MPa and (b) 350°C, (c) 450°C, (d) 550°C, and (e) 650°C. Labels correspond to (□) t-ZrO_2, (■)m-ZrO_2, (◇)AlO(OH), (◆) α-Al_2O_3

7.4.2 Surface area and pore characterization

Results from the characterization of the surface area and pores of the supports are presented in Table 1. After hydrothermal treatment at 350°C, ZrAl was mostly unchanged, with only a slight decrease in surface area. A noticeable increase in surface area was seen after hydrothermal treatment at 450°C; pore volume was unchanged, although the average pore radius slightly decreased from 38 Å to 29 Å. The large

increase in pore size after exposure to supercritical water at 550°C is likely due to the collapse of smaller pores while extensive sintering at 650°C, indicated by the large decrease in pore volume, decreases the average pore size.

Table 7.1: Surface Area, Average Pore Size, and Pore Volume of Binary Oxides After Calcination and Subsequent Hydrothermal Treatment at 25 MPa

	ZrAl			ZrTi			TiAl		
	Surface Area ($m^2 g^{-1}$)	Average Pore Radius (Å)	Pore Volume (cc/g)	Surface Area ($m^2 g^{-1}$)	Average Pore Radius (Å)	Pore Volume (cc/g)	Surface Area ($m^2 g^{-1}$)	Average Pore Radius (Å)	Pore Volume (cc/g)
Calcined	81.7	38	0.15	30.8	172	0.26	118.5	61	0.36
350°C	80.5	37	0.15	31.9	171	0.27	55.3	110	0.30
450°C	105.3	29	0.15	21.9	105	0.11	21.6	85	0.09
550°C	19.9	132	0.13	17.4	51	0.04	10.0	50	0.02
650°C	8.3	41	0.02	19.5	61	0.06	6.0	44	0.01

ZrTi had the lowest initial surface area of the binary oxides prepared. Like ZrAl, it was largely unaffected after exposure to subcritical water at 350°C and 25 MPa. At 450°C there was a decrease in surface area and pore volume with more extensive sintering at 550° and 650°C. Of the three binary oxides tested, however, ZrTi retained the largest surface area and pore volume after hydrothermal treatment at the most severe condition.

The TiAl sample, while having the largest surface area of the three binary oxides following calcination, sintered extensively after all hydrothermal treatments. Whereas the other two oxides were stable at 350°C, TiAl lost over 50% of its surface area through sintering after exposure to subcritical water at 350°C. The degree of sintering increased with further increases in temperature.

7.5 Conclusions

The hydrothermal stability of binary oxides of titanium, zirconium, and aluminum was evaluated in sub- and supercritical water at 25 MPa over the temperature range 350°-650°C. The TiO_2/Al_2O_3 sample had the highest initial surface area but sintered extensively after all hydrothermal treatments, with alumina in the samples being hydrolyzed in subcritical water and transformed to corundum in supercritical water. Anatase titania was transformed to rutile only at 650°C. ZrO_2/Al_2O_3 maintained high surface area up to 450°C, but sintered above this temperature as a result of phase transformation of both ZrO_2 and Al_2O_3. The compound $ZrTiO_4$ was crystallographically stable at all conditions. In subcritical water $ZrTiO_4$ maintained its pore structure and surface area. In supercritical water its surface area was reduced by approximately 30%, but at the most severe condition it retained the largest specific surface area and pore volume of the three compounds evaluated.

References

1. Yu, J.; Savage, P. E., Catalyst activity, stability, and transformations during oxidation in supercritical water. *Applied Catalysis B: Environmental* **2001,** 31, 123-132.

2. Elliott, D. C.; Sealock, L. J.; Baker, E. G., Chemical Processing in High-pressure Aqueous Environments. 2. Development of Catalysts for Gasification. *Industrial Engineering Chemistry Research* **1993,** 32, 1542-1548.

3. Osada, M.; Sato, O.; Arai, K.; Shirai, M., Stability of Supported Ruthenium Catalysts for Lignin Gasification in Supercritical Water. *Energy and Fuels* **2006,** 20, 2337-2343.

4. Byrd, A. J.; Kumar, S.; Ramsurn, H.; Kong, L.; Gupta, R. B., Hydrogen production from catalytic gasification of switchgrass biocrude in supercritical water. *International Journal of Hydrogen Energy* **2011**.

5. Elliott, D. C.; Hart, T. R.; Neuenschwander, G. G., Chemical Processing in High-Pressure Aqueous Environments. 8. Improved Catalysts for Hydrothermal Gasification. *Industrial Engineering Chemistry Research* **2006,** 45, 3776-3781.

6. Kennedy, G. C., A portion of the system silica-water. *Economic Geology* **1950,** 45, 629-653.

7. Yamaguchi, A.; Hiyoshi, N.; Sato, O.; Bando, K. K.; Osada, M.; Shirai, M., Hydrogen production from woody biomass over supported metal catalysts in supercritical water. *Catalysis Today* **2009,** 146, 192-195.

8. Matsumura, Y.; Xu, X.; Antal, M. J. J., GASIFICATION CHARACTERISTICS OF AN ACTIVATED CARBON IN SUPERCRITICAL WATER. *Carbon* **1997,** 35, (6), 819-824.

9. Kumar, K.-N. P.; Keizer, K.; Burggraf, A. J., Stabilization of the porous texture of nanostructured titania by avoiding a phase transformation. *Journal of Materials Science Letters* **1994,** 13, 59-63.

10. Santos, J. G.; Ogasawara, T.; Correa, R. A., Synthesis of nanocrystalline rutile-phase titania at low temperatures. *Material Science Poland* **2009,** 27, 1067-1076.

11. Block, S.; Jornada, J. A. H. d.; Piermarini, G. J., Pressure-Temperature Phase Diagram of Zirconia. *Journal of the American Ceramic Society* **1985,** 68, 497-499.

12. Gitzen, W. H., *Alumina as a Ceramic Material*. The American Ceramic Society, Inc.: Columbus, Ohio, 1970.

13. Ito, S.; Umehara, N.; Hidenori, T.; Fujii, T., Phase transition of g-Al2O3 under hot isostatic pressure. *Solid State Ionics* **2004,** 172, 403-406.

14. Reddy, B. M.; Rao, K. M.; Reddy, G. K.; Bharali, P., Characterization and catalytic activity of V2O5/Al2O3-TiO2 for selective oxidation of 4-methylanisole. *Journal of Molecular Catalysis A: Chemical* **2006,** 253, 44-51.

15. Reddy, B. M.; Chowhurdy, B., Dispersion and Thermal Stability of MoO3 on TiO2-ZrO2 Mixed Oxide Support. *Journal of Catalysis* **1998,** 179, 413-419.

16. Zou, H.; Lin, Y. S., Characterization and catalytic activity of V2O5/Al2O3-TiO2 for selective oxidation of 4-methylanisole. *Applied Catalysis A: General* **2004,** 265, 35-42.

17. Newnham, R. E., Crystal Structure of ZrTiO4. *Journal of the American Ceramic Society* **1967,** 50, 216.

18. Cosentino, I. C.; Muccillo, E. N. S.; Muccillo, R.; Vichi, F. M., Low-Temperature Sol-Gel Synthesis of Single-Phase ZrTiO4 Nanoparticles. *Journal of Sol-Gel Science and Technology* **2006,** 37, 31-37.

19. Reddy, B. M.; Sreekanth, P. M.; Yamada, Y.; Kobayashi, T., Surface characterization and catalytic activity of sulfate-, molybdate- and tungstate-promoted Al2O3–ZrO2 solid acid catalysts. *Journal of Molecular Catalysis A: Chemical* **2005,** 227, 81-89.

20. Amairia, C.; Fessi, S.; Ghorbel, A., Sol gel derived Pd/Al2O3-ZrO2 as catalysts for methane combustion: effect of zirconium loading. *Journal of Sol-Gel Science and Technology* **2010,** 54, 29-35.

21. Soisuwan, S.; Panpranot, J.; Trimm, D. L.; Praserthdam, P., A study of alumina–zirconia mixed oxides prepared by the modified Pechini method as Co catalyst supports in CO hydrogenation. *Applied Catalysis A: General* **2006,** 303, 268-272.

22. Dominguez, J. M.; Hernandez, J. L.; Sandoval, G., Surface and catalytic properties of Al2O3–ZrO2 solid solutions prepared by sol–gel methods. *Applied Catalysis A: General* **2000,** 197, 119-130.

23. Byrd, A. J.; Gupta, R. B., Stability of cerium-modified gamma-alumina catalyst support in supercritical water. *Applied Catalysis A: General* **2010,** 381, 177-182.

8. Overall Conclusions

This dissertation has focused on production strategies for the environmentally friendly energy carrier hydrogen from renewable resources by catalytic gasification and reforming in supercritical water. The associated problem of instability of catalyst supports in the supercritical water environment has also been addressed by developing several new metal oxide supports. Parametric studies have been performed for the catalytic reforming of the simple molecules ethanol and glycerol, as well as glucose and biocrude which have more complex reaction networks. In these studies the effect of temperature, pressure, feedstock concentration, residence time, and catalyst has been investigated. Many parallels can be drawn from the results of the glucose, glycerol and ethanol studies. Hydrogen yields increase with increasing temperature, as can be expected from thermodynamic equilibrium, however further increases in pressure in the supercritical region studied had negligible effect on product yields. In all cases hydrogen concentration in the product gases was highest when the feed concentration was low, while methane dominated with higher feed concentrations. Hydrogen yield is maximized when the formation of methane is minimized, as hydrogen is consumed in the formation of methane. By operating the supercritical water reactor with a short residence time it is possible to suppress methanation to a large extent. General kinetic models were developed for hydrogen production in supercritical water and rate constants were reported over the temperature ranges studied.

In the studies using glucose, glycerol, and ethanol as a feedstock a commercially available Ru/γ-Al_2O_3 catalyst was used. While Ru was a good catalyst, the γ-Al_2O_3

support was unstable at the temperatures and pressures associated with supercritical water. Accordingly, a suite of catalysts were developed for testing in the supercritical water gasification of biocrude. Further, the catalysts were characterized by XRD, BET, and TGA to evaluate their stability in supercritical water and tendency toward char formation. Switchgrass was first liquefied in subcritical water using a batch reactor before catalytic gasification in a separate step. Fixed temperature, pressure, feed concentration, and space time were used to evaluate Ru, Ni, and Co catalysts on anatase TiO_2, monoclinic ZrO_2, and $MgAl_2O_4$ supports to make a total of nine catalysts. This was the first report of $MgAl_2O_4$ being used as a support in supercritical water. In spite of the lower inherent surface acidity of the support material, it was seen to char extensively and rapidly upon exposure to a carbonaceous feedstock. A given metal supported on ZrO_2 gave a higher conversion of biocrude than those supported on TiO_2 due to the catalytic activity of zirconia, although charring at the face of the catalyst bed led to reactor plugging within a few hours for ZrO_2 supported catalysts. No plugging was observed for TiO_2 supported catalysts, which also had the smallest amount of char formation. The highest hydrogen yield was obtained with Ni/ZrO_2, while the lowest was with Ru/ZrO_2, which gave a product gas composed of mostly methane and CO_2. The anatase titania and monoclinic zirconia were crystallographically stable, but both lost significant amounts of surface area through hydrothermal sintering. Following SCW exposure $MgAl_2O_4$ also sintered and was found to partially transform to α-Al_2O_3.

Other support materials were also developed as potential catalyst supports for the severe supercritical water environment. A series of Ce-modified γ-aluminas were prepared by an incipient wetness method followed by a reducing treatment which were

then exposed to supercritical water for several hours at 250 bar and 500 - 700°C. XRD and BET studies showed that the inclusion of cerium slowed phase transformations in the supercritical water environment; however, the γ-phase was transformed in all cases and was accompanied by the loss of a large percentage of surface area. Compared to plain alumina samples, the Ce-modified aluminas showed some resistance to being hydrolyzed at 500°C, while at higher temperatures the transformation towards the thermodynamically stable α-Al_2O_3 was slowed. The first observation was made of transition through the κ-Al_2O_3 phase during the transformation sequence towards corundum. Low cerium loadings (1-2 wt%) maintained the highest BET surface areas at 500-600°C, while at 700°C all loadings retained approximately 30-40 m^2 g^{-1}, compared to 2 m^2 g^{-1} for unmodified alumina.

Binary oxides of aluminum, titanium, and zirconium were also synthesized and tested as potential support materials for supercritical water applications. These oxides were tested at 250 bar in both sub- and supercritical water over the temperature range 350 – 650°C. The TiO_2/Al_2O_3 sample had the highest initial surface area but sintered extensively after all hydrothermal treatments, with alumina in the samples being hydrolyzed in subcritical water and transformed to corundum in supercritical water. Anatase titania was transformed to rutile only at 650°C. ZrO_2/Al_2O_3 maintained high surface area up to 450°C, but sintered above this temperature as a result of phase transformation of both ZrO_2 and Al_2O_3. The compound $ZrTiO_4$ was crystallographically stable at all conditions. In subcritical water $ZrTiO_4$ maintained its pore structure and surface area. In supercritical water its surface area was reduced by approximately 30%,

but at the most severe condition it retained the largest specific surface area and pore volume of the three compounds evaluated.

9. Directions for Future Work

There is still much work to be done to develop hydrogen production strategies from biomass derived feedstocks. With small molecules like ethanol and glycerol it is possible to feed high concentrations to the reactor without coke formation on the catalyst; however, thermodynamics dictates a higher selectivity towards methane when the feed concentration is increased. We have seen that methanation can be suppressed by utilizing a short reaction time. Here lies an opportunity for design of more complex reactors than the simple tubular packed beds that were employed in this research. Reactors having better heat transfer characteristics could heat reactants to the desired temperature quickly and prevent lowering of temperature in the reactor from the endothermic reactions taking place, especially as throughput is increased to further reduce residence time. Working with the more complex feedstock biocrude it was also found that char formation took place primarily at the face of the catalyst bed where heating was taking place. Since it is known that char formation is related to heating rate, the rapid heating rate that could potentially realized with new reactor designs would further minimize char formation and increase gas yields.

Continued efforts are needed to further develop support materials capable of withstanding the supercritical water environment and to find less expensive catalytic materials. Some of the catalyst supports developed in this research were able to retain their morphological properties under limited high temperature and high pressure aqueous conditions, but this remains a challenge for future researchers to develop materials able of retaining high surface areas. Ruthenium metal has been found to be a good catalyst in

supercritical water gasification; however its high cost makes it prohibitive for large scale applications. Other researchers have found that noble metals can be replaced with combinations of base metals in other applications, in some cases exceeding the activity of the most active single element catalysts. Perhaps bimetallic base metal catalysts have a place in hydrogen production that has not been discovered by researchers yet.

Another area of study ripe with opportunity stemming from this research is the development of effective strategies for gas separation. The research of this dissertation has not addressed separation or purification of the produced gases. One promising possibility is a catalytic membrane reactor with *in situ* hydrogen separation. The development of a catalytic membrane reactor for hydrogen separation would offer several advantages. First, it would provide a high purity hydrogen stream for any application. Secondly, it would replace expensive processes such as pressure swing adsorption commonly used for hydrogen purification. A third boon lies in the ability of a membrane reactor to achieve conversions beyond the dictations of thermodynamics. As the product hydrogen is removed *in situ*, the equilibrium is shifted towards products. A reactor of this type can also serve to minimize methanation. Hydrogen produced in the reactor will be separated so it cannot react with other products to form methane.

The high pressures and temperatures found in supercritical water reactors provide large driving forces for porous ceramic membranes, the permeance of which scales directly with pressure. Proton conducting membranes have been recently studied for use in solid oxide fuel cells and could be further developed for hydrogen separation. A major shortcoming of both of these types of inorganic membranes is poor mechanical strength

and poor stability in a hydrothermal environment. These materials could add significantly to hydrogen production technologies if these limitations are overcome.

Appendix 1 – Determination of Gas Composition

An SRI 8610C gas chromatograph equipped with a 15' x 1/8" Supelco 60/80 Carboxen 1000 and a thermal conductivity detector was used to determine gas composition in all supercritical water gasification and reforming experiments. The oven was operated isothermally at 200°C, and nitrogen or helium supplied at 15 psi_g was used as carrier gas. An online 150 μLgas sampling loop from Supelco was used to inject the sample. The GC essentially has two parts: a packed column in an oven to separate the mixture into its components and a detector to quantify them. The detector compares the thermal conductivity of the carrier gas flowing in a reference cell to another gas in the sample cell and registers the difference as a mV signal via a Wheatstone bridge. As a gas passes through the detector the signal will quickly rise then fall back to the baseline. When plotted against time the signal will show a series of peaks for each component.

The area of each peak is proportional to it's concentration in the mix. A gas having a known composition similar to a typical product gas was used for calibration. Composition of a typical calibration gas is given in Table A1. To calculate the response factor from the calibration gas, first the number of moles of each gas was found by multiplying the total moles in the sample loop by each specie's molar concentration and assuming ideal gas behavior. Pressure and temperature were precisely known from an electronic gas flowmeter. Knowing the order of elution of the gases from the column manufacturer, a multiplication factor having units of moles per area could be calculated for each gas. By multiplying the peak area obtained from a sample of unknown concentration by this factor, the number of moles of each component can be calculated.

Table A1.1: Composition of Calibration Gas in mol%

H2	CO	CH4	CO2	C2H4	C3H6
50.886	9.709	9.907	19.800	4.844	4.854

Appendix 2 – Calculation of Gas Flow using Viscosity Correction

In Chapters 2,3,4, and 5 gas flow was measured by an Omega 1607A mass flowmeter. This flowmeter measures the pressure drop across a venturi tube and calculates flowrate for a given gas using the viscosity. The flowmeter was operated in hydrogen mode as it was typically the major component of the product gas. The gas flow being measured, however, is not a single component but a mixture. In order to obtain accurate information from the flowmeter the viscosity of the mix must be calculated. Viscosity of the mix was calculated from Wilke's empirical formula:

$$\mu_{mix} = \sum_{\alpha=1}^{N} \frac{x_\alpha \mu_\alpha}{\sum_\beta x_\beta \Phi_{\alpha\beta}} \qquad \text{Eq. A.2.1}$$

where

$$\Phi_{\alpha\beta} = \frac{1}{\sqrt{8}}\left(1+\frac{M_\alpha}{M_\beta}\right)^{-1/2}\left[1+\left(\frac{\mu_\alpha}{\mu_\beta}\right)^{1/2}\left(\frac{M_\beta}{M_\alpha}\right)^{1/4}\right]^2 \qquad \text{Eq. A.2.2}$$

and where M_i is the molecular weight of species i, μ_i is the viscosity of species i, and x_i is the mole fraction of species i. Dividing the viscosity of hydrogen by the calculated viscosity of the mix gives a correction factor to multiply the measured flowrate by to obtain the flowrate of the gas mix.

Appendix 3 – List of Publications and Presentations

JOURNAL ARTICLES

1. Byrd, Adam J.; Gupta, Ram B. **Stability of Binary Oxides of Aluminum, Titanium, and Zirconium in Sub- and Supercritical Water**. (submitted to Industrial & Engineering Chemistry Research)
2. Byrd, Adam J.; Kumar, S.; Kong, L.; Ramsurn, H.; Gupta, R. B. **Hydrogen Production from Catalytic Gasification of Switchgrass Biocrude in Supercritical Water.** International Journal of Hydrogen Energy (2011) available online doi:10.1016/j.ijhydene.2010.12.026
3. Byrd, Adam J.; Gupta, Ram B. **Stability of cerium-modified γ-alumina catalyst support in supercritical water.** Applied Catalysis, A: General (2010), 381(1-2), 177-182.
4. Byrd, Adam J.; Pant, K. K.; Gupta, Ram B. **Hydrogen production from glycerol by reforming in supercritical water over Ru/Al_2O_3 catalyst**. Fuel (2008), 87(13-14), 2956- 2960.
5. Byrd, Adam J.; Pant, K. K.; Gupta, Ram B. **Hydrogen Production from Ethanol by Reforming in Supercritical Water Using Ru/Al_2O_3 Catalyst**. Energy & Fuels (2007), 21(6), 3541-3547.
6. Byrd, Adam J.; Pant, K. K.; Gupta, Ram B. **Hydrogen Production from Glucose Using Ru/Al_2O_3 Catalyst in Supercritical Water**. Industrial & Engineering Chemistry Research (2007), 46(11), 3574-3579.

CONFERENCE PRESENTATIONS

1. Byrd, Adam J.; Kumar, S.; Gupta, R.B. **Hydrogen Production From Liquefied Switchgrass in Supercritical Water Over Ru, Ni, and Co Catalysts.** AIChE National Meeting, Salt Lake City, UT, United States, 2010

2. Kumar, S.; Byrd, A.J.; Gupta, R.B. **Sub- and Supercritical Water Technology for Biofuels: Swithchgrass to Ethanol, Biocrude, and Hydrogen**. 31st Symposium on Biotechnology for Fuels and Chemicals. San Francisco, CA, United States. 2009.
3. Byrd, Adam J.; Gupta, Ram B. **Stability of Ce-Doped Alumina Catalyst Support in Supercritical Water**. AIChE National Meeting, Nashville, TN, United States, 2009.
4. Byrd, Adam J.; Kumar, S.; Gupta, R.B. **Cellulose Liquefaction and Hydrogen Production in Supercritical Water**. AIChE National Meeting, Salt Lake City, UT, United States, 2008.
5. Byrd, Adam J.; Pant, K. K.; Gupta, Ram B. **Hydrogen Production from Glucose Using Ru/Al_2O_3 Catalyst in Supercritical Water**. AIChE National Meeting, Salt Lake City, UT, United States, 2007.
6. Byrd, Adam J.; Gupta, Ram B. **Hydrogen production by reforming in supercritical water.** 231st ACS National Meeting, Atlanta, GA, United States, March 26-30, 2006.

Posters

1. Byrd, Adam J.; Gupta, R.B. **Hydrogen Production by Reforming in Supercritical Water**. Alternative Energy Solutions from Alabama's Natural Resources. Auburn, AL, United States, 2006

2. Byrd, Adam J. and Gupta, Ram B. **Stability of Binary Oxides of Al, Ti, and Zr in Sub- and Supercritical Water**. AIChE National Meeting, Salt Lake City, UT, United States, 2010